Morgan, J., Gulick, S., Mellett, C.L., Green, S.L., and the Expedition 364 Scientists
Proceedings of the International Ocean Discovery Program Volume 364
publications.iodp.org

https://doi.org/10.14379/iodp.proc.364.102.2017

Expedition 364 methods[1]

S. Gulick, J. Morgan, C.L. Mellett, S.L. Green, T. Bralower, E. Chenot, G. Christeson, P. Claeys, C. Cockell, M. Coolen, L. Ferrière, C. Gebhardt, K. Goto, H. Jones, D. Kring, J. Lofi, C. Lowery, R. Ocampo-Torres, L. Perez-Cruz, A.E. Pickersgill, M. Poelchau, A. Rae, C. Rasmussen, M. Rebolledo-Vieyra, U. Riller, H. Sato, J. Smit, S. Tikoo, N. Tomioka, J. Urrutia-Fucugauchi, M. Whalen, A. Wittmann, K. Yamaguchi, L. Xiao, W. Zylberman, and the Expedition 364 ESO Team[2]

Keywords: International Ocean Discovery Program, IODP, International Continental Scientific Drilling Program, ICDP, *L/B Myrtle*, Mission Specific Platform, Expedition 364, Site M0077, Hole M0077A, Gulf of México, Yucatán shelf, Chicxulub, impact crater, crater modification, multi-ring basin, peak ring, uplifted continental crust, impact melt rock, planar deformation features, Cretaceous/Paleogene boundary, PETM, K-Pg boundary, Cretaceous-Paleogene mass extinction, shock metamorphism, carbon isotope excursions, hydrothermal, geomagnetic reversal, shatter cone, ejecta, suevite, granitoid, pelagic limestone, tsunamite

Contents

Introduction

This chapter documents the operational, curatorial, and analytical procedures and methods used during the offshore and onshore phases of International Ocean Discovery Program (IODP) Expedition 364. The information presented in this chapter concerns the shipboard and Onshore Science Party (OSP) methods only. Methods for postexpedition research conducted on Expedition 364 samples and data will be described in individual scientific contributions. Detailed drilling, coring, and logging operations are described in the Operations section of each results chapter.

Operations

Numbering of sites, holes, cores, and samples

Expedition numbers for IODP expeditions are sequential, starting with 301. Drilling sites are numbered consecutively, and for a European Consortium for Ocean Research Drilling (ECORD) Science Operator (ESO) operated platform, numbering started with Site M0001 (the "M" indicates the ESO-operated mission-specific platform [MSP]). For Expedition 364, the Site was M0077. Although not applicable to Expedition 364, multiple holes may be drilled at a single site. For all IODP drill sites, a letter suffix distinguishes each hole drilled at one site. The first hole drilled is assigned the site number with the suffix "A," the second hole takes the site number and the suffix "B," and so forth. For Expedition 364, a single hole was drilled at a single site; therefore, the hole takes the suffix "A" (Hole M0077A).

Recovered cores are numbered sequentially starting at 1, and each core is divided into sections numbered sequentially from the top, starting at 1 (Figure **F1**). Sections have a maximum length of ~1.5 m, taking advantage of any natural breaks in the recovered core. By convention, material recovered from the core catcher is treated as a separate section labeled "CC" and is placed below the last section recovered in the liner. The core catcher is assigned to the top of the cored interval if no other material is recovered. Due to the high integrity of recovered core, the core catcher was often wrapped around a continuous piece of core protruding from the overlying liner. In these cases, the core catcher was removed and the core was archived with the appropriate section number resulting in no core catcher section for that core.

Any sample removed from a core is designated by distance measured in centimeters from the top of the section to the top and bottom of the sample removed. A full identification number for a sample consists of the following information: expedition, site, hole, core number, core type, section number, and interval in centimeters measured from the top of the section. For example, a sample identification of "364-M0077A-2R-2, 35–40 cm," represents a sample removed from the interval 35–40 cm below the top of Section 2, Core 2R ("R" indicates core type; see below), from Hole M0077A during Expedition 364 (Figure **F1**). For Expedition 364, the only core type used was a diamond rotary corer (equivalent to the rotary core barrel [RCB] system used on the research vessel *JOIDES Resolution*), which has the unique identifier "R." A key aspect of the drilling rig used for Expedition 364 is that it drills at higher rotations per minute and lower weight on bit than the *JOIDES Resolution* RCB sys-

[1] Gulick, S., Morgan, J., Mellett, C.L., Green, S.L., Bralower, T., Chenot, E., Christeson, G., Claeys, P., Cockell, C., Coolen, M.J.L., Ferrière, L., Gebhardt, C., Goto, K., Jones, H., Kring, D., Lofi, J., Lowery, C., Ocampo-Torres, R., Perez-Cruz, L., Pickersgill, A.E., Poelchau, M., Rae, A., Rasmussen, C., Rebolledo-Vieyra, M., Riller, U., Sato, H., Smit, J., Tikoo, S., Tomioka, N., Urrutia-Fucugauchi, J., Whalen, M., Wittmann, A., Yamaguchi, K., Xiao, L., Zylberman, W., and the Expedition 364 ESO Team, 2017. Expedition 364 methods. *In* Morgan, J., Gulick, S., Mellett, C.L., Green, S.L., and the Expedition 364 Scientists, *Chicxulub: Drilling the K-Pg Impact Crater.* Proceedings of the International Ocean Discovery Program, 364: College Station, TX (International Ocean Discovery Program). https://doi.org/10.14379/iodp.proc.364.102.2017

[2] **Expedition 364 Scientists' addresses.**

MS 364-102: Published 30 December 2017

Figure F1. IODP recovery and naming conventions used during Expedition 364. * = cores are not representative of the numbered core but only illustrate the naming conventions described.

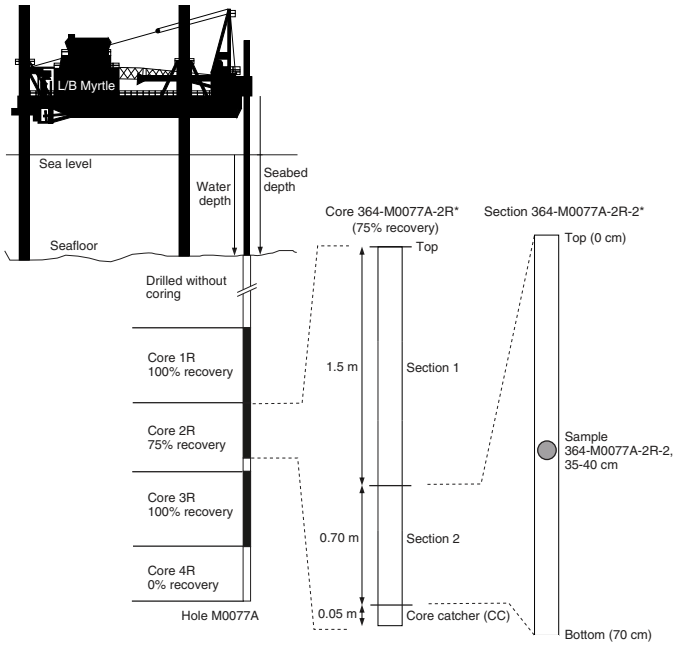

tem. These differences result in slower rates of penetration, but in the lithologies encountered during Expedition 364, it also resulted in significantly higher core recovery than typically achieved with the *JOIDES Resolution* RCB system.

Depth scale terminology

Depth in hole was measured by the drillers as the sum of all drill string components below the rig floor. To determine the depth of the hole below the seafloor, the length of drill string from the rig floor to the seafloor was subtracted from the total length of the drill string. The resulting reference depth for both the open hole and cored interval is drilling depth below seafloor (DSF).

Core depth, the distance from the seafloor to a target within a recovered core, is calculated by adding the curated length of the core to the top depth of the cored interval as measured by the drillers. This depth scale is equivalent to the IODP core depth below seafloor depth scale, Method A (CSF-A; **https://www.iodp.org/policies-and-guidelines/142-iodp-depth-scales-terminology-april-2011/file**). Here, this depth scale is cited as meters below seafloor (mbsf) and allows overlaps in core depth where the curated length is greater than the cored interval (e.g., due to drill pipe stretch and/or expansion of fractures that were initially closed during drilling but later opened during core retrieval). When the recovered core is shorter than the cored interval, the top of the core, by convention, is equated to the top of the cored interval to achieve consistency in reporting depth in core. In addition, a coring gap can occur between cores (i.e., some cored interval was lost during recovery, was never cut, or washed away), although such gaps were minimized due to the type of drill rig used during Expedition 364.

Wireline log depth below seafloor (WSF) is the distance, measured from the wireline, between the target and the seafloor calculated by subtracting the distance between the rig floor and the seafloor return from the total length of the wireline.

Figure F2. IODP depth scales used during Expedition 364. DSF = drilling depth below seafloor, mbsf = meters below seafloor (curated core depth), WSF = wireline log depth below seafloor, CCSF-A = core composite depth below seafloor (reference depth for CT data).

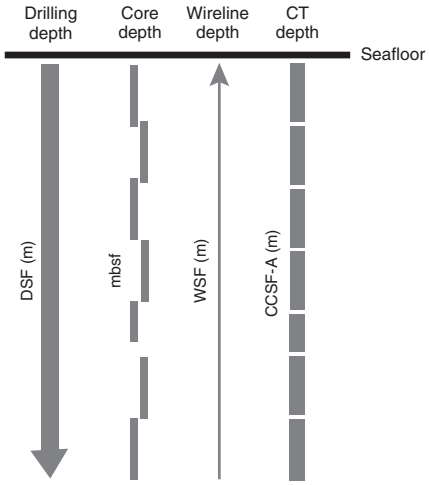

The depth scale for computed tomography (CT) data is a composite depth calculated by stacking the curated length of all the cores. This method does not compensate for overlaps, resulting in an artificially lengthened depth scale. Here, CT depth is cited as core composite depth below seafloor, Method A (CCSF-A).

The depth scales applied during the offshore and onshore phases of Expedition 364 are detailed in Figure **F2**. Corrected depth scales have not yet been applied but will be required postexpedition. The two additional depth scales that will be required are core depth below seafloor, Method B (CSF-B) and core composite depth below seafloor, Method C (CCSF-C). The CSF-B scale is the CSF-A depth with a compression applied to get the cored interval to map back to drilling depth. In other words, 3.1 m of core gets compressed back to the 3 m of cored interval it came from. A final corrected depth scale, CCSF-C, is the distance from the seafloor to a target within the recovered core using a scale of adjusted depths constructed to resolve gaps in core recovery, overlaps of curated lengths, and any depth inconsistencies. This scale is effectively the CSF-B depth calculated more carefully by using the borehole images and/or CT data to precisely resolve any gaps in recovery.

Site location

For Expedition 364, GPS coordinates from pre-expedition site surveys were used to position the *L/B Myrtle* on site (Figure **F3**). Once the *L/B Myrtle* was in position, the legs were lowered and the vessel was jacked up out of the water. The final site position was determined by GPS data collected from an antenna above the drill rig during a period of several hours while the *L/B Myrtle* underwent its preload procedure (see Table **T1** in the Expedition 364 summary chapter [Gulick et al., 2017a]). An additional check of the GPS position was taken at the drill rig positioned on the bow of the vessel.

Platform

For Expedition 364, the maximum target depth (TD) of the borehole was 1500 m DSF. The water depth at Site M0077 is shallow (19.8 m), so a liftboat equipped with a coring rig was selected to carry out expedition operations. The drilling platform, the *L/B Myrtle*, a three-legged, self-propelled 245 class liftboat (Figure **F4**), was selected by Drilling, Observation and Sampling of the Earth's Conti-

Figure F3. Drill site location map. Site bathymetry modified from Goff et al., (2016). Regional bathymetry from Amante et al., (2009).

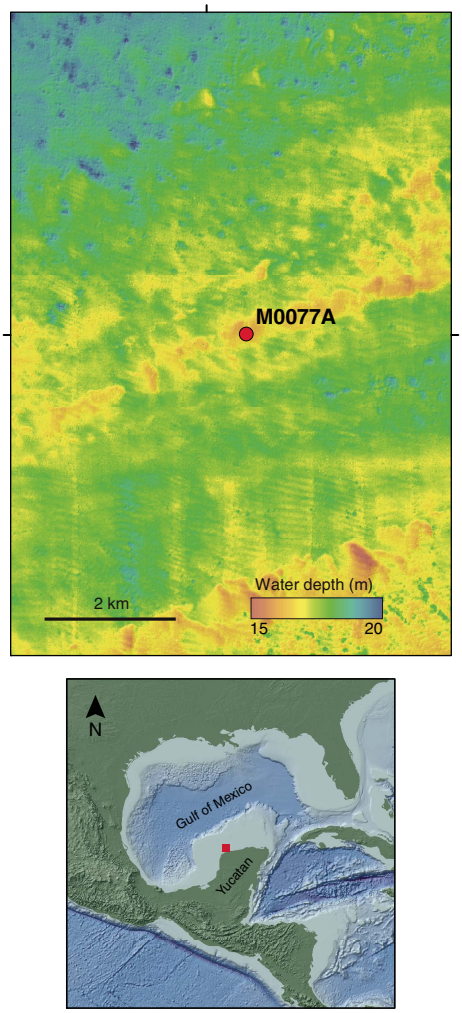

Figure F4. *L/B Myrtle* on site at Site M0077. The drilling rig is visible, cantilevered off the bow. (Image courtesy of L. Perez-Cruz.)

nental Crust (DOSECC) on behalf of ESO. The *L/B Myrtle* had sufficient capacity by way of food and accommodation for 24 h operations but required weekly resupply by a contractor-arranged supply boat (the *Linda F*).

Figure F5. Layout of containerized laboratories on the *L/B Myrtle*. (Image courtesy of D. Smith.)

ESO and DOSECC containerized laboratories were mobilized on the vessel (Figure F5). The containers included the following:

- One "reefer" unit,
- A physical properties multisensor core logging laboratory,
- Core curation facilities,
- A geochemistry clean laboratory,
- A science office,
- An ESO office,
- A database and data management office,
- An ESO logging tools container,
- A DOSECC workshop, and
- A DOSECC spares container.

Drilling and coring rig

The coring rig utilized was the International Continental Scientific Drilling Project (ICDP) Atlas Copco T3WDH mining rig, utilizing flush-jointed mining drill strings and a modified top drive. The rig had a mast capable of handling 6 m string lengths, and coring was conducted using a specially built coring top drive system installed in the mast (Figure F6). Wireline operation of the core barrel was conducted through broken, locked drill string. The coring rig was cantilevered off the bow of the *L/B Myrtle* (Figure F4). The drilling and coring plan was carefully designed to allow the greatest number of options for casing, drill rod/barrel, and core diameters.

An AMC Heli-Portable Solids Removal Unit (HP-SRU) was utilized to reduce the environmental impact and cost efficiency of the hole through a drilling fluid recycling system. Cuttings and drilling fluid were returned to the drill floor once open-hole drilling commenced. The drilling fluid was cleaned and filtered within the HP-SRU. The cleaned drilling fluid was added to a batch of newly mixed drilling fluid before being returned to the borehole. At 79 m DSF, drilling fluid did not return to the drill floor due to a loss of circulation. Below this depth, the remainder of the open-hole interval was drilled using seawater, with the occasional addition of drilling mud to reduce friction.

The HP-SRU was also used in the cored interval. A variable drilling fluid program comprising combinations of seawater, mud products, and loss circulation material (LCM) was used, depending on borehole conditions. Several zones of lost circulation were encountered.

Figure F6. Drilling rig. (Image courtesy of D. Smith.)

Wireline coring

Due to favorable borehole conditions, only two of the possible four wireline coring methods, Oversize PQ3 and Standard PQ3, were utilized.

Diamond rotary corer

The diamond rotary corer used is equivalent to a standard diamond rotary corer used in the mining industry and is designed to core in hard formations. Advancement was by rotary coring, with flushing occurring at the point where the core entered the core barrel. The core barrel was retrieved after each core run by wireline. For Expedition 364, the formation being cored was competent. Therefore, a core spring was used to break the core from the formation at the base of each core run and retain it in the core barrel.

The standard core run length was 3.05 m. However, the length of a core run was chosen to maximize core recovery and maintain hole stability, even at the expense of overall penetration rate. In fragmented or otherwise challenging formations, core runs were less than the 3.05 m maximum. To allow core runs to coincide with pipe additions, it was occasionally necessary to extend the run length to 3.1 m. There was adequate spare length liner capacity tube to accommodate any additional material recovered.

Drilling and coring methodology

The drilling and coring strategy was designed to maximize the probability of achieving the target drilling depth while minimizing the risks associated with a single-hole strategy. Due to the depth and uncertainty in expected lithologies, a number of different open-hole and coring systems of reduced diameter were available. The final strategy adopted involved open-hole drilling from the seafloor to ~500 m DSF, followed by casing the open hole and then continuously coring from ~500 m DSF to TD. Figure F7 is a schematic representation of the final borehole configuration.

Figure F7. Final configuration, Hole M0077A.

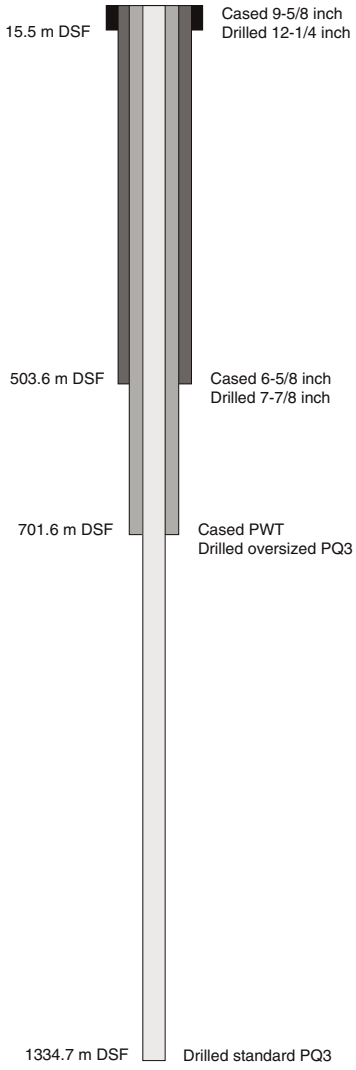

Open-hole drilling

A 13⅜ inch conductor pipe was lowered to the seafloor beneath the rig floor of the *L/B Myrtle*, ensuring that the first drill bit would penetrate the hard seafloor vertically while also providing the drill string with protection from metocean conditions. In addition, the conductor pipe ensured the bottom-hole assembly (BHA) could easily reenter the hole if it had to be retrieved to deck.

The initial open-hole drilling was performed using a 12¼ inch tricone rock roller to 15.5 m DSF. This interval was cased and cemented to establish a riser, allowing the cleaning of cuttings from recirculated drilling fluid. Open-hole drilling then continued from 15.5 to 503.6 m DSF using a drill string comprising a 7⅞ inch polycrystalline diamond (PCD) tricone bit on a CHD drill rod; the hole was subsequently cased and cemented.

Coring

At 503.6 m DSF, prior to coring, the hole was cleared of some debris. This resulted in the hole being advanced by 2.1 m to 505.7 m DSF.

Coring commenced at 505.7 m DSF, using a wireline core barrel. Drilling fluid was used to stabilize the hole and keep the bit cool

while simultaneously flushing drill cuttings out of the hole. When necessary, LCM was used to prevent the continued loss of drilling fluid into the formations. The drill string consisted of a BHA with an oversized PQ3 bit and CHD134 drill. The outer core bit size was ~149 mm, and the core collected was PQ3 size (~83 mm) in diameter, which is larger than the IODP "standard" diameter of ~62 mm. At 701.7 m DSF, the oversized PQ3 string was retrieved. The choice of oversized PQ3 bit allowed for PWT casing to be inserted into the hole and enabled the recovered core diameter to remain at 83 mm through the use of PHD V-wall drill rods and a standard PQ3 bit that could be used through the PWT casing.

Coring continued with a PQ3 coring BHA and PHD V-wall drill rods until the TD of 1334.69 mbsf was achieved. The outer core bit size remained at ~122 mm for the remainder of the borehole, and recovered cores consistently had diameters of ~83 mm.

Downhole logging tools

Downhole logging services were contracted and managed by the European Petrophysics Consortium (EPC). An overview of the logging program is given in **Downhole logging**, and the results are presented in the Downhole logging section of each results chapter.

Curatorial procedures

Cuttings

During open-hole drilling, cuttings were returned to the drill floor via the drilling fluid recycling unit. The initial strategy was to collect cuttings samples at regular intervals (every 5 m of hole advancement). However, cuttings were not always returned to the drill floor due to loss of circulation in some formations. Any cuttings returned were assigned the drilling depth at the time they were taken. The exact depth in the formation from which they came is unknown. In total, 17 samples of cuttings were recovered from between 0 and 75 m DSF.

Two grain-size fractions of cuttings were recovered from the drilling fluid recycling unit. The coarser cuttings (larger than sand sized) were recovered at the shaker table, and the finer fraction (smaller than silt sized) were recovered from the centrifuge. The cuttings samples were curated following IODP procedures.

Offshore core handling

As soon as a core was retrieved on deck, it was immediately curated by the ESO curators. This involved first marking the long axis with black permanent marker to aid later orientation of the core in combination with CT and downhole data. The core was cut into sections (maximum 1.5 m length). Each section was sealed at the top and bottom by attaching color-coded plastic caps: blue at the top of a section and clear at the bottom. A yellow cap was placed on section ends where a whole-round sample was removed, and the sample code was written on the yellow cap. Core section liners were permanently labeled with an engraving tool. The length of the core in each section and the core catcher sample were measured to the nearest centimeter; this information was logged into the Offshore Drilling Information System (OffshoreDIS). No core splitting took place during the offshore phase of Expedition 364.

In parallel with the initial curation, geochemists and microbiologists were given access to the cores to sample for ephemeral properties. Every 9 m, a 5 cm whole round for interstitial water was planned. However, following test squeezing on two samples, these samples were not taken due to the indurated nature of the lithology. Sampling for microbiology postexpedition requests was also conducted offshore, with a 4 cm whole round collected every 9 m throughout and a 2 cm whole round collected every 3 m in the uppermost 100 m of the cored interval.

The core catcher, or a subsample from the core catcher, was given to the micropaleontologists and impact geologists for initial description. The shipboard scientists also took the opportunity to describe the core sections through the clear plastic liners. Samples from the core catcher were taken for preliminary carbon isotope and trace metal analysis to better constrain future sampling during the OSP.

Core sections were allowed to thermally equilibrate before they were run through the multisensor core logger (MSCL) that sequentially measured gamma ray attenuation (GRA) bulk density, *P*-wave velocity, noncontact electrical resistivity, magnetic susceptibility, and natural gamma radiation (NGR) (see **Physical properties**). After these measurements and core descriptions were complete, the core was moved to refrigerated storage.

The offshore core flow is illustrated in Figure **F8**.

Onshore Science Party

The OSP was held at the Bremen Core Repository (BCR; Germany) from 21 September to 15 October 2016. Prior to the OSP, CT scanning was carried out on the unsplit cores, as detailed in **Computed tomography**.

After being taken out of refrigerated storage, cores were split lengthwise into working and archive halves. All cores were split along the axis marked by a black line offshore, allowing cores to be oriented relative to CT data and downhole images. The black line was positioned so that it lies on the bottom of the archive half, ensuring the split face of the cores is the same as the XZ plane in the CT images. The cores were split using a diamond saw.

After splitting, a digital line-scan image of the archive half was taken. Visual core description was carried out on the archive half, aided by digital images, CT images, thin sections, and smear slides

Figure F8. Layout of the *L/B Myrtle* working deck and offshore core flow. Cores arrived (1) on deck and were transferred to (2) the core bench for initial core curation. Final curation occurred in (3) the curation container, where samples for IODP standard measurements and postexpedition research were taken. After curation, cores were transferred to (4) the petrophysics container for MSCL and NGR measurements. Later, cores were stored in (5) the reefer.

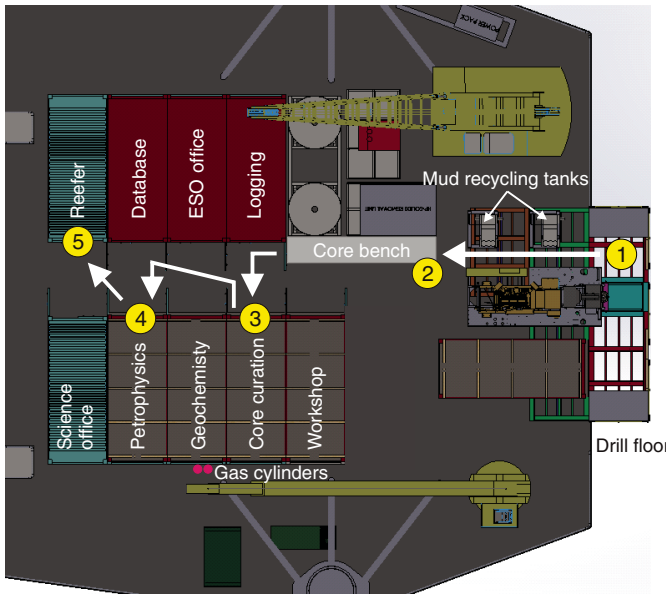

(see **Core description**). Simultaneously, color reflectance measurements were undertaken on the working half of the core (see **Physical properties**). Close-up color photographs were taken of particular features for illustrations, as requested by individual scientists. After core description and imaging, the archive half was used for thermal conductivity measurements (see **Physical properties**).

The working half of the core was sampled for IODP standard measurements (biostratigraphy, thin sections, XRD, X-ray fluorescence [XRF], total carbon [TC]/total organic carbon [TOC], paleomagnetism, and discrete physical properties: thermal conductivity, moisture and density [MAD], and *P*-wave velocity) and post-expedition research (Figure **F9**). Each sample was logged into ExpeditionDIS by location and the name of the investigator receiving the sample. The IODP curator and ExpeditionDIS maintain information about all samples taken. Samples were sealed in plastic bags, labeled, and stored as appropriate.

Following initial IODP standard measurements and sampling, both halves of the cores were wrapped in film and placed in labeled plastic D-tubes that were sealed and transferred to refrigerated storage at the BCR. At the end of the moratorium period, the cores will be permanently archived at the Gulf Coast Repository (USA).

The onshore core flow is summarized in Figure **F9**.

Figure F9. Onshore core flow and IODP standard measurements undertaken during the Expedition 364 OSP. CT scanning was conducted prior to arrival at the BCR.

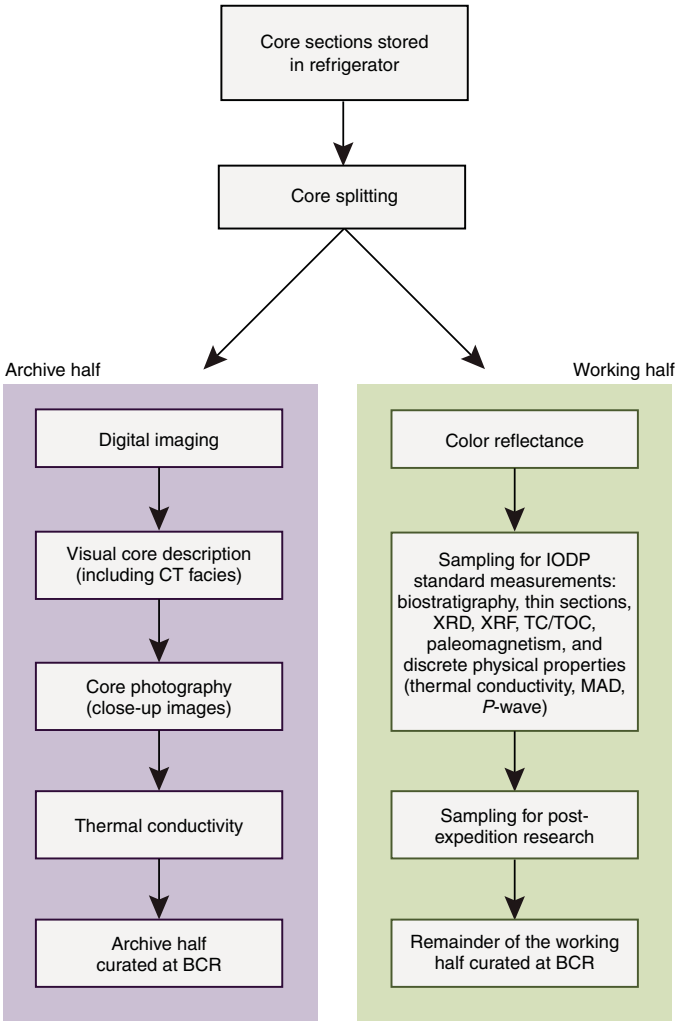

Data handling, database structure, and access

Data management during the offshore and onshore phases of Expedition 364 took place in two stages. The first stage was the capture of metadata and data during the offshore and onshore parts of the expedition. Central to this was the ExpeditionDIS, which stored information about drilling, core curation, sampling, and primary measurements. The second stage was the longer term post-expedition archiving of Expedition 364 data sets, core material, and samples. This function was performed by the International Council of Scientific Unions World Data Center (WDC) for Marine Environmental Sciences (PANGAEA) and the BCR.

The ExpeditionDIS is a flexible and scalable database system originally developed for the ICDP and adapted for ESO. The underlying data model for the ExpeditionDIS is compatible with those of the other IODP implementing organizations and ICDP. For the expedition-specific configuration and workflow requirements of Expedition 364, the ExpeditionDIS data model, data import pumps, and user interfaces were adapted to form the Chicxulub Impact Crater ExpeditionDIS (DIS Version 6.02). This system also included some new functionality, such as setting up predefined sample series for quicker entry of samples, as well as new forms for mud and cuttings samples.

The ExpeditionDIS was implemented in SQLServer-2008 R2 installed on a central server with Microsoft-based client PCs connecting to the system through a Microsoft Access 2010 user interface. The work on DIS development is carried out by Smartcube GmbH (Potsdam, Germany).

Offshore, the ExpeditionDIS was used to capture metadata related to core and sample curation; store core catcher, core close-up, and cuttings photographs along with smear slides, thin sections, and downhole logging metadata; and print section, sample, and subsample labels. During Expedition 364, cuttings samples were taken, and the resulting samples were captured in the ExpeditionDIS. In addition, the database also stored primary measurements data: MSCL data and visual core descriptions (VCDs) of core catcher material and core sections (through liner).

The expedition scientists and ESO staff also generated a variety of spreadsheet files, text documents, and graphics containing operations and scientific data, geological descriptions, and interpretations. Therefore, in addition to the structured metadata and data stored in the ExpeditionDIS, all data files were stored in a structured file system on a shared file server. The primary server was replicated on a secondary server, and backups of the ExpeditionDIS and the file server were made daily. The EPC was responsible for capturing and processing MSCL and downhole logging data.

On completion of the offshore phase of the expedition, the ExpeditionDIS database and file system were transferred to the BCR to continue data capture during the OSP. Additionally, between the offshore and onshore phases all core sections underwent CT scanning by Weatherford Laboratories (Houston, Texas [USA]). The raw CT data were processed, and subsequently a Virtual Core CT project was created by Enthought, Inc. (Austin, TX, USA).

Onshore, additional data types were captured in the ExpeditionDIS, including core close-up images, high-resolution line-scan images, and red-green-blue color space (RGB) data; CT, CT density, and CT atomic number images; color reflectance data; thin sections; and full VCDs of the split cores. All other data were loaded onto the shared file server. A new virtual server at the Center for Marine Environmental Sciences (MARUM; Germany) was used for this expedition. Contents on the server were backed up daily. The file server was also accessible remotely via a web browser using a

cloud system, and the ExpeditionDIS was accessible using the XDIS web interface during both the onshore phase and moratorium.

During the onshore phase, line-scan images and CT, CT density, and CT atomic number images were imported from the ExpeditionDIS into the Corewall-Corelyzer application for visualization purposes to aid with core description, which was useful. Expedition scientists also used the Corewall-Corelyzer software on their laptops during the onshore phase. Virtual Core software was used for viewing the CT project, including a 3-D viewer. Other data such as downhole logging and line-scan images were imported to Virtual Core to view alongside the CT images. Licenses of the Virtual Core software were granted by Enthought to the participants for use during this expedition. The high-volume CT project (~4.7 TB) was copied to scientists' external hard drives. Work with Virtual Core continued after the expedition.

Subsequent to completion of the onshore phase, the sampling and core curation data were transferred from the ExpeditionDIS to the Curation Drilling Information System (CurationDIS), the long-term BCR core curation system.

During the second stage, all Expedition 364 data were archived in the PANGAEA information system. PANGAEA is a member of the WDC system. It has a flexible data model that reflects the information processing steps in earth science fields and can handle any related analytical data (Diepenbroek et al., 1999, 2002; Collier et al., 2015). It is used for processing, long-term storage, and publication of georeferenced data related to earth sciences. Essential services supplied by PANGAEA are project data management and the distribution of visualization and analysis software. Data management functions include quality checking, data publication, and metadata dissemination that follows international standards.

The data captured in the Chicxulub Impact Crater ExpeditionDIS and stored in the shared file server were transferred to PANGAEA following initial validation procedures. The data transfer process was completed by the time of publication of the Expedition reports section of this *Proceedings* volume. Until the end of the moratorium period, data access was restricted to the expedition scientists. Following the moratorium, all data except downhole wireline data were published online (**https://pangaea.de**), and PANGAEA will continue to acquire, archive, and publish new results derived from Expedition 364 samples and data sets. Raw and processed downhole wireline data were archived at **http://brg.ldeo.columbia.edu/logdb** with a link from PANGAEA.

The central portal for all IODP data, including Expedition 364 data, is the Scientific Earth Drilling Information Service (SEDIS; **http://sedis.iodp.org**). IODP MSP data are also downloadable from the MSP data portal (**http://iodp.pangaea.de**).

Core, section, and sample curation using the Chicxulub Impact Crater ExpeditionDIS

Expedition 364 followed IODP procedures and naming conventions in core, section, and sample handling (see **Numbering of sites, holes, cores, and samples**). The ExpeditionDIS captured the curation metadata and printed the appropriate labels, also to IODP standards. Curation metadata comprise the following:

- Expedition information,
- Site information (latitude, longitude, water depth, start date, and end date),
- Hole information (hole naming by letter, latitude, longitude, water depth, start date, and end date),
- Core data (core number, core type, top depth, bottom depth, number of sections, core catcher availability, curator, core on deck date and time, and any additional remarks),
- Section data (section number, section length, curated length, and curated top depth of section),
- Sample information (repository, request, request part, code observer, expedition, site, hole, core, section, half, sample top, sample bottom, and sample volume),
- Calculated core recovery percentage on the basis of the drilled or cored length and the curated recovery, and
- Calculated section recovery on the basis of the section length and the curated length.

No correction was made in cases where the recovery exceeded 100%. Top and bottom depths of the section (mbsf scale) were calculated on the basis of the core top depth determined by the DSF scale. Curation of subsections was possible but not used during Expedition 364. Section and sample label formats follow the standard IODP convention. They include bar codes of the section/sample code and the complete section/sample code (Expedition-Site-Hole-Core-Core type-Section-Half-Interval and sample request code). This standardization guarantees data exchange between the repositories and enables information flow between the implementing organizations.

Computed tomography

This section describes the X-ray CT scanning and data processing performed on Expedition 364 cores. It explains the procedures for handling and CT scanning the cores, processing the raw CT data, creating CT image volumes, and generating bulk density (ρ_b) and effective atomic number (Z_{eff}).

CT has emerged as one of the most effective nondestructive methods for understanding the composition and internal structure of cores. The CT technique has undergone many refinements since its invention in the 1970s, and whole-core CT scans can now provide a 3-D model of the bulk density and chemical composition of the entire core at a resolution up to 0.3 mm^3. Duliu (1999) provides a detailed theoretical background of CT methodology and specific considerations for use when studying rock samples. Expedition 364 is the first IODP MSP expedition for which all cores were CT scanned as a standard measurement.

CT scanning

CT scanning for Expedition 364 cores was performed by Weatherford Laboratories. The cores arrived by truck at Weatherford Laboratories on 15 June 2016 in a 20 ft refrigerated container which was kept at 4°C during shipping. The cores were unloaded from the container, with effort made to minimize the time exposed to higher temperatures, and staged in a refrigerated storage room at 4°C during processing. The core was not exposed to strong magnetic fields during storage or scanning.

The scanning was performed using a Toshiba Aquilion Prime Dual Energy Helical CT scanner (Figure **F10**). This machine performed two scans of each core section: one scan was performed at a higher X-ray energy level (135 kV) and the other at a lower energy level (80 kV). Dual-energy scanning can provide additional insight into the physical properties of the core. Each core section was oriented according to the black line marked on the core tube offshore. The machine produces a series of axial cross-section "slices" or im-

Figure F10. Expedition 364 core scanning at Weatherford Laboratories.

Figure F11. Unprocessed high- and low-energy CT images of the hundredth slice from the interval between 697.09 and 698.09 m CCSF-A. CT number values are in Hounsfield units.

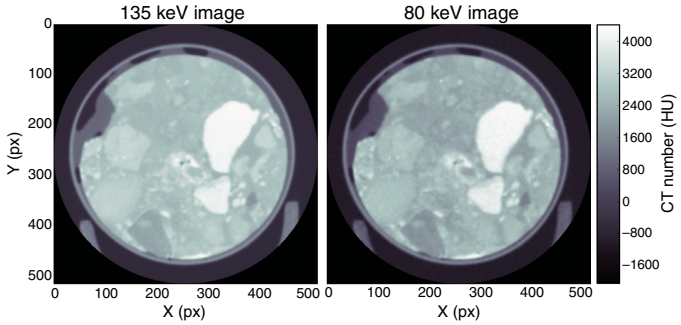

ages (Figure **F11**). Each slice represents a thickness of 0.3 mm, which results in approximately 3300 slices per meter of core. The images have a spatial resolution of 250 µm.

Weatherford Laboratories completed scanning the cores on 6 July 2016. The complete CT scan consisted of over 5 million slice images representing the scans at both energy levels. These images were stored as industry standard Digital Imaging and Communications in Medicine (DICOM) files comprising 3 TB of raw data in total.

CT data processing

The raw data were shipped to Enthought, Inc. (Austin, TX, USA), and received on 14 July 2016. Enthought has developed a series of processing algorithms called Clear Core to clean and correct CT data (Hall and Govert, 2016). The first step during processing is combining the raw data into a convenient scientific data storage format. HDF5 is the high-performance scientific data model and archive format used to store the raw and processed data. Libraries such as H5Py (Collette, 2013) can be used to load HDF5 data into high-performance numerical arrays suitable for fast computation and visualization.

Expedition 364 CT data were cleaned by removing the dominant noise artifacts. Because core tends to fracture along bedding or other planes of weakness, contiguous pieces of core can be detected. First, the axis and radius of each section were estimated and the type of liner was identified because corrections are dependent on liner type. Voxels containing liner and residual mud were removed. The median CT value of the center region of the core along the axis was used to correct for beam hardening. CT number offsets between adjacent sections were identified and used to normalize the data in different sections. Fractures and void space in the core (e.g., due to unconsolidated sediment or rubble) were removed. The end result was a continuous core with a normalized CT intensity corrected for beam hardening.

Figure F12. Explanation of the orientation of core CT images and the cylinder unwrap from the CT volumes.

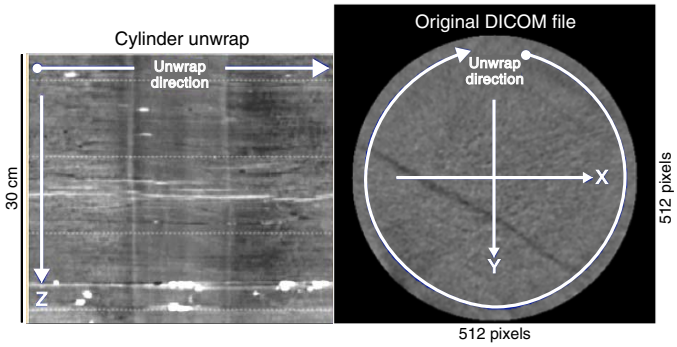

During processing, various 2-D images were generated from the 3-D CT volume. These images are oriented in reference to the Cartesian coordinate system shown in Figure **F12**. The *X*- and *Y*-directions define the plane of the cross-sectional images, and *Z* points downward along the axis of the core. The core is oriented so the black marker line is at the top (12 o'clock) position on the cross-section in the right image of Figure **F12**. For example, the "CT Cleaned: XZ Slice" is an image of the central plane of the entire core extracted along a plane parallel to the *x*-axis. The cylindrical unwrap is a 2-D image of the CT values around a given circumference within the core. This image is unwrapped and presented in the direction shown in the figure.

The CT processing results are stored in a project file that can be viewed with the Virtual Core software or other CT imaging software. Virtual Core, provided for the Expedition 364 Science Party by Enthought, provides a visualization tool for 1-D, 2-D, and 3-D core data and images. It also provides tools for depth shifting and rotational orientation, which are necessary to orient the cores, and for plotting additional data, like logs (log ASCII standard [LAS] files) and acoustic borehole images (digital log interchange standard [DLIS]). Figure **F13** shows a screenshot of Virtual Core with various types of data added.

It was necessary during processing to create a contiguous CT depth scale. The cores were supplied with their curated depths (in mbsf), which overlap between some sections. Processing (and display) of the CT images require that each location within the core has a unique depth. The CT depth scale was created by adding the curated lengths together. This depth scale is labeled CT depth in the CT processing/viewing software and is referred to by IODP as core composite depth below seafloor (CCSF-A) (see **Depth scale terminology**). A translation table was created so that CT images could be exported from Virtual Core and named according to their curated lengths. The processed CT data were delivered to ESO on 26 August 2016. The final project file size was 4.7 TB, delivered on a large-capacity external hard drive.

Dual-energy analysis

Weatherford Laboratories performed a full dual-energy scan on the Expedition 364 cores. In dual-energy CT scanning, the specimen is scanned twice at two different energy levels. At higher ener-

Figure F13. Virtual Core visualization software. Left to right: Mini-Map (navigation tool), CT density, sonic well log and MSCL density, CT XZ slice, CT unwrapped, acoustic borehole image, and CT cleaned histogram.

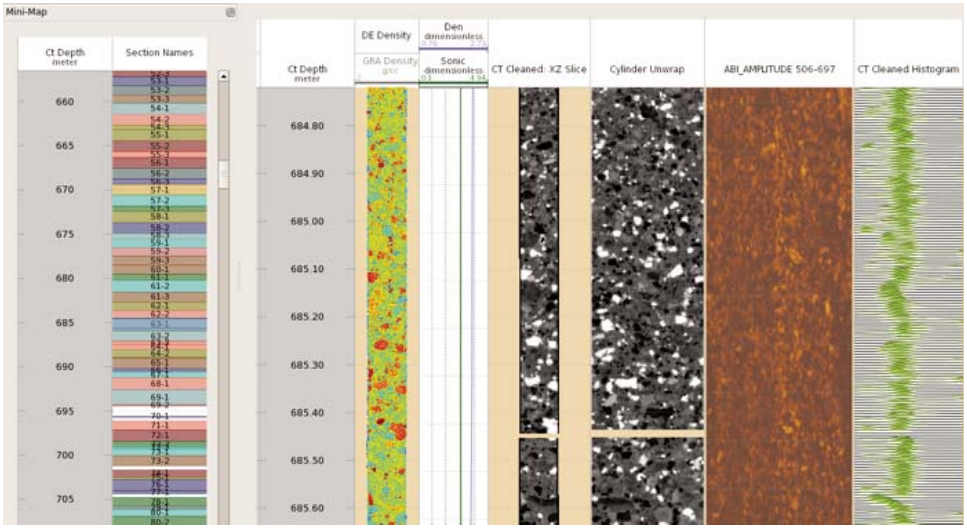

Table T1. Calibration coefficients for dual energy calculations, Expedition 364. **Download table in CSV format.**

Coefficient	Value
m	–1.17847
p	2.341677
q	1,743.256
r	54,221.69
s	–65,748.2
t	–1.3E–7

gies (above 100 kV), X-rays interact with matter mainly through Compton scattering. The amount of Compton scattering is sensitive to the electron density (and thus bulk density). At X-ray energies below 100 kV, the predominant interaction mechanism is photoelectric absorption, which is sensitive to the effective (bulk) atomic number.

Siddiqui and Khamees (2004) proposed a technique to calculate bulk density (ρ_b) and effective atomic number (Z_{eff}) from dual-energy CT data. They give the following equations to calculate density from the high and low energy data:

$$m \times CTN_{low} + p \times CTN_{high} + q = \rho_b, \quad (1)$$

and

$$r \times CTN_{low} + s \times CTN_{high} + t = [0.9342 \times \rho_b + 0.1759] \times Z_{eff}^{3.6}. \quad (2)$$

CTN_{low} and CTN_{high} are the CT numbers of the low- and high-energy scans, respectively. The coefficients m, p, q, r, s, and t are dependent on core lithology and need to be determined empirically. For Expedition 364, preliminary coefficients were obtained by performing a dual-energy scan of three different materials of known ρ_b and Z_{eff} and obtaining the CTN_{low} and CTN_{high} response. This scanning provided data to solve three unknowns, from which Weatherford Laboratories determined the coefficients shown in Table **T1**. These calibration coefficients are considered preliminary and will be more accurately determined as part of the postexpedition research.

Figure F14. XZ slice images of ρ_b and Z_{eff} for CT depth range 697.09–698.09 m CCSF-A. These values are not yet calibrated for Expedition 364 cores; calibration will be completed as part of the postexpedition research.

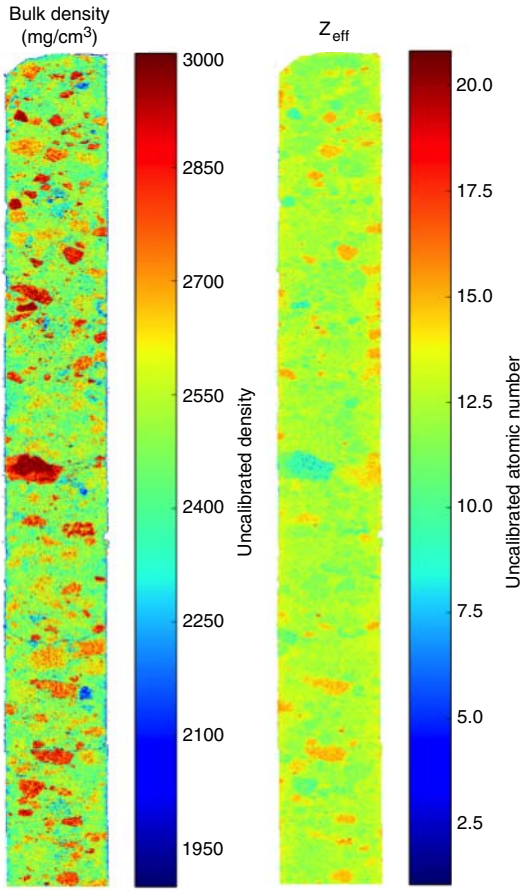

Using the XZ slice of the unprocessed high and low CT data, ρ_b was obtained for every pixel location using Equation **E1** and the corresponding locations in the high and low CT data. Once obtained, Equation **E2** can be used to find Z_{eff}. Figure **F14** shows a typ-

ical result of this calculation for CT depth range 697.09–698.09 m CCSF-A. This method was applied to the entire core, and XZ slice images of ρ_b and Z_{eff} were generated and exported for every section. Comparisons with other physical properties data indicated that these CT density values are too high and the calibration coefficients will need additional adjustment postexpedition. XZ slice images for both the high- and low-energy scans are provided in CT_IMAGE in **Supplementary material**. The full CT data are available through the BCR (**https://www.marum.de/en/Research/IODP-Bremen-Core-Repository.html**).

Core description

Initial core descriptions occurred offshore on unsplit cores through the clear plastic core liner; more detailed core descriptions were carried out during the OSP on split cores. The procedures for both these methods are described below.

Offshore methodology

This section summarizes the offshore methodology for description and documentation of the lithostratigraphy of cores recovered during the offshore phase of Expedition 364. Most of these methods overlap in detail with procedures during the onshore phase and will be addressed more thoroughly in that section. To avoid redundancy, this section will only outline specific procedures carried out offshore that differ from onshore description and documentation.

Visual core descriptions

Lithologies of the core intervals recovered were represented on the VCDs by sketching graphic patterns in the Sketch column. In the Post-Impact Sedimentary Rocks interval, the major lithology is shown in the Lithology column, and some distinctive secondary lithologies, such as interpreted ash layers, are included graphically. The additional VCD columns include Veins and alteration, used for vugs and hydrothermal minerals (note that veins are actually shown in the Sketch column); Structure, used for specific sedimentary structures; MBio, used for bioturbation; and Core disturbance, used to report preexisting and drilling-induced fractures. Notes and details were added in the Description column.

In the upper sedimentary section, graphic lithologies were used for all components that compose 25% or more of the total section length. Below the top of the Upper Peak Ring interval at 617.33 mbsf to the bottom of the hole, graphic lithologies were used where the length of a given rock type exceeded 10 cm. Rock types of shorter length were noted in comments and/or sketches. Sedimentary rocks were characterized mainly as marlstones and limestones on the basis of color and the presence (for marlstone) or absence (for limestone) of darker, more clay-rich laminae identified visually or through smear slide analysis (see **Core catcher analyses**).

In the Upper Peak Ring and Lower Peak Ring intervals, the major lithology was documented. The additional VCD columns used include Veins and alteration, used for sketches of the orientation of veins and the presence of vugs and other diagenetic mineralization, and Core disturbance, used to report open fractures or drilling-induced damage to the core. Notes and details were added in the Description column. Units 2 and 3 (suevites and impact melt rocks) were characterized on the basis of their clast compositions, clast sizes, contents, and matrix composition. It is possible that some of the dikes within the basement lithologies that were classified as impact melt rocks offshore are magmatic and not impact related. Basement lithologies were characterized broadly on the basis of their overall composition (felsic, intermediate, and mafic), and their texture was noted in the Description column.

Relative abundances of lithologies reported in this way are useful for general characterization of the sedimentary rocks, impactites, and igneous units but do not constitute precise, quantitative observations. The nomenclature applied offshore was revised based on detailed visual core description carried out during the OSP.

A legend of the symbols used on offshore VCDs is provided in Figure **F15**.

Core catcher analyses

Core catcher material provided the only opportunity offshore to view lithologies directly rather than through the transparent liner. Throughout the core, in particular the suevite interval (Unit 2), mineralogy and compositional assessment of core catcher material was aided by the use of a reflected light binocular microscope. In addition, smear slides were prepared for use with a transmitted light microscope. Smear slides were prepared by two different methods depending on the character of the material. (1) For sedimentary rocks and more friable suevite, a small amount of the sample was crushed with a mortar and pestle and mixed with a small amount of water. The resulting slurry was pipetted onto coverslips and dried with the use of a hot plate. Once dry, the coverslips were set onto glass slides using Norland optical adhesive 61 and then cured under anultraviolet (UV) lamp for several minutes. (2) For hard Lower Peak Ring rocks, the edge of a sample was shaved off with a dull blade directly onto the glass slide. Larger particles were removed or crushed on the slide. Optical adhesive and two square coverslips per slide were added. The adhesive was hardened under a UV lamp for several minutes.

Figure F15. Legend for offshore visual core description, Expedition 364.

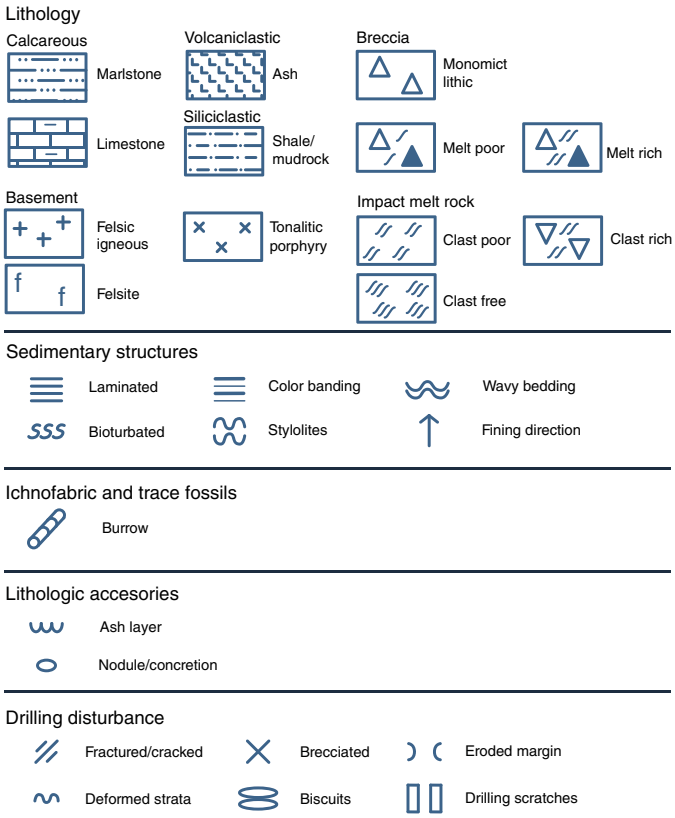

Core summary

The written description for each core in the Description column contains a brief overview of major and minor lithologies, color, and notable features such as sedimentary structures and major disturbances resulting from the coring process (see **Onshore methodology** for details). All VCDs were scanned and uploaded to the ExpeditionDIS as PDFs, and observations of lithology and structures were entered into the ExpeditionDIS for each core and section. However, these VCDs were later superseded by the onshore VCDs.

Onshore methodology

During the OSP, cores were split, and much more detailed descriptions of lithology and other features were possible. Information here concerns onshore operations and analyses described in the relevant results chapters. Offshore visual core description and observations based on core catcher samples were consulted in making these descriptions.

General methodology

Unsampled archive halves of split cores arrived in the visual core description laboratory of the BCR along with paper copies of VCDs that included the line-scan image of the accompanying core section on the left side of the sheet. The archive half was examined, and visual observations were recorded manually on the VCDs. This information was then condensed and entered into the ExpeditionDIS to generate a simplified database of each core section unit described. Handwritten VCDs were scanned and archived (see SCANVCD in **Supplementary material**).

Apart from the naked eye, visual aids used for core description included hand lenses and a microscope camera with an LED light (eScope DP-M01; 20× magnification) that was placed on the core surface. Munsell charts (Munsell Color Company, Inc., 1988) were placed on the cores for color estimation, and plastic grain size charts and rulers were also used. For better visibility, the archive halves were often sprayed with distilled water from a plastic spray bottle. Diluted hydrochloric acid (10%) was used locally to test for the presence of carbonate minerals. In the Lower Peak Ring interval, broken segments of the core sections were temporarily removed from the liner to inspect the fracture surfaces for the presence of shatter cones and fault striations. Where present, the orientation of striations was measured with a steel protractor (see STRUCTURAL in **Supplementary material**). Description was enhanced by the use of Corewall software and three flat-screen monitors that displayed line-scan images and CT scans of the cores (see **Computed tomography**).

Thin sections

Polished petrographic thin sections of specific intervals within cores were prepared to allow material to be examined under an optical (polarizing petrographic) microscope using transmitted light. A total of 49 thin section billets were taken during the offshore phase, and 36 billets were taken during the early part of the OSP to give a representative overview of all lithologies. After the thin section billets were cut with a diamond saw, they were dried in a furnace for 24 h at not more than 25°C. Thin section billets were sent to two different outside contractors (Dettmar Dissection Technology GmbH & Co., Bochum, Germany, and MKfactory, Stahnsdorf, Germany) to produce standard-sized, 30 µm thick thin sections. In some cases, they were first impregnated in epoxy to ensure that the sample remained intact throughout thin section preparation.

Before detailed investigations of the thin sections were made, most of the thin section billets were photographed to associate a given thin section to the macroscopic sample from which it was prepared (see **Core descriptions**). All thin sections were also scanned using a Plustek OpticFilm 8200i film scanner (and SilverFast 8 software), which created ~1 MB JPEG images of the entire thin section. By sandwiching the thin section between two polarizing filters, cross-polarized light scans were obtained (allowing preliminary identification of some of the rock-forming minerals). Noteworthy features found in the thin sections were photographed with a digital camera mounted on the microscope.

Computed tomography

A complete set of 3-D X-ray CT images was collected from whole-round cores prior to the OSP using facilities at Weatherford Laboratories and computational processing by Enthought (see **Computed tomography**). CT images were provided to the visual core description team using the Corelyzer software application of Corewall (see CT_IMAGE in **Supplementary material**). Additionally, the visual core describers had access to the full CT volumes using the Virtual Core software provided by Enthought.

CT scans provide useful additional information that helps characterize and describe the different lithologic units. In particular, features like cracks and shear faults, veins, alteration zones, and enhanced or reduced porosity can be recognized, as well as primary minerals or mineral clast components. Images are displayed as negatives, with cracks and voids as black features, low-density minerals and rocks as dark features, and high-density minerals and rocks as bright features.

All cores were described with the use of four images with the upper image being the photographic line scan. The lower three images were CT images showing a core slice in the plane of the split core on the workbench, the XZ plane (see **Computed tomography**). These CT images are (1) a map of CT number, (2) an uncalibrated map of density (ρ_b), and (3) an uncalibrated map of effective atomic number (Z_{eff}). CT facies were then described alongside the core descriptions. Lithostratigraphic units were described with simple terminology on the barrel sheet. CT number facies were described as black (B), dark gray (DG), light gray (LG), or white (W), and density and atomic number were described as high or low. Unusual features were described in more detail, and reoccurring lithologies were often abbreviated (e.g., "granite facies" and "dolerite facies").

Post-impact sedimentary rocks

Lithostratigraphy

This section provides a summary of the onshore procedures for the description and documentation of the stratigraphy and sedimentology of cores recovered during Expedition 364. It outlines the methodology of the visual core description and our system for sedimentary rock classification.

Visual core description and rock classification

Members of the onshore sedimentary geology team conducted visual inspection and description of the core recovered during Expedition 364. Descriptions were initially made by hand on the VCDs. These featured a high-resolution line-scan image of each core section (see LINESCAN in **Supplementary material**) with a series of columns for manual entry of graphics or symbols to denote lithology and illustrate aspects such as lithologic variations and sedimentological features (Figures **F16**, **F17**). Grain size divisions for

Figure F16. Sample onshore sedimentary rock visual core description (VCD) sheet, Expedition 364. From left to right, the sheet has a line-scan image of the core with a scale in centimeters and columns for unit numbers as defined by the VCD team, lithology, veins and alteration, structures, burrows, ichnofabric index (Droser and Bottjer, 1991), fossils, core disturbance, and general description.

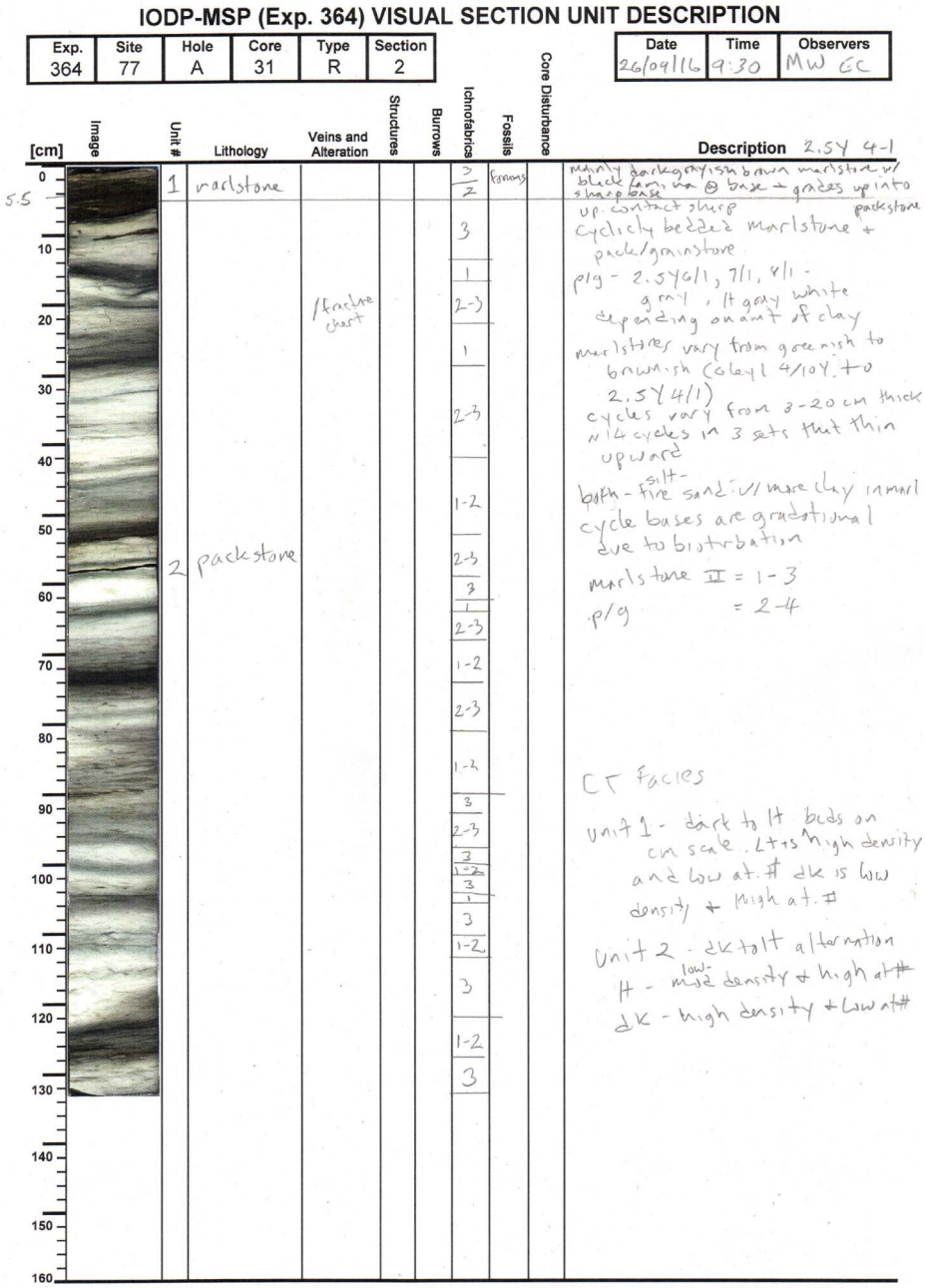

clay, silt, sand (very fine, fine, medium, coarse, and very coarse), granules, and pebbles were defined in accordance with Wentworth (1922) and used in the description of siliciclastic facies. Carbonate rocks were classified according to the scheme of Dunham (1962) as modified by Embry and Klovan (1972) (Figure **F18**). Fine-grained rocks with approximately equal proportions of lime mud (micrite) and clay minerals were classified as marlstones, and the modifier "marly" was commonly used for carbonate rocks that appeared to contain significant but less than 50% clay minerals based on visual inspection and reaction with dilute hydrochloric acid.

Lithologies were assessed through visual comparison using hand lenses, the eScope DP-M01, and grain size cards. Color was noted with reference to the Munsell color chart to assign an estimated value; however, cores were also analyzed with an automated color reflectance procedure (see **Physical properties**), which provides a quantification of Munsell index color. Composition was estimated using a combination of the eScope DP-M01, microscopic observations of smear slides (see **Offshore methodology**), and visual comparison charts of grain size, sorting, and grain percentages.

A wide variety of features that characterize the sedimentary rocks were indicated in the columns to the right of the graphic log on the VCDs and included items such as sample locations, veins and alteration, primary sedimentary structures, bioturbation intensity and burrows, fossils, core disturbance, and general description.

Where apparent, contacts between different sedimentary units are given in the Description column. Authigenic and diagenetic products such as glauconite, pyrite, silicification, carbonate nodules, and veins or other alteration products were noted on the VCDs either in the Description or Veins and alteration column (Figure F16). These features, as well as the positions of sedimentary features, were recorded as accurately as possible with respect to stratigraphic position on the VCDs. A full set of symbols used on the VCDs is given in Figure F17.

Figure F17. Patterns for lithologies and symbols for sedimentary structures, burrows, fossils, postdepositional alteration products, and core disturbance, Expedition 364.

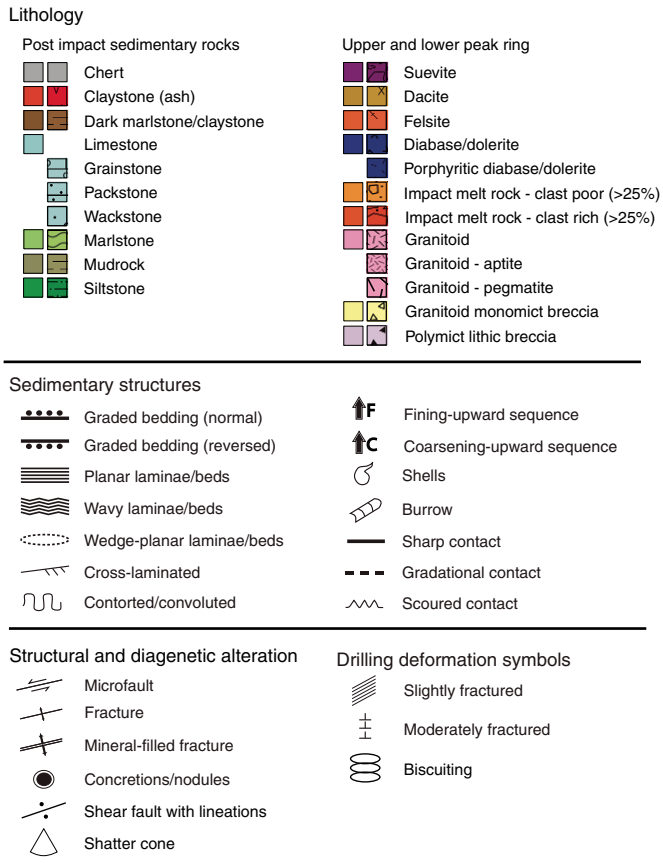

Ichnological analysis included evaluation of the intensity of bioturbation and documentation of individual well-defined traces. Bioturbation intensity (1–5) was determined semiquantitatively using the ichnofabric index of Droser and Bottjer (1991) (e.g., 1 = bioturbation absent, 3 = moderate bioturbation, and 5 = total biogenic homogenization of sediment).

Visual core description thus allowed for semiquantitative estimates of the relative grain size, sorting, ratio of grains to matrix, ichnofabrics, and bioclastic composition to produce a sedimentary rock classification. Generic or interpretive terms such as pelagic, hemipelagic, or turbidite were avoided because the aim was to provide a purely descriptive account of the sedimentary rocks.

Thin sections

Specific intervals within cores were prepared as thin sections to allow material to be examined under a petrographic microscope using transmitted-polarized and cross-polarized light. This technique is particularly useful for examining microscopic details of carbonate grain types, microfossils, and sedimentary textures. Attributes that were determined included dominant grain types, microfossils, accessory minerals, authigenic or diagenetic components, and mineralogy of matrix or cement between or within grains. Thin section mineralogy was also used as a check on visual core descriptions. Fine-grained components (especially microfossils) can be difficult to identify except under higher magnification. Thin sections provided additional means to identify more accurately the components of marlstones and fine-grained carbonate lithologies.

Locations of thin section samples were marked on the VCDs, and the location and orientation of samples for thin section preparation were flagged on the cores.

Upper Peak Ring rocks

Rock classification

The nomenclature of impactites of the Upper Peak Ring interval utilizes the provisional International Union of Geological Sciences (IUGS) nomenclature described by Stöffler and Grieve (2007); the implementation of this scheme during the OSP is described in Table T2. The nomenclature was revised based on detailed visual core description carried out during the OSP.

Figure F18. Carbonate rock classification (adapted from Dunham [1962] as modified by Embry and Klovan [1972]).

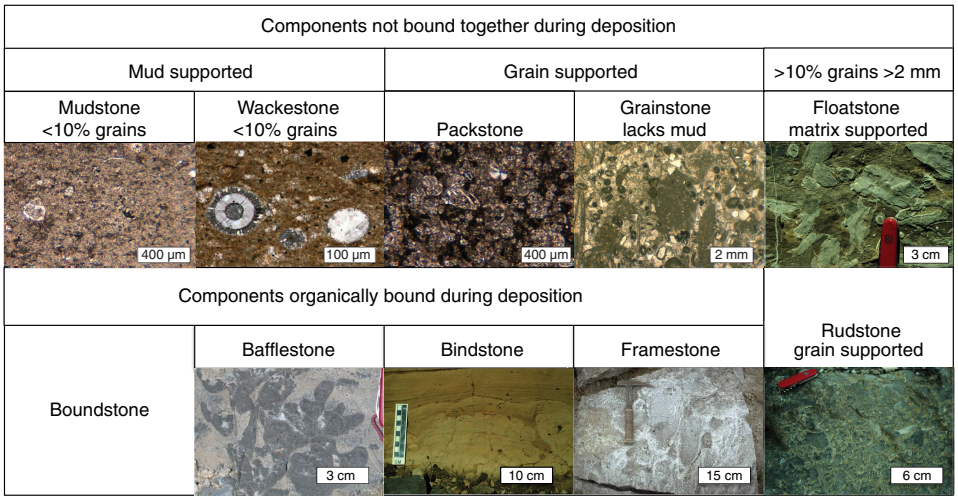

Table T2. Implementation of the provisional IUGS nomenclature guide of impactites (Stöffler and Grieve, 2007) used during Expedition 364. **Download table in CSV format.**

Lithology	Criteria
Shocked target rocks	
Granitoid	Coarse-grained, granitic, or syenitic rock.
Granitoid—pegmatite	Ultracoarse-grained, granitic, or syenitic rock.
Granitoid—aplite	Fine-grained, granitic, or syenitic rock.
Felsite	Fine-grained intrusive felsic rock.
Dacite	Porphyritic rock with phenocrysts of plagioclase feldspar, quartz, and alkali feldspar in a groundmass of plagioclase and mafic minerals.
Diabase/dolerite	Medium-grained mafic rock; contains pyroxene crystals visible to the naked eye, <2 mm.
Porphyritic diabase/dolerite	Medium-grained, porphyritic mafic rock; contains plagioclase feldspar laths visible to the naked eye, ~2 mm or greater, and pyroxene crystals visible to the naked eye, <2 mm.
Monomict breccia	
Granitoid	Authigenic breccia with clastic matrix of granitoid composition (see above).
Polymict breccia	
Lithic impact breccia	Polymict impact breccia with clastic matrix containing shocked and unshocked mineral and lithic clasts but lacking cogenetic melt particles.
Suevite	Polymict impact breccia with particulate matrix containing lithic and mineral clasts in all stages of shock metamorphism, including cogenetic impact melt particles, which are in a glassy or crystallized state.
Impact melt rock	Crystalline, semihyaline, or hyaline rock solidified from impact melt containing variable amounts of clastic debris of different degrees of shock metamorphism.
Clast rich	>25% clasts.
Clast poor	0%–25% clasts.
Clast free	0% clasts.

For visual core description and classification of the different types of rocks encountered, we characterized the type of clast, clast size, sorting (Figure **F19**), roundness (Figure **F20**), nature of matrix (color), and other features, such as coarsening- and fining-upward packages. Clast sizes of the suevites and impact melt rocks are highly variable, ranging from silt to boulder. We measured the long axis length of the largest clast as a representative maximum size of clasts in each section (or each part where clast size significantly changed). In some intervals, clast size shows a more or less bimodal distribution, and in such cases we measured maximum sizes for each mode. We described sorting features following four categories: very well sorted, well sorted, poorly sorted, and very poorly sorted (Figure **F19**). We described grain shape following five categories: angular, subangular, subrounded, rounded, and well rounded (Figure **F20**). We described the overall texture as matrix supported or grain supported (Figure **F21**) and documented the color of the matrix using the Munsell color system.

Thin sections

Thin sections were investigated using both plane- and cross-polarized light. Different components (matrix, clasts, etc.) and rock-forming minerals were identified and listed according to their relative abundances. Most minerals (and phases) are easily identified (i.e., different minerals have different optical properties); however, in a few cases, complementary methods beyond the scope of standard IODP measurements such as micro-Raman spectroscopy or electron microscopy will be necessary to confirm the precise nature of the minerals (and melts and glasses) and their alteration products.

Figure F19. Examples of sorting in suevite in the Upper Peak Ring (Unit 2), Site M0077. A. 40R-2. B. 41R-1. C. 57R-3. D. 65R-1.

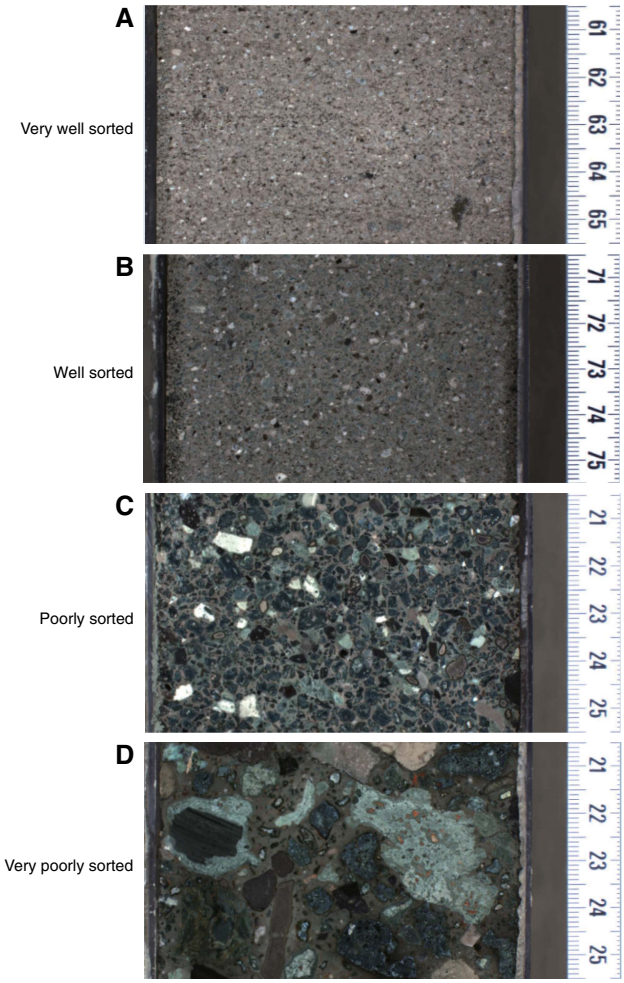

General petrographic characteristics, such as the nature of the matrix (i.e., lithic versus impact melt rock), shape and size of the crystals or clasts, different types of clasts (rock and mineral clasts, glass, and melt rock particles), textural relationship(s), replacements (alteration), and so on, were carefully investigated and reported on specific description sheets. Particular attention was given to shock-induced deformation and transformation types; all types of fractures and features in all possible minerals were described. The prepared thin sections provided an additional means of more accurately identifying the different minerals and fine-grained matrix, which cannot be properly determined macroscopically.

Lower Peak Ring rocks

Rock classification

The classification of the Lower Peak Ring rocks utilized the same provisional IUGS nomenclature scheme (Stöffler and Grieve, 2007) used for the Upper Peak Ring interval. Shocked target rocks were also described based on estimations of standard geological descriptors of composition and texture for magmatic rocks (e.g., QAPF diagram; Streckeisen, 1974). The implementation of the impactite classification scheme and the rock unit names is described in Table **T2**. Note that the correct petrographic terminology for these lithologies requires bulk chemical analysis. The designation of these lithologies will therefore most likely be subject to change. For

Figure F20. Examples of clast shapes in suevite in the Upper Peak Ring (Unit 2), Site M0077. A. 73R-2. B–E. 71R-1.

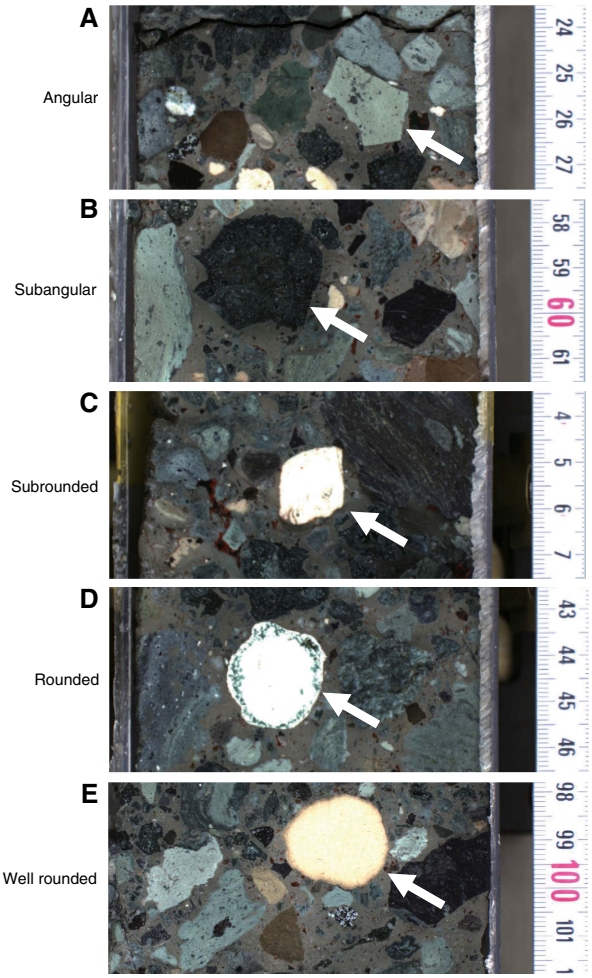

example, preliminary geochemical analyses of samples from dikes described as "diabase/dolerite" plot within the foidite and tephrite-basanite fields of the TAS diagram (Le Maitre et al., 2002).

Petrographic (macroscopic) observations

No specific checklist was followed for petrographic observations, but a certain number of characteristics were typically reported, starting with the rock name; in the case of very fine grained rocks, thin sections were used to resolve features not visible to the naked eye. Rock alteration, typically visible due to a variation of rock color, was described. Whenever possible, alteration minerals were identified. Color, grain size (and/or variations in grain size and clasts), matrix, and minerals (names), or at least their color and their relative abundance (mentioned if one is particularly common), were reported.

Structural observations

Deformation in the Lower Peak Ring interval was assessed on a number of structural characteristics. These included the shape-preferred orientation (SPO) of elongate rock-forming minerals, mostly plagioclase, alkali-feldspar, and quartz, collectively defining the mineral fabric of the rock. Prominent brittle deformation structures were indicated in the ExpeditionDIS in terms of thickness, length, and spacing. Breccia zones, melt rock zones, open fractures, distinct

Figure F21. Grain and matrix-supported suevite in the Upper Peak Ring (Unit 2), Site M0077. A. 82R-1. B. 71R-1.

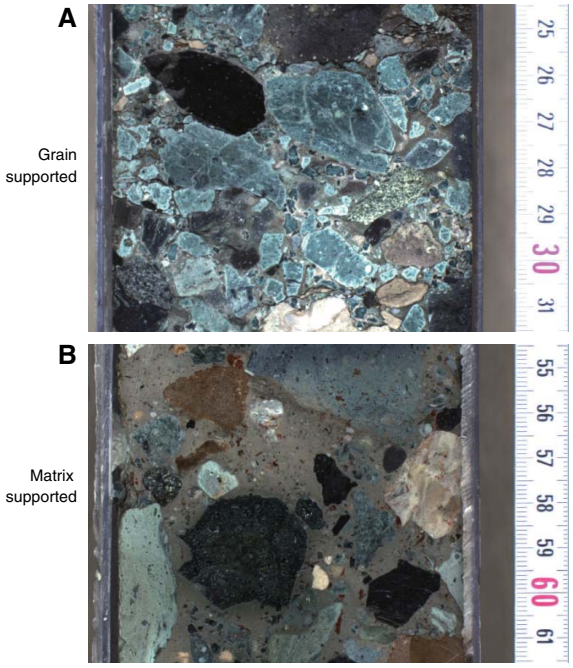

faults, and well-defined zones characterized by enhanced SPO (foliation) were noted (Figure F22). Deformation intensity of each core section was labeled as either undeformed or weakly, moderately, or strongly deformed based on visual appraisal of brittle fault characteristics. Occurrences of shatter cones were specifically noted.

In addition to the visual assessment of brittle deformation, orientation measurements of mesoscopic shear faults displaying slip lineations and slip sense were of particular importance. Orientations of shear faults and lineations in the archive half were measured with a steel protractor. Core sections were carefully removed from the liner to access the shear surfaces. The convention for recording brittle fault data used was as follows:

- Any planar structure (S) was measured as a dip direction and dip with respect to the top direction of the core (Z-axis). Dip measurements were measured as the maximum angle that the plane made with the surface along which the core was halved (XZ plane).
- Any lineation (L) found on a planar structure (S) was measured as a plunge direction and plunge. Plunge directions were measured between the z-axis and the projection of the lineation onto the XZ plane. Plunge values were measured as the angle between lineation and the XZ plane.
- Sense of slip on a fault plane was indicated by either a "+" or "–" symbol, indicating a reverse or a normal fault, respectively. The sense of slip was determined relative to the core's orientation on the visual core description workbench, not to the top of the drill core. An indication of the confidence of the observer in determining the slip sense was made as an integer estimate from 1 to 4, where 1 indicates complete confidence in the assessment and 4 indicates that the observer was unable to determine the sense of shear.

For orientation data, see STRUCTURAL in **Supplementary material**. These data are not corrected regarding their orientation to geographic north. Due to time constraints and the quality of the

Figure F22. Alteration and structural modification, Site M0077. A. White veins cutting across a shear fault in granitoid. B. White vein in felsite with an altered mafic xenolith. C. Vug along vein partially filled with quartz (inset = magnified view). D. Vein of cataclastic material, possibly with melt rock. E. Vein of cataclastic material. F. Fault plane cutting through the sawn surface of a half core. G. Fault surface with striations through a half core. H. Shatter cone in felsite. G and F are perspective photos; scale can be determined from core diameter (86 mm).

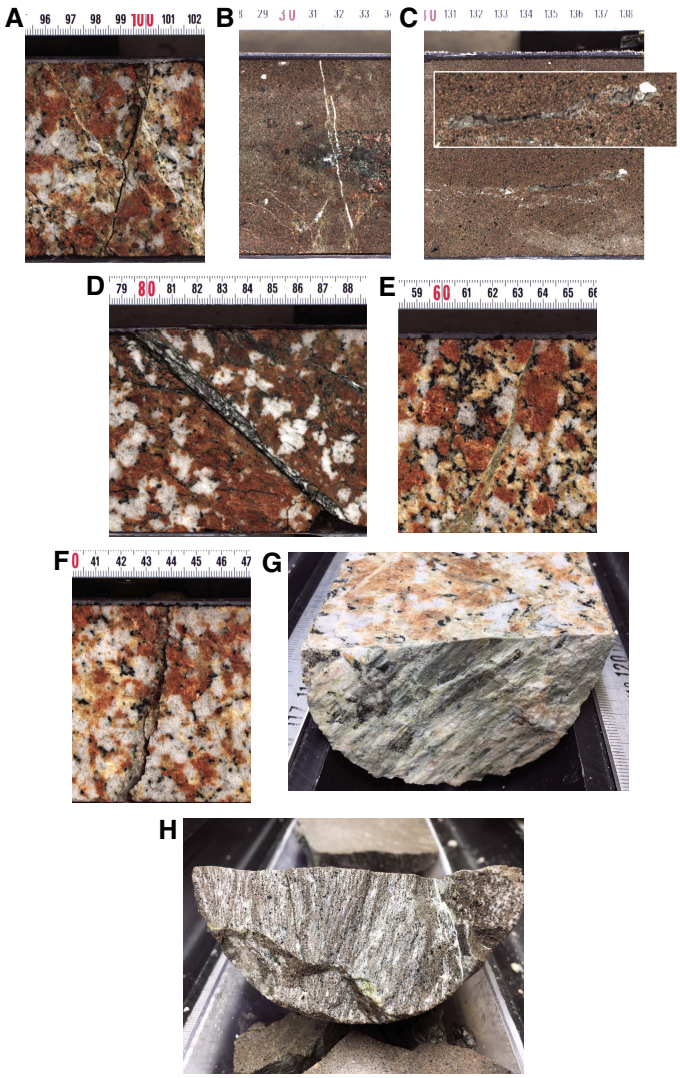

CT images, planes of deformation without lineations were not measured by hand.

Thin sections

Inspection of thin sections in plane- and cross-polarized light was instrumental in capturing petrographic and structural characteristics of the target rocks. Aside from identifying the overall mineralogical composition, including accessory minerals, petrographic characteristics aided in differentiating between feldspar types and their magmatic and postmagmatic signatures (twinning, zoning, and solid-solutions). Moreover, the type of (hydrothermal) alteration and mineralogical transformation of rock-forming minerals (saussuritization and sericitization) was recorded. In terms of deformation, evidence for strain, including impact-induced grain-scale modification and shape change, was examined. Observations were captured in terms of the geometry of grain/grain contacts, subgrain

Figure F23. Shock features in basement rocks (granite Sample 364-M0077A-125R-3, 61–63 cm; cross-polarized light). A. Multiple sets of planar deformation features in quartz. B. Kinked biotite.

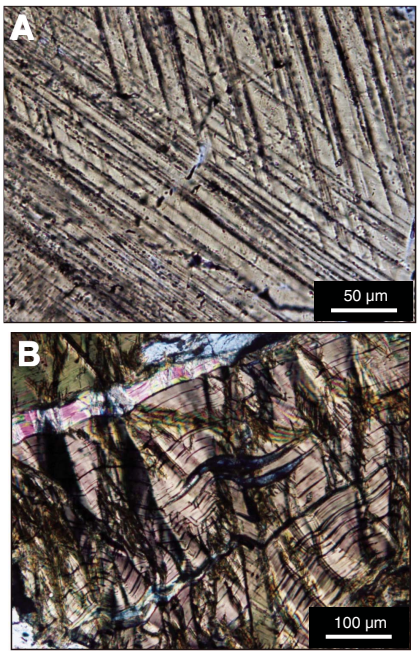

formation, lattice distortion, inter- and intragranular fragmentation, and displacement magnitudes. The characterization of brittle deformation mechanisms on the grain scale was of particular importance. In this regard, the appearance of structural relationships of cataclasite zones, melt zones, and deformation gradients was drafted on the VCDs. Evidence for impact-induced deformation included the recognition of planar fractures, planar deformation features, and feather features in plagioclase, alkali-feldspar, and quartz and kink banding in biotite (Figure **F23**).

Biostratigraphy

Biostratigraphic age assignments are based on the identification of calcareous nannofossil and planktic foraminifer highest occurrence (HO) and lowest occurrence (LO) datums using the standard zonation schemes explained below. Biozone boundaries are cited as the midpoint between the datum sample and the adjacent sample without the datum taxon. The integrated calcareous nannofossil and planktic foraminiferal biozonation used during Expedition 364 is illustrated in Figure **F24** (Gradstein et al., 2012). In addition, relative abundances of species and groups of calcareous nannofossils, planktic and benthic foraminifers, and other sedimentary material (e.g., radiolarians, sponge spicules, echinoid spines, fish debris, etc.) were used as paleoenvironmental indicators.

Initial age determinations were based on 41 samples collected on the ship at 3 m intervals (i.e., from the base of each core) plus an additional sample at the base of Section 37R-1. During the OSP, additional samples were taken from split cores to refine the age model. These were collected from the middle of each core for Cores 1R–37R for a combined offshore-onshore resolution of 1.5 m and at 25 cm intervals in Cores 37R–40R. Additional samples were taken in Sections 37R-1 and 40R-1 across clear changes in lithology and within the black shale in Section 37R-1. Samples were taken every 3 m from the Upper Peak Ring suevite Cores 40R–85R, both from the matrix and from selected limestone clasts, to help characterize the

Figure F24. Combined planktic foraminifer and calcareous nannoplankton biozones and magnetic polarity reversals for the middle Eocene (Ypresian) to basal Paleocene (Danian). *P. eugubina* = *Parvularugoglobigerina eugubina*. Modified from TSCreator 7.0 (**http://www.tscreator.org**).

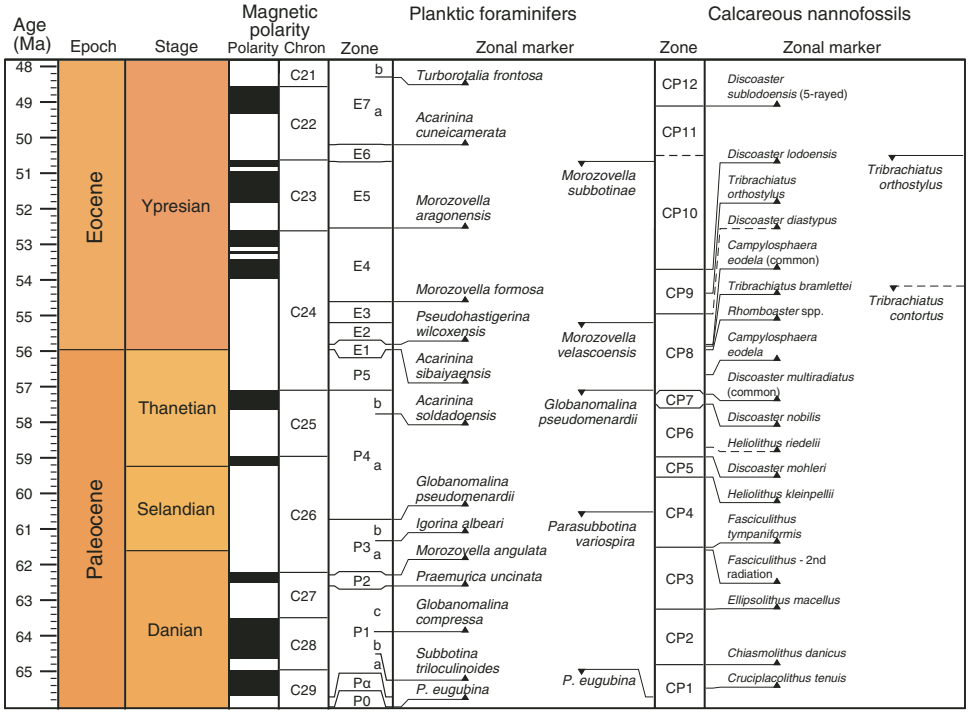

components of this interval. In total, 196 washed samples were analyzed for foraminifer and calcareous nannoplankton biostratigraphy. A total of 17 additional thin sections in indurated intervals were analyzed for planktic foraminifers during the OSP to further refine the age model. It should be noted that due to the importance of obtaining an age model, distribution tables and range charts produced both shipboard and during the OSP are biased toward biostratigraphically significant taxa.

Calcareous nannofossils

Zonal scheme and taxonomy

Calcareous nannofossil age determination is based primarily on the CP zonation scheme of Okada and Bukry (1980) and secondarily to additional biohorizons within each zone (e.g., Agnini et al., 2007). The zonal scheme and additional biohorizons were calibrated with orbital chronology by Westerhold et al. (2008) and Agnini et al. (2007), respectively. Taxonomic concepts are those given in Perch-Nielsen (1985) and Bown et al. (1998).

Methods of study

Because samples are indurated, slides were prepared using a mortar and pestle. A small chip of material was placed in a mortar, covered in water, and tapped lightly with a pestle. The liquid was decanted into a beaker. This process was repeated three times. The liquid was then placed on a coverslip using a pipette, dried on a hot plate, and adhered to a slide with Norland optical adhesive. All slides were examined with an Olympus BX51 light microscope using cross-polarized and plane-transmitted light. Thin section preparation techniques were identical on the ship and at the OSP.

Abundance estimates were performed at 1000×, with lower magnification used to scan for rare biostratigraphic marker taxa. Qualitative assessment of calcareous nannofossil preservation was recorded as follows:

G = good (little or no evidence of dissolution and/or overgrowth, little or no alteration of primary morphological features, and specimens are identifiable to the species level).
M = moderate (minor dissolution or crystal overgrowth observed, some alteration of primary morphological features, but most specimens are identifiable to the species level).
P = poor (strong dissolution or crystal overgrowth, significant alteration of primary morphological features, and many specimens are unidentifiable at the species and/or generic level).

A qualitative assessment of the total abundance of calcareous nannofossils for each sample was estimated as follows:

V = very abundant (50 specimens/field of view [FOV]).
A = abundant (11–49 specimens/FOV).
C = common (1–10 specimens/FOV).
Fr = frequent (1 specimen/1–10 FOVs).
F = few (1 specimen/11–50 FOVs).
R = rare (1 specimen/50 FOVs).
P = present (1 specimen/>50 FOVs).
B = barren (no specimens encountered in 500 FOVs).

The abundance of individual species for each sample was estimated as follows:

V = very abundant (50 specimens/FOV).
A = abundant (11–49 specimens/FOV).
C = common (1–10 specimens/FOV).
Fr = frequent (1 specimen/2–10 FOVs).
F = few (1 specimen/11–50 FOVs).
R = rare (1 specimen/50 FOVs).
P = present (1 specimen/>50 FOVs)

Questionable occurrences are indicated with a question mark.

Planktic and benthic foraminifers

Zonal scheme and taxonomy

Paleogene planktic biozonation follows the P and E zones of Berggren and Pearson (2005) as modified by Wade et al. (2011). Age estimates for planktic foraminiferal datums follow Gradstein et al. (2012). Taxonomic concepts of Paleogene planktic foraminifers follow Olsson et al. (1999) and Pearson et al. (2006), as well as figures on **http://www.mikrotax.org/pforams**. Thin section identifications follow the work of Postuma (1971) and van Konijnenberg et al. (1998). Taxonomic concepts and water depth assignments of Paleogene benthic foraminifers follow Bolli et al. (1994), Alegret and Thomas (2001), and Holbourn et al. (2013). In general, effort was made to identify benthic foraminifers associated with either the shallow (middle neritic; <200 m water depth) Midway-type "fauna" (Berggen and Aubert, 1975) or the deep (bathyal; 500–2000 m water depth) Velasco-type "fauna" (Schnitker, 1979) to give general depth estimates for the Chicxulub post-impact basin throughout the Paleocene and Eocene. Generally, the Midway assemblage includes shallower dwelling benthic foraminifers like *Gavelinella*; *Anomalinoides*; various nodosariids, lenticulinids, and vaginulids; and shelf-dwelling agglutinated benthic foraminifers like textulariids (Berggren and Aubert, 1975). The Velasco assemblage is characterized by generally deeper dwelling benthics like *Nuttalides, Osangularia, Aragonia, Gyroidina, Uvigerina*, and various buliminids, as well as agglutinated benthics like *Tritaxia* and *Gaudryina* (e.g., Berggren and Aubert, 1975; Alegret and Thomas, 2001).

Methods of study

Washed residues

Forty core catcher sediment samples and one additional midcore sample from the Post-Impact Sedimentary Rocks interval were collected and washed on the *L/B Myrtle*. During the OSP, 62 additional post-impact samples were collected from this interval to refine the shipboard age model. Both on the ship and at the OSP, samples were soaked in a 10% solution of hydrogen peroxide for at least 2 h and then washed with tap water over a 63 µm sieve for Eocene samples and over a 45 µm sieve for Paleocene samples. Some indurated limestone samples were broken up into ~1 cm pieces with a mortar and pestle and soaked in an 80% solution of acetic acid for up to 3 h, following the techniques of Lirer (2000) as modified by S. Galeotti (pers. comm., 2012). Acidified samples were then buffered with Calgon and allowed to soak for ~20 min before sieving. Unfortunately, there was no difference in disaggregation between samples soaked in acetic acid and samples soaked in peroxide or sieved immediately after being broken up with a mortar and pestle. Sieved samples were then placed in an oven or in a beaker on a hot plate to dry before examination. To minimize contamination on the ship, sieves were placed in an ultrasonic bath for 15 min between uses and then checked for lingering contaminants. At the OSP, sieves were dipped in methylene blue dye after ultrasonication to flag any contaminants in subsequent samples (dye was not available on the ship). Methylene blue dye was also used during the OSP to help enhance the details of wall structure on poorly preserved foraminifers in some washed residues. All samples were examined with an Olympus SZX7 microscope; on shore, this microscope had a 2× objective lens, allowing more robust identification of small Paleocene foraminifers. The relative abundance of foraminifers and foraminifer-sized sediment particles (including total radiolarians) were estimated from the >63 µm size fraction (>45 µm for lower Paleocene) based on the following criteria:

D = dominant (>30% of sediment particles).
A = abundant (>10%–30% of sediment particles).
F = few (>5%–10% of sediment particles).
R = rare (>1%–5% of sediment particles).
P = present (<1% of sediment particles).
B = barren.

Foraminiferal species abundances are reported as follows:

A = abundant (>50 specimens on the tray).
C = common (20–49 specimens on the tray).
F = few (10–19 specimens on the tray).
R = rare (2–9 specimens on the tray).
P = present (<2 specimens on the tray).
B = barren.

Specimens that were clearly reworked are designated as "RW." Questionable occurrences are indicated with a question mark; specimens which do not fit the sensu stricto definition of a species but clearly have an affinity for that species are indicated as "aff."

Additionally, the preservation status of planktic and benthic foraminifers was estimated as follows:

E = excellent (glassy preservation).
VG = very good (no evidence of overgrowth, dissolution, or abrasion).
G = good (little evidence of overgrowth, dissolution, or abrasion).
M = moderate (calcite overgrowth, dissolution, and/or abrasion are common but minor).
P = poor (substantial overgrowth, dissolution, and/or fragmentation).
VP = very poor (foraminifers are present but cannot be speciated).

Thin sections

In addition to washed residues, 17 thin sections were taken and observed during the OSP. They were taken at ~9 m intervals in the Eocene section (Cores 1R–36R), at ~3 m intervals in the Paleocene section (Cores 37R–40R), and at several points of interesting lithology. Additionally, thin sections in the suevite were examined for any biotic debris. Brief counts of the relative abundance of planktic foraminifers, benthic foraminifers, and radiolarians were conducted based on evaluation of 10 FOVs at 100× magnification on an Olympus SZX16 and Olympus BX41 phase-contrast microscope. From some lithified intervals where thin sections were not available, chips were taken from the cores and polished on glass plates on one or two sides using carborundum powder sizes (grain size = 120, 360, and 600). The chips were submerged in a methylene blue solution to help highlight foraminifers, dried and mounted on a glass slide with silly putty, and covered with a coverslip using UV-hardening Norland optical adhesive.

Paleomagnetism

Shore-based paleomagnetism studies had two goals: (1) produce a polarity magnetostratigraphy for the recovered sedimentary rock succession overlying the Chicxulub impact structure and (2) produce a preliminary characterization of the natural remanent magnetization (NRM) of suevites, impact melt rocks, granitoids, and pre-impact dikes within the peak ring of the crater. These objectives were achieved by conducting measurements of the NRM and limited alternating field (AF) demagnetization of discrete paleo-

magnetism samples collected from the working half of the core at a minimum frequency of one sample per 3 m core spanning the entire length of the Expedition 364 drill core. Regions of special interest (i.e., the expected Paleocene/Eocene Thermal Maximum interval and the post-impact recovery interval) were sampled at a higher rate of one sample every ~25 cm.

Samples

The lithologies of the samples recovered during the expedition (which include hard impact melt rocks, suevites, granitoids, pre-impact dikes, and indurated sedimentary rocks) prevented collection of U-channel or sediment cube paleomagnetic samples. Therefore, sample plugs were obtained by drilling into the cores. Plugs were trimmed into cylindrical samples 12.25 cm^3 in volume (25 mm diameter × 25 mm height). We established a right-hand-rule geographic coordinate system for sample collection in which the $-z$ direction points up the drill core (i.e., toward the surface) and the $+x$ direction points from the interior of the half core toward the split saw–cut face (Figure **F25A**). Due to geometric requirements of the magnetometer sample handler, the discrete sample plugs were oriented in a different system for measurements: the $+x$ direction (in magnetometer coordinates) corresponds to the $-z$ direction in the real core coordinate system described above, the $+z$ direction (in magnetometer coordinates) corresponds to the $-x$ direction in the real core coordinate system, and the $+y$ direction (in magnetometer coordinates) corresponds to the $-y$ direction in the real core coordinate system (Part B). Prior to interpretation, data were rotated from the magnetometer coordinate system into the real core coordinate system.

Instrumentation

Paleomagnetic measurements were conducted using a 2G Enterprises Cryogenic Rock Magnetometer (Model 755 HR, long core version) at Faculty 5 Geosciences, University of Bremen. The magnetometer is equipped with automated AF demagnetization and a sample handler that can hold up to 8 samples at a time. The room containing the magnetometer is not magnetically shielded.

Measurements

Measurement of the NRM and stepwise (5 mT increment) AF demagnetization up to a minimum of 15 mT was performed on all samples. Samples with magnetic moment ≥1 × 10^{-9} Am^2, such as suevites, impact melt rocks, granitoids, and pre-impact dikes were demagnetized up to 20 mT. In contrast, the post-impact sedimentary rocks carried a very weak and/or unstable NRM, and their magnetization intensities were often the same order of magnitude as the magnetometer sample handler (~1 × 10^{-11} Am^2) at AF 20 mT demagnetization. For this reason, the post-impact sedimentary rocks were instead demagnetized up to a maximum of 15 mT. Demagnetization to higher AF levels was reserved for postexpedition research in laboratories equipped with magnetically shielded rooms and potentially lower magnetic moment sample holders that will permit higher sensitivity measurements. To test for the presence of secondary magnetic overprints, AF demagnetization up to 100 mT was performed on two samples of post-impact sedimentary rocks (see **Paleomagnetism** in the Site M0077: Post-Impact Sedimentary Rocks chapter [Gulick et al., 2017b]). Because the NRMs of impact melt rock samples often exceeded the saturation limit of the magnetometer, these samples were measured by changing the measurement range setting from 1× (default) to 1000× and the background level setting from 1 × 10^{-5} (default) to 1 × 10^{-1}.

Figure F25. A. Orientation of the paleomagnetic plug with respect to the Expedition 364 drill core with orthogonal coordinate axes defined. B. Orientation of the paleomagnetic plug on the sample handler of the magnetometer at MARUM relative to the magnetometer internal coordinate system.

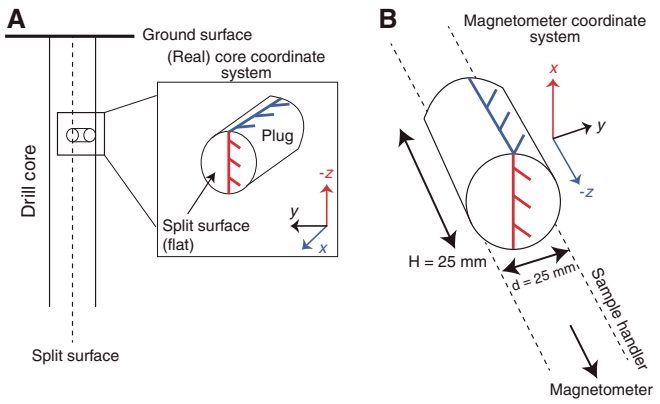

Age model and mass accumulation rates

Age model

The age model for post-impact sedimentary rocks at Site M0077 is based on planktic foraminifer and calcareous nannofossil age determinations. Biostratigraphic datums are placed as midpoints between adjacent samples. Datum placements represent uncertainty in age-depth plots. See **Biostratigraphy** for a detailed discussion of the biostratigraphic datums and identification scheme. Age determinations are based on the geologic timescale by Gradstein et al. (2012) and are illustrated in Figure **F24**.

Uncertainty estimates for the age model were calculated based on the stratigraphic uncertainty of the datum placement. Maximum and minimum sedimentation rates were calculated based on the highest and lowest possible depths for each datum; the average sedimentation rate is calculated from the midpoint between these bounding depths.

Impact-associated sedimentary rocks are assumed to have accumulated at a timescale orders of magnitude faster than background geologic processes and are therefore excluded from both the age model and mass accumulation rate calculations.

Linear sedimentation rate

A linear sedimentation rate (LSR) curve for Site M0077 was constructed from biostratigraphic datums (see Figure **F25** in the Site M0077: Post-Impact Sedimentary Rocks chapter [Gulick et al., 2017b]). Magnetochronology was not incorporated into the age model presented here due to a pervasive magnetic overprint that could not be removed from the post-impact sedimentary rocks during the OSP AF demagnetization experiments (which were limited to applied fields below 15–20 mT) (see **Paleomagnetism**). The LSR curve follows the mbsf scale on the depth axis and is drawn through the most robust planktic foraminifer and nannoplankton zonal boundaries (particularly avoiding those truncated by unconformities), avoiding age inversions and intervals of core overlap.

Some biostratigraphic datums were excluded from the linear sedimentation rate curve (see Figure **F25** in the Site M0077: Post-Impact Sedimentary Rocks chapter [Gulick et al., 2017b]) based on the following criteria:

- Stratigraphic uncertainty due to taxon rarity or intervals of poor preservation, and
- Chronologic uncertainty based on Gradstein et al. (2012).

The slope of the line segment between datum points is the linear sedimentation rate. Hiatuses are identified based on clusters of datums near a certain depth and, where possible, are marked at a specific depth (rather than interpolated between datums) based on sedimentological observations.

Mass accumulation rate

Mass accumulation rates (MARs) for Site M0077 were calculated based on the linear sedimentation rates and dry bulk density (DBD) measurements conducted during the OSP (see **Physical properties**) (see Figure **F26** in the Site M0077: Post-Impact Sedimentary Rocks chapter [Gulick et al., 2017b]). MARs for bulk carbonate ($CaCO_3$) and TOC (see Figures **F27** and **F28** in the Site M0077: Post-Impact Sedimentary Rocks chapter [Gulick et al., 2017b]) are calculated by multiplying the MAR by the weight percent $CaCO_3$ or TOC measured during the OSP.

Calculation of MAR, bulk carbonate accumulation rate (CAR), and organic carbon accumulation rate (OCAR) follows these equations:

$$\text{MAR} = \text{LSR (cm/ky)} \times \text{DBD (g/cm}^3\text{)},$$

$$\text{CAR} = \text{LSR} \times \text{DBD} \times \text{CaCO}_3 \text{ (wt\%)},$$

and

$$\text{OCAR} = \text{LSR} \times \text{DBD} \times \text{TOC (wt\%)}.$$

Time steps for MAR are 500 ky, determined by the sampling density of dry bulk density and geochemical measurements. Dry bulk density, TOC, and $\%CaCO_3$ were resampled at this time step by averaging the values of all samples that fall within each time interval.

Geochemistry

Offshore interstitial water sampling and analysis

The offshore pore water sampling plan was envisioned to include routine sampling at 9 m intervals (5 cm whole-round cores). However, this plan was not possible because core material consisted of very hard rocks: marlstones, limestones, suevites, impact melt rocks, and granitoids. Squeezing tests were performed on two samples to gauge the feasibility of pore water sampling using the conventional squeezing method described below. For this, we squeezed two 5 cm long whole-round core samples in the ESO Teflon-lined titanium squeezer (piston-cylinder design; described in detail at **https://www.marum.de/Acquisition.html#Section3194**). The first whole-round core sample was cut from marlstones at the bottom of Core 364-M0077A-3R (Section 3R-1, 84–87 cm), which were considered unlikely to be undisturbed by drilling. The second sample tested came from the base of Core 40R (Section 40R-3, 28–32 cm). The samples were scraped clean on all surfaces to remove drilling mud and material from the outer surface that may have been smeared down the core liner. The material was then covered in sterilized aluminum foil, crushed in a vise, and further reduced to smaller pieces with a hammer. The samples were introduced into the squeezer using a funnel. Once in the squeezer, material was contained when under pressure (not exceeding 15 tons, applied by a hydraulic press) by a circular titanium screen at the base of the cylinder overlain by a paper filter (Whatman #1, 70 mm ϕ). Any pore water present would have been pushed through an online filter (0.2 µm; 25 mm ϕ; cellulose acetate) and into a 20 mL all-plastic syringe. All parts of the squeezer that touched the sample are polytetrafluoroethylene (PTFE), titanium (Grade 2), or Polyamid plastic (Delrin).

No pore water was obtained from the two test samples due to the degree of lithification. Both samples were photographed, along with the procedure from the squeezing tests. Residues of the two samples were kept as squeeze-cake samples and documented in the ExpeditionDIS.

Onshore chemical analyses

In situ bulk geochemical analysis of whole-rock samples (México)

We measured trace and major elements in 106 samples that were oven-dried at 40°C, using an in situ (handheld) Thermo Scientific Niton XL3t GOLDD XRF analyzer equipped with a 50 kV X-ray tube at the Institute of Geophysics at National University of México. We collected spectral data and performed quantification of the bulk chemical composition of our samples. For calibration we used HISS-1 and MESS-4 certified reference materials for trace metals and other constituents (see **http://www.nrc-cnrc.gc.ca/eng/solutions/advisory/crm/certificates/hiss_1.html** and **http://www.nrc-cnrc.gc.ca/eng/solutions/advisory/crm/certificates/mess_4.html**).

We measured each sample three times at different positions on their surfaces, and the measurements were averaged. Data are reported in weight percent (wt%) and parts per million (ppm) with an error of <5%.

Water samples (Onshore Science Party)

No water samples were analyzed onshore because no pore water was obtained from the two test samples squeezed offshore.

Whole-rock samples (Onshore Science Party)

We analyzed ~300 whole-rock samples with a minimum weight of 12 g. One sample was taken per core (approximately every 300 cm). These samples were taken as a subset of the samples extracted for, and measured by, the physical properties team. Therefore, all samples analyzed for geochemistry were also measured for physical properties. Before processing, all samples were photographed and then dried in an oven at 40°C for a minimum of 10 h.

We crushed, ground, and homogenized each sample to a fine powder (~20 µm) using an agate mortar and a planetary ball mill Fritsch "Pulverisette 7." We split every powder into three subsets for the following analyses: (1) TC/TOC (2 g), (2) X-ray diffraction (2 g), and (3) XRF (4 g).

Total carbon/total organic carbon

We measured TC and TOC using a LECO CS-300 carbon-sulfur analyzer. To measure TC, we weighed a 65 mg aliquot of ground and homogenized sample in a sterile disposable ceramic boat and combusted it at 2200°C in the furnace unit of the carbon-sulfur analyzer in a stream of purified oxygen (carrier gas). The evolved CO_2 and SO_2 were measured with a nondispersive infrared detector to measure the sedimentary TC and total sulfur (TS) content.

To measure TOC, another 65 mg aliquot of the same sample was weighed in a new sterile disposable ceramic boat. The sample was then decalcified using 12.5% HCl by washing the sample twice in

HCl, followed by washing the sample twice with purified (distilled, demineralized, and deionized) laboratory water. The sample was then dried in the ceramic boat at 50°C for 2 h on a hot plate. Once the sample was dry, it was combusted and measured using the procedure described above for TC. Total inorganic carbon (TIC) was then calculated by subtracting the decalcified (TOC) fraction from the TC fraction. All values are reported in dry weight percent.

X-ray diffraction

We analyzed the mineral assemblage of the same homogenized powder, devoid of macrofossils, claystone, or nodules, using a Philips X'Pert Pro multipurpose diffractometer. Samples were prepared using a Philips backloading system to prevent any kind of preferred orientation, using the procedure described by Moore and Reynolds (1997). The diffractometer uses a Cu-tube K_α under 45 kV and 40 mA, a fixed divergence slit of (typically) ¼°, a 16-sample changer, a secondary monochromator, and the X'Celerator detector system. The goniometer scanned from 3° to 85° 2σ for each run, with a calculated step size of 0.016° 2σ. A measuring time of 1 h was used for each sample.

Minerals were identified by the position of their main diffraction peaks on the X-ray diffraction (XRD) run, whereas semiquantitative estimates were produced in relation to their intensity (relative intensity ratio; RIR) using the Philips software X'Pert HighScoreTM. The RIR values were calculated as the ratio of the intensity X-rays diffracted from the most intense reflex of a specific mineral phase to the intensity of the most intense reflex of pure corundum (I/Ic) referring to the "matrix flushing method" after Chung (1974).

X-ray fluorescence

We measured elemental concentrations of the same ~300 discrete samples by energy dispersive X-ray fluorescence (ED-XRF) spectroscopy using a PANalytical Epsilon 3-XL benchtop ED-XRF spectrometer. We assessed the analytical quality of the measurements by repeated analyses of the certified standard reference materials JB-1b (basalt; Terashima et al., 1998) and JG-2 (granite; Imai et al., 1995) and replicate analyses of samples.

Quality assurance and quality control

We took care throughout to avoid contamination of samples. Samples were handled exclusively with nitrile gloves, and analytical grade ethanol, and disposable laboratory tissues were used to clean samples and processing tools.

X-ray fluorescence scanning of half cores

X-ray fluorescence line scan

Section 40R-1 merited additional analytical attention because the K-Pg boundary was suspected to occur in this interval. To characterize the chemical composition of this core, we scanned its split core surface with an AVAATECH XRF Core Scanner II at MARUM—University of Bremen (Germany). The split core surface was covered with 4 µm thick SPEX CertiPrep Ultralene foil to avoid contamination of the XRF measurement unit and desiccation of the core material. We acquired the XRF data with a Canberra X-PIPS silicon drift detector (Model SXD 15C-1150-500) with 1550 eV X-ray resolution, the Canberra digital spectrum analyzer DAS 1000, and an Oxford Instruments 50W XTF5011 X-ray tube with rhodium target material. We processed the raw data by analyzing X-ray spectra using the iterative least squares software WIN AXIL from Canberra Eurisys. To obtain sufficient resolution, we chose a slit size of 12 mm and a step size of 10 mm. We produced three line scans to determine a range of element concentrations across the core section. For the first scan, we used an accelerating voltage of 50 kV and a beam current of 1 mA with a sampling time of 20 s to determine the concentrations of Ba and Sr. For the second scan, we used an accelerating voltage of 30 kV and a beam current of 1 mA with a dwell time of 20 s to determine the concentrations of Sr, Rb, Zr, Zn, Pb, and Ni. For the third scan, we used an accelerating voltage of 10 kV and a beam current of 0.15 mA with a dwell time of 20 s to determine the concentrations of Al, Si, K, Ca, Ti, Fe, Mn, and S. Averaged dead times for the three scans were 5%, 6%, and 11%, respectively.

X-ray fluorescence mapping

We obtained XRF maps on four ~20 cm long quarter-core subsections of Section 40R-1. We used the new generation Bruker M4 Tornado table-top energy-dispersive µXRF scanner (Bruker Nano GmbH, Berlin, Germany) with a rhodium source and two XFlash 430 silicon drift detectors from the University of Bremen. XRF allows characterization of the elemental abundances in a sample from the fluorescence spectrum emitted after the sample is excited by an X-ray source (Norrish and Chappell, 1967). The µXRF technique combines the advantages of an automated microscope-guided high-precision movable stage system with the spectral resolution of a high-energy X-ray source to allow fast, nondestructive, and high-resolution (25 µm) elemental analysis (de Winter and Claeys, 2016). To achieve the small spot size needed for high-resolution measurements, X-rays from a rhodium source are focused using a polycapillary lens. This technique focuses the X-ray beams with minimized energy loss, enabling the instrument to yield well-resolved XRF spectra of small surfaces on the sample. The polycapillary-focusing and XYZ-moving stage of the table-top µXRF device enables the formation of line scans and 2-D maps on the sample surface. The dimensions of the µXRF device's vacuum chamber make it possible to measure sample surfaces of up to 200 mm × 160 mm. No sample coating is necessary, and the method is completely nondestructive. We selected the most appropriate locations for different sampling purposes, based on changes in lithology. For our analyses, we chose an excitation energy of 30 W and an acquisition time of 1 ms/pixel with a spot size of 25 µm under a vacuum of 20 mbar to obtain well-resolved, accurate point-spectra in the lower energy part of the spectrum (<5 keV). After we set up the measurements with maximized source energy settings of 600 µA and 50 kV acceleration voltage, the automated scans took between 2 and 6 h to complete.

Acknowledgments

This research used data acquired at the XRF Core Scanner laboratory at the MARUM—Center for Marine Environmental Sciences, University of Bremen.

Physical properties

Offshore physical measurements

Offshore measurements of physical properties were undertaken to characterize recovered core material and to help inform drilling and sampling decisions. Data were acquired on whole-round cores using a Geotek MSCL provided by the EPC. These data are important for understanding the physical properties of the recovered rocks and linking the geological observations made on the core to the downhole logging data and regional geophysical survey results.

The MSCL is equipped with five sensors that sequentially measure GRA bulk density, *P*-wave velocity, noncontact electrical resistivity, magnetic susceptibility, and NGR. Two additional secondary sensors allow these primary measurements to be corrected for core diameter and temperature. MSCL data were acquired at 2 cm intervals, except for NGR measurements, which were acquired at 10 cm intervals. Core was allowed to equilibrate to ambient temperature for a minimum of 6 h prior to MSCL acquisition. Nominal temperature in the MSCL container was set to 20°C but slightly fluctuated because of difficulties regulating temperature in the hot and humid environment.

A full calibration of the MSCL sensors was conducted at the start of the expedition (Table **T3**). Calibration checks were then performed approximately once every 6 h for the gamma density, *P*-wave velocity, noncontact resistivity, and magnetic susceptibility sensors and once per week for the NGR sensor. The 6 h calibration check involved logging three calibration reference pieces at 6 cm intervals and comparing the results to the values derived during the full calibration (Table **T3**). The weekly NGR calibration check consisted of placing a potassium sulfate calibration standard in the lead cube of the sensor. The potassium sample has an easily identifiable single peak at 1460.75 keV. When this peak deviates by >5% (when measuring total natural gamma rays) from the known energy, the detectors need to be recalibrated. No NGR recalibrations were required offshore during Expedition 364.

Gamma ray attenuation bulk density

The GRA densitometer on the MSCL operates by passing gamma rays from a ^{137}Cs source through a whole-round core and into a sodium iodide (NaI) detector located directly behind the core. The input gamma ray peak has a principal energy of 0.662 MeV and is attenuated as it passes through the core. Attenuation of gamma rays, mainly by Compton scattering, is related to electron density and thereby material bulk density (ρ_b) by the following equation:

$$\rho_b = \rho_e w/2\Sigma N,$$

where

ρ_b = bulk density,
ρ_e = electron density,
w = molecular weight, and
N = atomic number of elements in the material.

For the majority of elements and for rock-forming minerals, $2\Sigma N/w$ is ~1, whereas for hydrogen it is 1.9841. Therefore, for a known sample thickness, the gamma ray count is proportional to density.

The standard sampling interval was set at 2 cm and the count time to 10 s. The resolution with this setup is 0.5 cm. Initial full calibration was performed using a standard core liner containing a stepped aluminum calibration piece centered inside the liner, which was filled with distilled water ("wet calibration"). Gamma counts were taken for 60 s through each of the five aluminum steps of known thicknesses (8, 7, 6, 4, and 3 cm). In addition, the gamma count of the liner filled with only distilled water was recorded. All data were processed using the parameters from these wet calibrations. Calibration checks were made by logging the 0.35 g/L salinity fluid calibration piece at ~6 hour intervals during the core logging process.

Table T3. MSCL sensor specifications. **Download table in CSV format.**

Sensor	Pieces used for full calibration	Pieces used for calibration check	Acceptable departure from full calibration values
Gamma density	Stepped Al/H_2O (8, 7, 6, 4, 3, and 0 cm Al)	0.35 g/L saline fluid	±100 cps
P-wave velocity	Distilled water	0.35 g/L saline fluid	±1 µs
Resistivity	Saline fluids (35, 17.5, 8.75, 3.5, 1.75, and 0.35 g/L)	0.35 and 8.75 g/L saline fluid	±10 mV
Magnetic susceptibility	Impregnated resin	Impregnated resin	±5 SI
NGR	Potassium sulfate	Potassium sulfate	<5% keV

P-wave velocity

P-wave velocity is the rate at which a (compressional) *P*-wave travels through a medium per unit time, expressed in meters per second. *P*-wave velocity is dependent on the composition, porosity, bulk density, fabric, and temperature of the material, some of which are functions of consolidation and lithification, state of stress, and degree of fracturing. *P*-wave velocity was measured using two *P*-wave transducers aligned perpendicular to the core axis with *P*-waves passing through the core horizontally. A compressional wave pulse centered on a frequency of 250 kHz was transmitted through the core. Signal processing software picks the first arrival of the wave at the receiver, and the processing routine also corrects for the thickness of the liner. The *P*-wave transducers also function as displacement transducers, monitoring the small variations of the outside diameter of the liner over which the traveltime was measured. These variations are ultimately used in processing the gamma density, *P*-wave velocity, and magnetic susceptibility data sets. Standard measurement spacing was set at 2 cm. Initial calibration was performed using a core liner filled with distilled water, measured at a known temperature. Calibration checks were made by logging the 0.35 g/L salinity fluid calibration piece at ~6 hour intervals during the core logging process.

Poor *P*-wave velocity data results occur where undersized core causes separation between the core material and core liner. This appeared to be the case for all Expedition 364 core; hence, all MSCL *P*-wave velocity values are considered unreliable.

Noncontact electrical resistivity

The noncontact electrical resistivity measurement is based on comparison of readings from the core (using one set of coils) with readings taken in air (using a second set of coils). The transmitter coil induces a high-frequency alternating magnetic field in the core, which induces electrical currents that are proportional to the core's conductivity (inversely proportional to resistivity). The very small magnetic fields regenerated by these electrical currents are measured by a receiver coil and normalized with the separate set of identical coils operating in air. The spatial resolution of this measurement is ~2 cm, which was set as the measurement interval. Resistivity (Ωm) is a good indicator of lithology, porosity, and fluid content.

Initial calibration was performed using six standard core liner sections containing water of known but varying salinity. Six standards were made up to NaCl concentrations of 35, 17.5, 8.75, 3.5, 1.75, and 0.35 g/L. Calibration checks were undertaken every ~6 h and consisted of logging the 8.75 g/L saline and 0.35 g/L saline standards.

Magnetic susceptibility

Magnetic susceptibility, κ, is a dimensionless measure of the degree to which a material can be magnetized by an external magnetic field:

$$\kappa = M/\mathrm{H}\ (\mathrm{SI}),$$

where M is the magnetization induced in the material and H is strength of an external field. Magnetic susceptibility varies in response to the type and concentration of magnetic grains, making it useful for identifying compositional variations. Whole-core magnetic susceptibility was measured on the MSCL using a Bartington MS2 meter coupled to a MS2C sensor coil. The loop used for Expedition 364 had an internal diameter of 120 mm and was operating at a frequency of 565 Hz, which means no correction factor needed to be applied to the data. The MS2 system operates on two fixed sensitivity levels, ×0.1 and ×1, corresponding to 10 s and 1 s sampling integration periods, respectively. For Expedition 364, all cores were measured using the 10 s (×0.1) setting. Magnetic susceptibility measurements were made at a sampling interval of 2 cm. The sensor automatically zeros and takes a free-air reading at the start and end of each run to account for instrument drift by subtraction of a linear interpolation between readings. Magnetic susceptibility data were recorded as corrected volume-specific units ($\times 10^{-5}$ SI). The accuracy of the magnetic susceptibility sensor was checked using a calibration standard made of impregnated resin, and calibration checks were carried out every ~6 h to check the reliability of the sensor.

Natural gamma radiation measurements

Gamma radiation is emitted from rock primarily as a result of the radioactive decay of ^{40}K and the decay of isotopes in the ^{238}U and ^{232}Th series. Measurement of natural gamma rays (in counts per second) from the recovered core provides an indication of the concentration of these isotopes. The sensor comprises NaI(Tl) detectors housed in 6 inch diameter lead shields. Emitted gamma rays hit the NaI(Tl) crystals, which produces a pulse of light that then strikes the photomultiplier tube, producing a small electrical current to give a voltage pulse, which is related to the energy of the gamma emission. Multiple detectors are used to ensure the measured signal is reliable because some natural rocks have very low natural radioactivity, and combining data collected with multiple detectors improves the data quality. Natural gamma total counts refer to the integration of all emission counts over the gamma ray energy range between 0 and 3 MeV; total counts were measured for 1 min every 10 cm of core.

Quality assurance

Quality assurance (QA) checks were carried out regularly during the offshore phase of the expedition. QA involved core quality description, use of hard copy and electronic MSCL log sheets and calibration sheets, repeat MSCL logging of calibration standards (calibration checks) every 6 h, and repeat logging of selected cores, as described below. Systematic cross-checks of electronic calibration, data files, and processed data were made after the offshore phase. The final data set was made available during the onshore phase of the expedition.

As part of the QA measurement plan during the offshore phase of the expedition, the reproducibility of the MSCL data was assessed by repeat logging of selected core sections, and cores were chosen at roughly every 30 m in depth to avoid any bias. Typically, sections were selected where there was close to 100% core recovery to ensure that accurate and representative measurements could be obtained from all sensors.

MSCL log sheets

Throughout the expedition, information was recorded on both hard copy and electronic MSCL log sheets in an attempt to ensure all information that affects the quality of the data was retained. This included

- Observations of core liner fill, fluid content, and cracks in the core;
- Top depths cross-checked with final DIS depths;
- Sections where there were possible sensor issues; and
- The presence of any metal in a section, cross-checked with the ExpeditionDIS.

Deletion of values around core end caps

MSCL operators deleted all data around the end caps that were clearly affected by these caps. As the amount of data affected varies for each sensor and the effect is gradational away from the end of the core, the MSCL operator was responsible for choosing how much data to delete. Before the OSP, the raw data (with no deleted values) was compared with the processed data to check for errors and consistency. In the final processed data, any bad data points that were considered to be caused by the end caps, metal in the liner, or open cracks in the core were removed.

Onshore physical measurements

Onshore petrophysical methods are described in the order in which they were performed through the core flow. Line-scanning and color reflectance measurements were conducted on split-core sections, immediately after splitting, to record accurate colors prior to core desiccation and oxidation. Digital images (line scans) of archive halves were made with a digital imaging system. Discrete color reflectance measurements of working halves were made with an MSCL system at a measurement interval ranging from 1 to 4 cm. *P*-wave and moisture and density (MAD) measurements were subsequently conducted on discrete samples (average volume of ~6 cm^3) taken from the working halves. A helium gas pycnometer was used to measure the matrix volume of discrete samples, with approximately one sample per core section. Discrete *P*-wave velocity measurements were performed with a Geotek DPW sensor at a regular interval of about one sample per core section. Core sections shorter than 50 cm were not sampled for either MAD or *P*-wave measurements. Thermal conductivity measurements were performed on archive halves approximately once every core in the Post-Impact Sedimentary Rocks and Upper Peak Ring intervals and one every three cores in the Lower Peak Ring interval. Thermal conductivity QA measurements were performed on working-half samples every 20 to 24 m (Cores 7R–62R).

Line scanning

Digital line-scan images of the split cores were obtained during the OSP using the Avaatech Superslit X-ray fluorescence (XRF) core scanner, provided by MARUM (Center for Marine Environmental Sciences). The XRF scanner has an option for line-scan camera and linear light source. The line scanner produces high-resolution color images and outputs accurate color data in red-green-blue (RGB) and Commission Internationale d'Eclairage (CIE) "L" (lightness; a total reflectance index ranging from 0% to 100%), "a" (green to red chromacity), and "b" (blue to yellow chromacity) units (L*a*b*) because of individual charge-coupled device pixel calibration. The

line-scan program uses the Stemmer Common Vision Blox (CVB) platform to acquire and process color images.

The camera system contains a 3 charge-coupled device camera using 3 × 2048 pixels with beam splitter and a manually controlled Pentax 50 mm lens. The image resolution is ~150 pixel/cm (70 μm/cm) in cross-core and downcore directions. An exposure time of 5 ms was used, which allowed a scan speed of 125 mm/s. Added to this is the time taken to initialize the scanner and reposition the camera after each scan. The image coverage is ~13.5 cm cross-core and a maximum of 153 cm in the downcore direction.

Every split core was imaged with a color/gray chart beside it, and the scans are available as original files. Three output files were generated for each core section: a high-resolution bitmap file (.BMP), a compressed image file (.JPEG), and a text file (.TXT) with numerical data in RGB and L*a*b* units. The line-scan system was calibrated every 24 h with black and white standards. All split cores were measured using aperture settings of *f*/6.7 and *f*/11. Additional apertures were used when necessary, but these were always run in addition to the scan with a standard aperture. Custom settings were not used, as this would have led to changes in settings between cores. Instead, equipment settings were consistent for the entire data set. In the setup used, the length of line-scan images was slightly longer than the curated core length, and the bitmap images were subsequently modified so that they matched the length of the cores. In cores from which a whole-round sample (e.g., for microbiology or geochemistry) had been removed offshore from the bottom of the core, a gray foam spacer was inserted in its place. The operator verified that the full core section had been imaged during the scan before the data were accepted.

Color reflectance spectrophotometry

During the OSP, working halves were measured for color reflectance in intervals: 2 cm (Sections 364-M0077A-1R-1 through 61R-3), 4 cm (Sections 62R-1 through 303R-3), and 1 cm (Sections 36R-1, 37R-1, and 40R-1). Badly disturbed core sections were not measured (Section 161R-CC). Measurements were performed using a Minolta spectrophotometer (Model CM-2600d) from MARUM mounted on a split-core MSCL system. On this integrated MSCL system, the spectrophotometer moves vertically, interlocked with the *P*-wave equipment. Color reflectance measurements were carried out with all other MSCL sensors switched off.

Prior to measurement, each core surface was covered with a clear plastic wrap (Hostaphan RN15, 120 mm width) in order to protect the spectrophotometer sensor from direct contact with the rock. Standard calibrations were performed daily after starting up the machine, and color calibration was checked twice a day. Adjustments of the spectrophotometer and the pusher were done before each run, and each core was measured as a separate run.

The spectrophotometer produces three different sets of data:

1. L*, a*, and b* values,
2. Munsell color values, and
3. Intensity values for 39 contiguous 10 nm wide bands across the 360–740 nm interval of the visible light spectrum.

The quality of color reflectance measurements is highly dependent on the integrity of the surface of the core. Degree and uniformity of rock fill, cracks, or other disturbances in the core and the smoothness of the plastic wrap (e.g., presence of air bubbles) directly affect the measurement. Comments on the quality of the core surface were appended to the spectrophotometer data to allow for better retrospective evaluation of data quality. It is recommended that these comments, along with line-scan data and core images, be used to filter out outliers and spurious data when examining color reflectance measurements in detail.

P-wave velocity from discrete samples

P-wave velocity was measured with the EPC's Geotek *P*-wave logger for discrete samples (DPW), using a source frequency of 250 kHz. The equipment consists of a mechanical section containing two transducers and receivers (between which the sample is placed), an associated electronics box, and a PC. Solid neoprene surfaces (pads on the transducers) are used to couple the acoustic sources to the sample. Acoustic coupling is improved by applying downward pressure on the sample between transducers and by wetting the neoprene with distilled water. A laser distance transducer measures the thickness of the sample. The DPW system can measure velocities on cubic or cylindrical, consolidated or lithified core specimens. The system allows measurement on core samples with flat surfaces.

The basic velocity equation is

$$v = d/t,$$

where

v = velocity through sample (m/s),
d = distance traveled through the material (m), and
t = traveltime (s).

A calibration check was performed twice a day. Calibration involved measurement of a standard sample of known length and *P*-wave velocity, and a measurement was also taken with the transducers touching (zero distance).

Traveltimes are corrected for time delays due to (1) the transducers and electronics (t_{delay}) and (2) the peak detection procedure (t_{pulse}). These delays were determined from the result of the zero-distance calibration. For routine measurements on discrete samples with the DPW system, the equation for the velocity is

$$v_{sample} = (1000 \times d_{sample})/(TOT - PTO),$$

where

v_{sample} = velocity through sample (m/s),
d_{sample} = measured thickness of the sample (mm),
TOT = measured total travel time (μs), and
PTO = delay correction (μs).

A pulse is sent to the transmitter sensor, which generates an ultrasonic compressional pulse at ~250 kHz that propagates through the sample and is received by the receiver sensor. The received signal is processed through an analog to digital converter before appearing in the software display. The signal is digitized using a sampling frequency of 12.5 MHz.

Before a transit time can be computed, the intercept of the first arrival must be picked. The acoustic signal is displayed in the software window, allowing the operator to check the waveform quality. Delay time (blanking window, i.e., time period in microseconds for which the first arrival detection will be skipped) and threshold voltage (noise level) are displayed on a virtual oscilloscope and can be adjusted by the operator. The software then picks the first amplitude value found after the blanking window that is greater than the threshold voltage defined by the operator. Calculated *P*-wave veloc-

ity is displayed in real time, taking into account the sample thickness.

During Expedition 364, *P*-wave measurements were made in the direction perpendicular to the split core surface. In most cases, the sample was taken near the MAD sample. Sample size was ~6 cm^3 with 2 cm diameter plugs except for samples from Cores 37R–39R (1 cm diameter) and 230R–247R (3 cm diameter). Preparation involved cutting the sample to ensure two flat, parallel surfaces to provide good acoustic coupling with the transducers. Three *P*-wave measurements were taken and averaged for each sample to produce a final *P*-wave velocity. The data files are in comma-separated value (CSV) format, containing a header with the core and sample ID followed by measured data (e.g., temperature and sample depth) and calculated velocity. The waveform is recorded as a change in voltage against time.

Because sample quality strongly affects the ability to acquire reliable *P*-wave velocity data, it was important to prepare the sample correctly to get good contact between the transducers. *P*-wave velocity is also sensitive to temperature (Leroy, 1969) and decreases with increasing temperature. Temperature was recorded at the time of each measurement and was so uniform during the OSP that no temperature corrections were considered to be required.

A batch of samples (one every 10 cores) was remeasured for QA at the end of the OSP in order to check the repeatability of the data and to verify the validity of the calibration. Discrete *P*-wave velocities for the remeasured samples were found to be consistent with the original measured velocities.

Moisture and density

MAD measurements (bulk density, dry density, grain density, water content, porosity, and void ratio) were calculated from measurements of the wet and dry masses of core plugs and dry volumes. Discrete samples were taken from the working halves, approximately once per section. Sample size was ~6 cm^3 with 2 cm diameter plugs except for samples from Cores 37R–39R (1 cm diameter). Samples were cut to reduce their height before being transferred into previously weighed 10 mL glass beakers. The top of each beaker was sealed with parafilm to prevent moisture loss, and beakers were always handled with gloves to avoid contamination. Adjacent samples of similar size were taken for the discrete *P*-wave velocity measurements.

Wet samples were weighed to a precision of 0.001 g using an electronic balance to determine the wet mass (M_{wet}). Samples were then dried in a convection oven at ~105°C for a period of at least 24 h followed by cooling to room temperature in a desiccator for at least 1 h. Dry sediments were weighed to determine dry mass (M_{dry}).

The volumes of the dried samples were analyzed using a Quantachrome pentapycnometer (helium-displacement pycnometer), provided by MARUM, with a nominal precision of 0.02 cm^3. This equipment allows the simultaneous analysis of four samples and one standard (calibration spheres). Volume measurements were repeated at least three times until the last three measurements exhibited <0.01% standard deviation, with a purge time of 1 min. Volume measurements were averaged per sample (V_{dry}). Calibration spheres were successively cycled between different pycnometer cells for each run to check for accuracy, instrument drift, and systematic error.

During the first few days of pycnometer measurements, several problems were identified. First, one of the cells stopped retaining pressure while measuring samples from Cores 16R and 17R, after which only four cells could be used, allowing the simultaneous analysis of only three samples instead of four and one standard. Second, the volumes for the cells with calibration spheres often showed a volume that differed by more than 0.02 cm^3 than expected. These cells were recalibrated, but the difference persisted. An investigation of the pycnometer revealed that the battery on the motherboard needed to be replaced. Starting on samples from Core 24R, all pycnometer cells were recalibrated twice a day, and additional recalibrations were performed if the volume differed by more than 0.02 cm^3 than expected. After the battery on the motherboard was replaced, starting on samples from Core 41R, the recalibrations were only performed if the volume differed by more than 0.04 cm^3. An error of 0.02 cm^3 resulted in bulk density differences of ~0.003 g/cm^3 and porosity differences <0.1%, and an error of 0.04 cm^3 led to bulk density differences of ~0.006 g/cm^3 and porosity differences <0.1%. Hence, volume differences of up to 0.04 cm^3 were considered to be acceptable.

The mass of the evaporated water (M_{water}) is given by

$$M_{water} = M_{wet} - M_{dry}.$$

The volume of pore water (V_{pw}) is given by

$$V_{pw} = M_{pw}/\rho_w,$$

where M_{pw} is the mass of the pore water and ρ_w is the pore water density, which is set at 1.024 g/cm^3.

Salt precipitated in sample pores during the drying process is included in M_{dry} and V_{dry} values, resulting in the following approximations:

- The mass of pore water (M_{pw}) is given by the mass of the evaporated water ($M_{water} = M_{pw}$).
- The mass of solids, including salt (M_{solid}), is given by the dried mass of the sample ($M_{dry} = M_{solid}$).
- The volume of solids, including salt (V_{solid}), is given by the measured dry volume from the pycnometer ($V_{dry} = V_{solid}$).

The mass of the evaporated water (V_{wet}) is given by

$$V_{wet} = V_{solid} + V_{pw}.$$

For all samples, water content (w) is expressed as the ratio of the mass of pore water to the wet sample (total) mass:

$$w = M_{pw}/M_{wet}.$$

Wet bulk density (ρ_{wet}), dry bulk density (ρ_{dry}), rock grain density (ρ_{grain}), and porosity (ϕ) are calculated from the previous equations (density is given in g/cm^3):

$$\rho_{wet} = M_{wet}/V_{wet},$$

$$\rho_{dry} = M_{solid}/V_{wet},$$

$$\rho_{grain} = M_{solid}/V_{solid},$$

and

$$\phi = V_{pw}/V_{wet}.$$

Thermal conductivity

Thermal conductivity is an intrinsic material property that depends on the chemical composition, density, porosity, structure, and fabric of the material. Thermal conductivity was measured with the TK04 system (TeKa, Berlin), provided by the EPC, using the line source method. Cores were measured at 4°–6°C in the refrigerated core repository in MARUM.

The line source method relies on measuring thermal conductivity with a cylindrical line source in an infinite medium (Carslaw and Jaeger, 1959; Von Herzen and Maxwell, 1959; Vacquier, 1985). The measuring principle is based on transient heating of a homogeneous and isotropic material with a known and constant heating power generated from a source with infinite length, finite radius, and infinite thermal conductivity for a finite measuring time. Thermal conductivity can then be determined from the temperature rise in the source. With the described geometry, temperature depends on the radial distance from the source only, and the problem can be reduced to two dimensions. After heating has started, the temperature (T) is related to thermal conductivity (λ) by

$$T = [q/(4 \times \pi \times \lambda)] \times (\ln(t) + C),$$

where q is the heat input per unit length, and both t (measurement time) and C are constants.

Generally, a first-order approximation made by picking T at times t_1 and t_2, from the temperature versus time measurement curve is used to calculate the apparent thermal conductivity $\lambda_a(t)$:

$$\lambda_a(t) = [q/(4 \times \pi)] \times \{[\ln(t_2) - \ln(t_1)]/[T(t_2) - T(t_1)]\}.$$

$\lambda_a(t)$ is called apparent because the above approximation is only valid for sufficiently large measurement times. This means that $\lambda_a(t)$ is not constant but dependent on the chosen time interval. The real thermal conductivity value (λ) of the material is approached only for sufficiently large heating durations.

In practice, the correct choice of the time interval (t_1 and t_2) is difficult to determine (TeKa, 2010). In the early stage of heating, the source temperature is affected by the contact resistance between the source and the surrounding material. In the later stage of heating, boundary effects caused by the finite length of the line source, assumed infinite in theory, affect the measurement. In between these extremes, there is a time interval in which the source temperature is dominated by the thermal conductivity of the material. This interval should be used for the calculation of $\lambda_a(t)$ in the equation above, and its position changes from measurement to measurement. A main advantage of the TeKa software is the SAM algorithm that automatically selects the optimal time interval to solve the equation, which ensures that only results of physical significance are considered.

Thermal conductivity was measured on split cores from Expedition 364 by placing a half-space probe on the plane surface of the archive half. Good contact was ensured by using silicone paste, and a layer of film was placed between the paste and core to protect the archive half from direct contact with the silicone. Thermal conductivity measurements were taken at one location on the core surface in the z-direction, and core sections were sampled at a frequency of one per core within Section 1 of Cores 1R–102R, where available, and one every three cores within Section 1 in Cores 105R–303R, where available. If core quality was poor, the nearest appropriate core section was selected for measurement. In addition, some measurements were performed in the y-direction (Cores 3R–60R). Measurements were performed for QA at a frequency of about 1 every 20–24 m (Cores 7R–62R) on 10 cm long rock samples from the working halves. Prior to measurement, the working samples were oven dried at a temperature of ~105°C for 24 h and subsequently cooled to 4°–6°C. This procedure was adopted to provide a measure of the importance of water content on the thermal conductivity measurement performed on the archive half.

For QA purposes, multiple measurements (up to five per thermal conductivity run) were taken at the selected depth within each core. Data quality was evaluated by the operator, and any spurious or poor data, potentially caused by poor contact between the core and the probe, were removed prior to the calculation of a mean thermal conductivity and standard deviation. Where possible, a minimum of three good quality measurements were chosen when calculating the mean thermal conductivity, and a variance of less than ±5% was sought.

Downhole logging

For all MSP expeditions, the downhole logging program, coordinated by the EPC, part of the European Consortium for Ocean Drilling (ECORD) Science Operator (ESO), is an integral part of offshore operations and is designed to help meet the expedition-specific scientific objectives and maximize scientific output in general.

MSPs employ various coring technologies and pipe sizes and drill in a variety of water depths, each of which provides constraints on the anatomy of logging operations.

For Expedition 364, downhole logging operations at Site M0077 were funded by the ICDP. Slimline downhole logging services managed by the EPC were contracted from the University of Montpellier (France) for wireline logging and from the University of Alberta (Canada) and the University of Texas at Austin (USA) for the vertical seismic profiles (VSPs). The logging equipment and staffing were selected to allow for seamless operations on the platform. The set of downhole geophysical tools used during Expedition 364 was determined in accordance with scientific objectives, drilling/coring technique (see **Operations**), hole conditions, and temperature at the drill site during operations.

Downhole logs are used to determine physical, chemical, and structural properties of the formations penetrated by the borehole. The data are rapidly collected, and measurements are taken at closely spaced depth intervals and measured in situ; these data can be interpreted in terms of stratigraphy, lithology, porosity, fluid content, geochemical composition, and structure of the formation. Where core recovery is incomplete or disturbed, log data may provide the only way to characterize the geological formation. Where core recovery is good, log and core data are complementary and may be interpreted jointly.

Downhole logs measure formation properties on a scale that is intermediate between those obtained from laboratory measurements on core samples and those from surface geophysical surveys. They are useful in calibrating the interpretation of geophysical survey data (e.g., through the use of synthetic seismograms) and provide a necessary link for the integrated understanding of physical properties on all scales.

During downhole logging operations, the following measurements were acquired in three sessions from slimline tools (Figure **F26**): spectral and total gamma radiation, sonic velocity, acoustic and optical borehole images, electrical resistivity, induction conductivity, magnetic susceptibility, caliper, borehole fluid parameters, and seismic traveltime versus depth from the VSPs (Tables **T4**,

Figure F26. Logging summary, Hole M0077A.

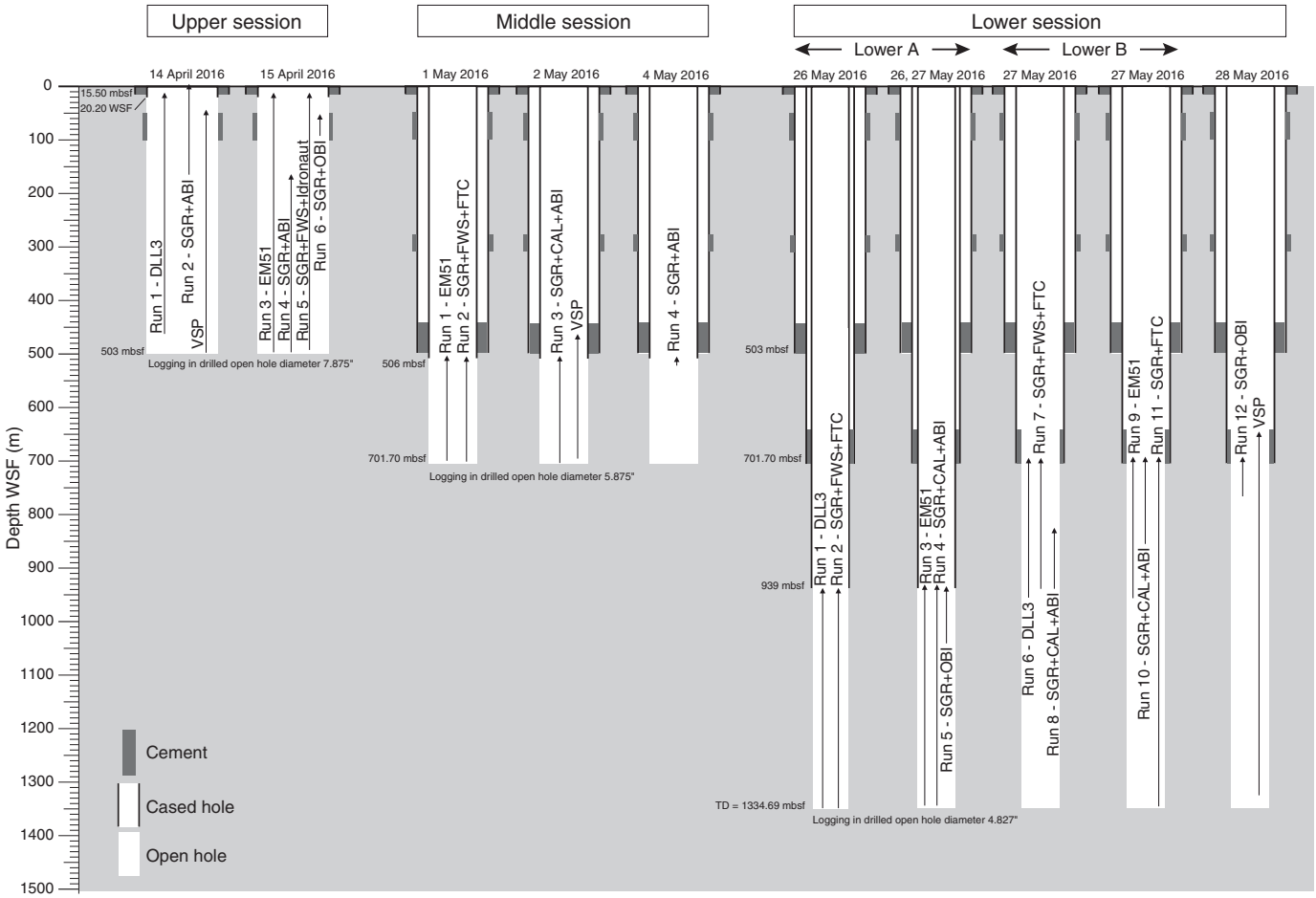

Table T4. Intervals and tools logged, Expedition 364. **Download table in CSV format.**

Table T5. Wireline slimline probes, Expedition 364. ALT = Advanced Logic Technology, QL = quick link. NA = not applicable. **Download table in CSV format.**

Tool acronym	Tool full name	Manufacturer	Position in tool string	Focus	Uplog measurement spacing interval (cm)
Stackable					
QL40-SGR	Spectral Gamma Ray Probe	ALT/Mount Sopris Instruments	In-line sub	Formation	5
QL40-FWS	Full Waveform Sonic	ALT/Mount Sopris Instruments	In-line sub	Formation	5–10
QL40-Ocean	Idronaut Ocean Seven	ALT/Mount Sopris Instruments	Bottom sub	Borehole fluids	5
QL40-CAL	3-arm Caliper	ALT/Mount Sopris Instruments	In-line sub	Borehole wall	5
QL40-FTC	Fluid Temperature and Conductivity	ALT/Mount Sopris Instruments	Bottom sub	Borehole fluids	5
QL40-OBI	Optical Borehole Imager	ALT/Mount Sopris Instruments	Bottom sub	Borehole wall, inclinometry	0.2–0.4
QL40-ABI	Acoustic Borehole Imager	ALT/Mount Sopris Instruments	Bottom sub	Borehole wall, inclinometry	0.2–0.4
Standalone					
DLL3	Dual Focused Resistivity	Geovista	NA	Formation	5–10
EM51	Magnetic Susceptibility and Induction	Geovista	NA	Formation	5–10

T5). Logs were recorded either with stand-alone logging tools (Figure F27) or with stackable tools (Figure F28) combined into tool strings (Figure F29), which were lowered into the hole after completion of coring operations over a given interval.

For the first time in IODP, Expedition 364 included the deployment of stackable slimline probes.

Wireline logging

The majority of measurements were performed in open borehole conditions (no casing), with the exception of some spectral gamma ray and acoustic borehole images that were acquired through the casing over short intervals (Table T4). The recovery

Figure F27. Stand-alone slimline logging tools used during Expedition 364.

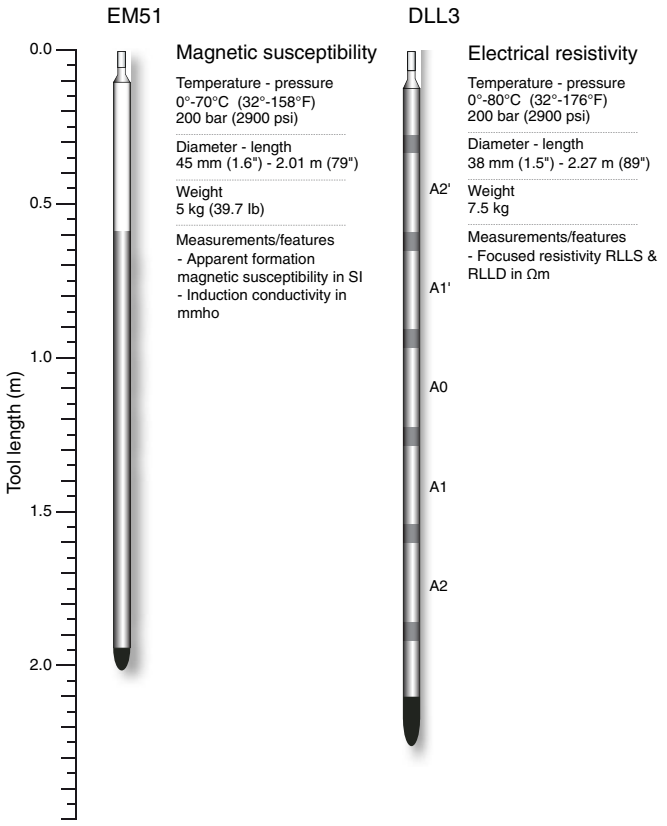

and overall quality of the downhole logging data are good in the upper part of the hole (~0–400 m WSF), improve with depth, and are excellent from ~400 m WSF to the total depth of the hole due to favorable borehole conditions.

The following nomenclature is used to refer to the logging acquisition stages and phases (Table **T4**):

- Logging session: a continuous period of time during which logging operations were uninterrupted or almost uninterrupted over a given interval. These intervals were labeled upper, middle, and lower sessions. In the lower session, wireline logs were acquired in two steps to avoid a zone of potential hole instability (where significant drilling fluid circulation loss was noted) and identified as Lower A (1334–938 m WSF) and Lower B (935–698 m WSF) sessions. Due to the robustness of the tool used, electrical logs were always acquired first through the open holes to ensure that the hole was in good condition before running more fragile tools.
- Run: what happens between the moment a tool or tool string enters the borehole and the moment it exits the borehole.
- Pass (either downhole or uphole): what happens between the beginning and the end of recording a data stream. It corresponds to a single data file. For each pass, data files were labeled "down" when data were acquired as the tools are lowered in the hole, and "up" when data are acquired as the tools move upward. In each run, if some tools were logged in several passes, passes are numbered sequentially.

Due to time constraints, it was not possible to log with all tools in every borehole section.

Logging procedure, acquisition chain, and data recording

During each logging session, slimline tools were logged either on an individual string or combined into a tool string (Figures **F27**, **F28**, **F29**; Table **T4**). A logging run commenced with zeroing the tool to a reference point (loggers zero) that corresponded either to the top of the drill pipe, located 0.86 m above the rig table (upper session), or the rig table (middle and lower sessions) (Figure **F30**, Part A).

After logging was completed, the data were processed and the depth scale shifted to wireline depth below seafloor (WSF) (Figure **F30**), which was determined using the step in NGR at the water/sediment interface.

Each logging pass was recorded and stored digitally. During acquisition, data flow was monitored in real time for both quality control and security using Advanced Logging Technology (ALT) acquisition boxes and ALT Logger software. Table **T4** summarizes the operations and acquisition parameters for each tool or tool string. Tools were raised at speeds that ranged from a minimum of 0.5 m/min for optical and acoustic borehole image logs to a maximum of 30 m/min for induction conductivity and resistivity logs. When time allowed, both up- and downlogs were recorded. Uphole acquisition was stopped once the casing/drill pipe was entered, with the exception of some gamma ray (GR) logs, which were also recorded in the steel casing along certain intervals. These GR logs were used for depth calibration purposes, through examining the match between GR logs on different sessions, runs, and passes. Acoustic borehole images were also acquired locally in pipe for acoustic caliper calibration. At the end of each log run, the instrument was re-zeroed at the top of the drill pipe to ensure that no depth discrepancies arose during data acquisition. After each run, the ALT WellCAD software package was used for visualization, processing, preliminary interpretation, and plotting the data.

Tool measurement principle

The logged physical properties and the principles used in the tools to measure them are briefly described in this section. The primary logs are listed in Table **T6**, and technical details for individual tools are shown in Figures **F27** and **F28**. More detailed information on the geological applications of downhole tools may be found in Serra (1984, 1986), Schlumberger (1989, 1994), Rider (1996), Goldberg (1997), and Ellis and Singer (2007), and on individual tools at the manufacturers' Web sites (**http://www.antares-geo.de**, **http://www.geovista.co.uk**, and **http://www.alt.lu**).

Spectral natural gamma probe (QL40-SGR)

The QL40-SGR (Figure **F28**) records the total gamma ray emissions of the geological formation and allows identification of the individual elements that emit gamma rays. Naturally occurring radioactive elements such as K, U, and Th emit gamma rays with a characteristic energy. K decays into two stable isotopes (Ar and Ca), and a characteristic energy of 1.46 MeV is released. U and Th decay into unstable daughter elements. The most prominent gamma rays in the U series originate from decay of ^{214}Bi, and those in the Th series originate from decay of ^{208}Tl. It is thus possible to compute the quantity (concentration) of parent ^{238}U and ^{232}Th in the decay series by counting gamma rays from ^{214}Bi and ^{208}Tl producing characteristic energy at 1.76 and 2.62 MeV, respectively.

The QL40-SGR detector for gamma rays is a bismuth germanium oxide scintillation crystal (2.22 cm in diameter, 10.16 cm in length), optically coupled to a photomultiplier. The bismuth germa-

Figure F28. Stackable slimline logging tools used during Expedition 364. Modified from **http://www.alt.lu**.

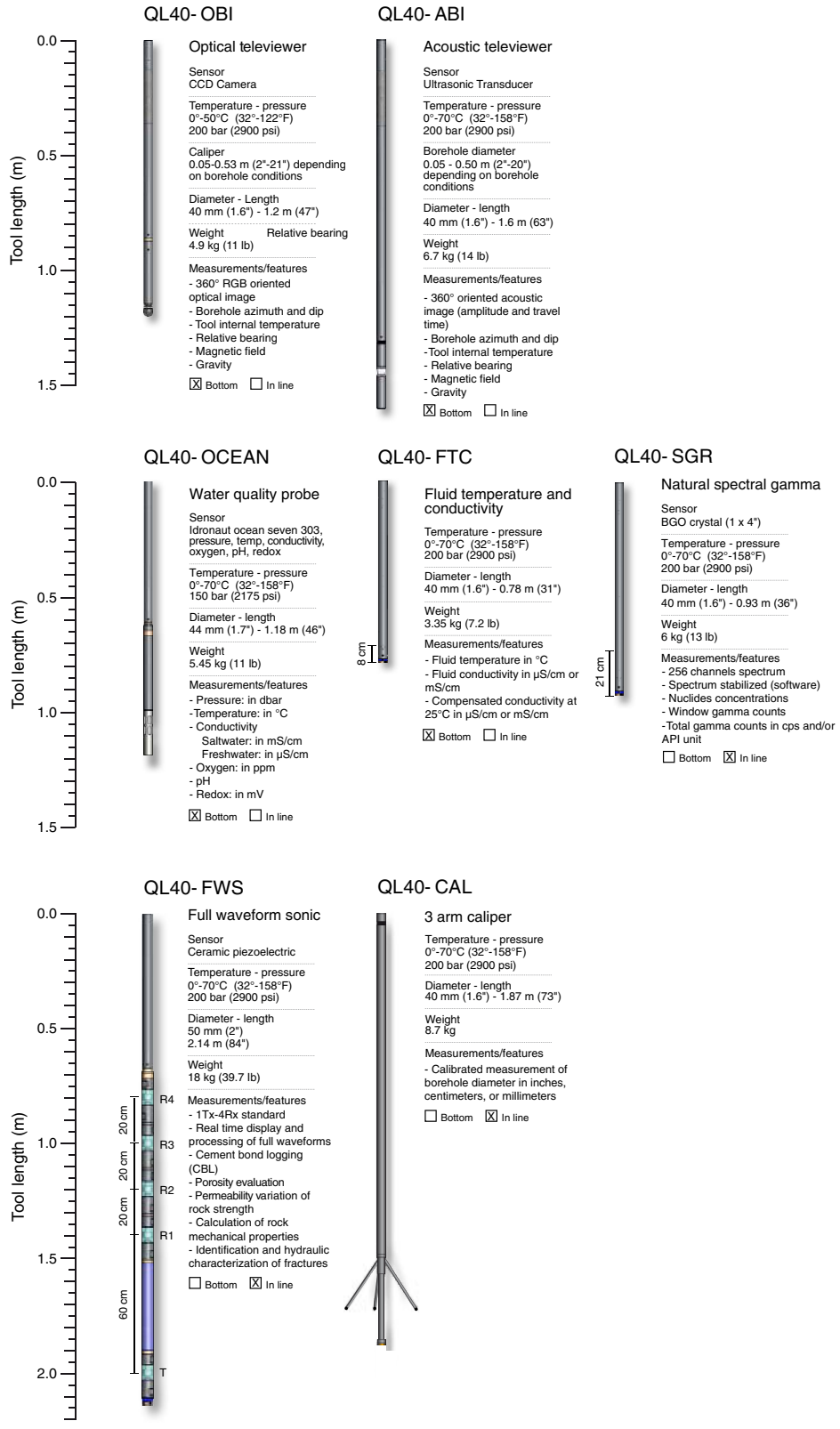

nium oxide detector has an absorption potential eight times greater than the more classic NaI crystal. The instrument was master-calibrated by the manufacturer.

As the probe moves up the borehole, gamma rays are sorted according to their emitted energy spectrum, and the number of counts in each of three preselected energy intervals is recorded.

Figure F29. Slimline tool strings used during Expedition 364.

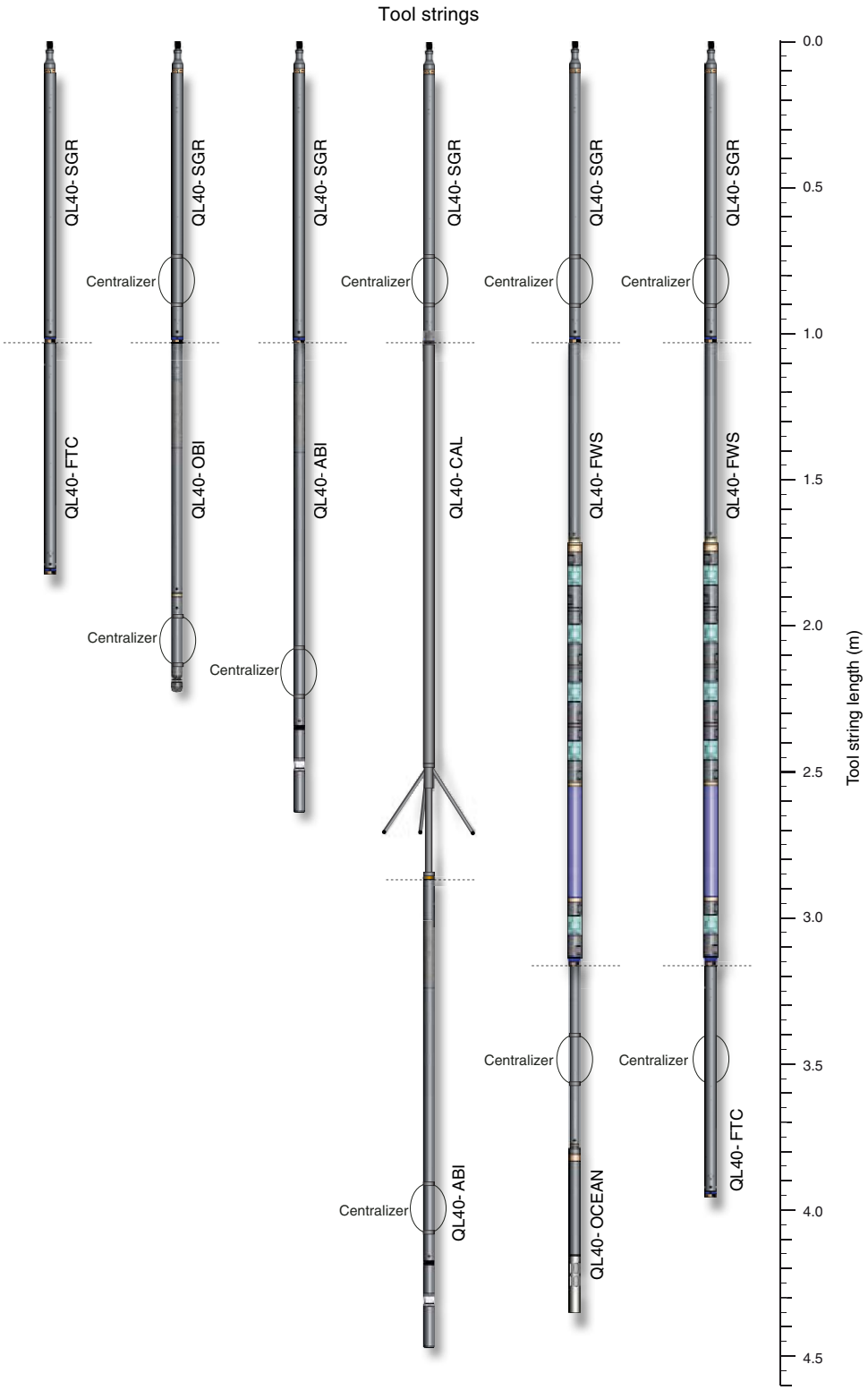

These intervals are centered on the peak values of ^{40}K, ^{214}Bi, and ^{208}Tl. Tool output comprises K, U, and Th in becquerel per kilogram and total gamma ray counts in API units. The vertical measurement interval was 0.05 m, and the vertical resolution of the tool is ~15 cm.

Full waveform sonic probe (QL40-FWS)

Under suitable borehole conditions and formations, the QL40-FWS (Figure **F28**) can detect compressional (*P*), shear (*S*), Stoneley, and tube wave arrivals. When lithology and bulk density are known

Figure F30. Depth setup during downhole logging operations, Expedition 364.

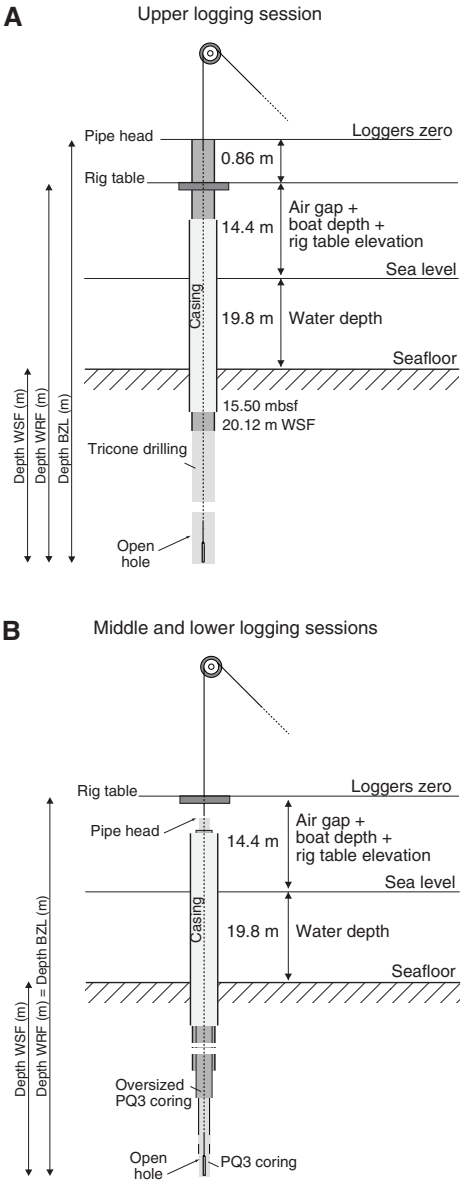

(e.g., from core), both elastic properties (bulk and shear moduli) and porosity estimates can be derived from sonic measurements.

The QL40-FWS can only be operated in a fluid-filled hole. The tool measures the time it takes for a sound pulse to travel from a monopole 6 kHz piezoelectric transmitter to four receivers. The transmitter and receivers are mounted on the same tool. The acoustic pulse generated by the transmitter travels in various different forms through borehole fluid to the rock interface, where some of the energy is critically refracted along the borehole wall. As a result of wavefront spreading (Huygen's principle), some of the refracted energy is transmitted back into the borehole fluid adjacent to each of the four receivers (RX1 to RX4), respectively located at 60, 80, 100, and 120 cm from the transmitter (Figure **F28**). The arriving wavefield is amplified and digitized with a sampling interval of 4 µs. Recorded waveforms are then examined, and wave arrival times (transit times of the acoustic energy) are manually or automatically selected (picked). Typically, the compressional wave (*P*-wave) travels through the rock (or pipe) and arrives first, followed by shear waves (*S*-wave). By measuring the first-arrival traveltime and knowing the distance between the successive receivers (20 cm), the sonic *P*-wave velocity of the rock is calculated.

During Expedition 364, the tool was centered with two centralizers. The downhole measurement interval was 0.05 m. To establish that the tool was working properly, recordings were made in the pipe while running downhole to confirm that the casing had a *P*-wave velocity typical of steel (56 µs/ft or 5400 m/s). The measured velocity was 5550 m/s; thus, formation velocities may be slightly overestimated (by <3%).

Water quality probe (QL40-Ocean)

The QL40-Ocean (Figure **F28**) is a fluid characterization probe equipped with six sensors to measure the following borehole fluid parameters: pressure, temperature, conductivity, dissolved oxygen, pH, and oxidation-reduction (redox) potential. The temperature sensor consists of a low–time response (50 ms) platinum resistance thermometer. The conductivity sensor is a flow-through cell with seven platinum ring electrodes. The polarographic type oxygen sensor was not available during Expedition 364. The pH sensor has a titanium body and a pH-sensitive glass tip. The redox sensor measures the oxidation-reduction potential of the redox couples present in the medium and consists of a platinum wire.

The QL40-Ocean log, like the QL40-FTC log, should ideally be acquired running downhole, as the first tool, after the borehole fluid reaches equilibrium with the ambient environment. During Expedition 364, the QL40-Ocean was only run with the tool moving upward in the upper logging session shortly after the drilling operations. The tool outputs should therefore be used with care and for qualitative interpretations only.

Caliper (QL40-CAL)

The QL40-CAL (Figure **F28**) is a three-arm caliper measuring the borehole diameter. As the three arms are mechanically linked together, they can only open by the same amount, which makes the measurement unreliable in asymmetric boreholes or when the hole is tilted due to the weight of the tool string. The output of the QL40-CAL is a nonoriented single caliper log. When available, the acoustic caliper derived from the QL40-ABI tool should thus be utilized instead.

Optical borehole televiewer (QL40-OBI)

The QL40-OBI (Figure **F28**) produces millimeter-scale, high-resolution optical images of the borehole wall and can be directly used for sedimentological and structural interpretation, as well as for core-log integration (Inwood et al., 2008). As for the QL40-ABI, the tool is coupled with a three-component magnetometer (accuracy = ±1.2°) and accelerometer (accuracy = ±0.5°) to orient the tool with respect to magnetic north and verticality. The tool incorporates a high-resolution, high-sensitivity charge-coupled device digital camera with matching Pentax optics. The camera, located above a conical mirror, captures the reflection of the borehole wall. The light source is provided by a light ring assembly located in the optical head. Azimuthal resolutions available are 90, 180, 360, and 720 points per recorded circle. By combining processed camera data with deviation sensor data, the tool can generate an unwrapped 360° oriented image. Image quality degrades with hole diameters larger than 15 cm (6 inches) and with the presence of mudcake in the borehole because the tool is designed for logs either in air or clear water.

Table T6. Main wireline log channels processed (*) and main log channels acquired. † = logged resulting from postacquisition processing. **Download table in CSV format.**

Tool	Output	Description	Unit
QL40-SGR		Spectral Gamma Ray Probe	
	GR*	Gamma ray	API
	K*	Potassium content	counts/s
	U*	Uranium content	counts/s
	TH*	Thorium content	counts/s
QL40-FWS		Full Waveform Sonic	
	V_p*†	*P*-wave velocity (postacquisition first-arrival picking)	m/s
	AMP	Amplitude	—
	WIDE-BAND, CHEVRON, TUBE, CBL	Waveforms	
QL40-Ocean		Idronaut Ocean Seven	
	TEMPERATURE*	Fluid temperature	°C
	COND(SW)*	Fluid electrical conductivity	µS/cm
	PRESSURE*	Fluid pressure	dbar
	REDOX*	Oxydo-reduction potential	mV
	PH*	pH	—
QL40-CAL		3-arm Caliper	
	CAL*	Caliper	mm
QL40-FTC		Fluid Temperature and Conductivity	
	TEMP*	Fluid temperature	°C
	COND*	Fluid electrical conductivity	µS/cm
QL40-OBI40		Optical Borehole Imager	
	TILT *	Inclination from vertical	°
	AZIMUTH*	Azimuth from magnetic north	°
	MAGNETIC FIELD*	Magnetic field intensity surrounding the borehole	µT
	GRAVITY*	Absolute value of Earth gravity	g
	IMAGE*	Oriented optical image (oriented to magnetic north)	RGB
	ACCELERATION	Tool acceleration	g
QL40-ABI40		Acoustic Borehole Imager	
	TILT*	Inclination from vertical	°
	AZIMUTH*	Azimuth from magnetic north	°
	MAGNETIC FIELD*	Magnetic field intensity surrounding the borehole	µT
	GRAVITY*	Absolute value of the Earth gravity	g
	ACCAL*	Acoustic caliper (postacquisition processing)	mm
	AMPLITUDE*	Echo amplitude image (oriented to magnetic north)	—
	TRAVELTIME*	Two-way traveltime image (oriented to magnetic north)	µs
	WNDTIME	Two-way traveltime of acoustic window reflection	µs
	ACCELERATION	Tool acceleration	g
DLL3		Dual-focused Resistivity	
	RLLD*	Deep resistivity	Ωm
	RLLS*	Shallow resistivity	Ωm
EM51		Magnetic Susceptibility and Induction	
	CIL*	Conductivity by induction	mmho
	MSUS*	Magnetic susceptibility	SI

During Expedition 364, optical borehole images (OBI) during uplogs were acquired with various resolutions of 360 samples × 4 mm or × 2 mm. The QL40-OBI was run only when the hole was flushed with seawater. The tool was run centered with one or two centralizers. The QL40-OBI40 images were affected by the presence of mudcake in the upper part of the lower B session logged.

Acoustic borehole televiewer (QL40-ABI)

The QL40-ABI (Figure **F28**) produces millimeter-scale, high-resolution acoustic images of the borehole wall and can be directly used for sedimentological and structural interpretation and for core-log integration (Inwood et al., 2008). A three-component magnetometer (accuracy = ±1.2°) and accelerometer (accuracy = ±0.5°) allow orienting the tool with respect to magnetic north and the vertical direction.

A voltage is applied in a piezoelectric ceramic to produce an acoustic wave generated at 1.2 MHz. On hitting a focalizing mirror, the wave is deflected perpendicularly, toward the borehole wall. Both the amplitude and two-way traveltime of its echo from the borehole wall (geological formation) are successively recorded. To obtain a 360° image, the mirror pivots on a central axis. The resolution is user defined and depends on the number of measurements made in one mirror rotation and the rate at which the tool is raised up the borehole while measurements are made. The azimuthal resolution can be set at 72, 144, or 288 points per revolution. The vertical resolution is typically set at 2 mm for full-resolution (288 points per revolution) logs. Full-resolution logs require slow logging speeds, typically 0.5 m/min, because they are limited by the communication bandwidth between the tool and the surface. During Expedition 364, acoustic borehole images (ABIs) during uplogs were acquired with various resolutions ranging from 144 samples × 4 mm in the upper session to 288 samples × 2 mm in the lower session.

The QL40-ABI produces two distinct images of the borehole wall. First, an acoustic impedance image (from the contrast between the borehole fluid and wall) is derived from the reflected wave amplitude obtained around the hole. The amplitude ratio between the emitted wave and the reflected wave provides information on the formation's capacity of absorption (low returned amplitude corresponds to a high capacity of sound wave absorption, i.e., soft formation). Second, a traveltime image is derived from the reflected-wave traveltime from the ceramic transducer to the borehole wall and back. The traveltime is directly proportional to the distance between the borehole wall and the probe and is used to compute acoustic caliper and determine borehole size and shape. The formation echo is detected within a time gate that can be adjusted manually. This gate is necessary when the signal is attenuated, for example, due to the presence of viscous drilling mud or when borehole width and shape are highly variable. For each of the two images, a set of false colors is assigned and a virtual image of the borehole wall is produced. This image is displayed as an unfolded representation of the 360° view. Image quality will degrade with hole diameters larger than 15 cm (6 inches) and with the presence of mud in the borehole fluid.

During Expedition 364, the QL40-ABI was run centered with one or two centralizers, the size of which depended on both the borehole diameter and the BHA minimum internal diameter. The ABI images do not appear to be affected by mudcake, if any was present on the borehole wall.

Fluid conductivity and temperature probe (QL40-FTC)

The QL40-FTC (Figure **F28**) provides borehole temperature and fluid conductivity measurements from fresh to highly saturated water. Borehole fluid passes by the temperature and fluid sensors as the probe is lowered into the hole. Temperature is measured with a sensor based on a fast-response semiconductor device whose output current changes proportionally to absolute temperature. Fluid conductivity is measured using a seven-electrode mirrored Wenner array. The QL40-FTC measures temperature in a range of −20° to 80°C with a precision of 0.004°C and fluid conductivity in a range of 5 to 2500 mS/cm with an accuracy of 1%.

As for the QL40-Ocean, the QL40-FTC should ideally be the first tool lowered downhole, with log data acquired while running downhole, after the borehole fluid reaches equilibrium with the ambient environment. During Expedition 364, the QL40-FTC was run in the middle and lower sessions shortly after the drilling operations. FTC up- and downlogs were acquired at a 0.05 m sampling interval, with the exception of the lower logging session, for which only downlogs were acquired at a 0.1 m sampling interval (Table **T4**). The tool outputs should thus be used for qualitative interpretations only.

Dual laterolog electric probe (DLL3)

The DLL3 (Figure **F27**) measures electrical resistivity within the formation, which reflects primarily lithology (composition and texture), formation porosity and saturation, and interstitial fluid properties. The DLL3 is a focused resistivity tool that provides both deep (>1 m) and shallow (<0.5 m) measurements. It has a central electrode, A0, from which a measured current is sent. This current is focused by means of a bucking current that flows from four guard electrodes (A1, A1′, A2, and A2′) (Figure **F27**). The electrical potential of the guard electrodes is held equal to the potential of the A0 electrode in order to force the electrical current to be perpendicular to the tool axis and to flow a larger distance into the formation. The measured current is proportional to formation resistivity. Shallow and deep resistivities are measured by alternating the role of the various guard electrode length and the return location of the bucking current. In shallow measurement mode, A1 and A1′ electrodes act as guards with the current returning to A2 and A2′ electrodes. In deep measurement mode, the pairs A1, A2 and A1′, A2′ act as guards with current returning to the electrical cable beyond an insulated logging cable. Tool output includes deep (RLLD) and shallow (RLLS) resistivities in ohm·meters (Ωm). The vertical measurement interval was 0.05 m. We note that the performance of the DLL3 is more reliable in high-resistivity formations.

Induction resistivity and magnetic susceptibility probe (EM51)

The EM51 (Figure **F27**) measures electrical conductivity and magnetic susceptibility of the formation using electromagnetic induction. Like the DLL3, variations in electrical conductivity of the geological formation primarily reflect variations in lithology, porosity, saturation, and interstitial fluid properties. The sonde includes a set of two coils for conductivity measurement and another set of two coils for magnetic susceptibility measurement. Each pair of coil sondes consists of a transmitter and a receiver. A high-frequency alternating current of constant amplitude is applied to the transmitter coil, which induces an alternating magnetic field around the sonde that, in turn, induces secondary currents in the formation. These currents create their own alternating magnetic field, which induces currents in the receiver coil of the sonde. The received signal is measured, and its size is proportional to the conductivity of the formation (penetration < 1 m). The "in-phase" (real component) signal is a measure of magnetic susceptibility in the formation. The EM51 probe is most effective in high-conductivity geological formations and with a low-conductivity borehole fluid, such as oil-based drilling mud or air. It has a high sensitivity to target conductivity but a low spatial resolution. Tool output comprises conductivity (IL) in mmho and magnetic susceptibility (MSUS) in SI units. The measurement window for magnetic susceptibility ranges from 10^{-5} to 2 SI units. The downhole measurement spacing interval was selected to be 0.05 m.

Vertical seismic profile

The majority of VSP measurements were performed in open borehole conditions (no casing), with the exception of data that were acquired through the casing over short intervals to fill some acquisition gaps (Table **T4**).

Logging procedure, acquisition chain, and data recording

Air gun source

The pneumatic acoustic sources for Expedition 364 VSPs were produced using a Sercel Mini generator-injector (GI) air gun system provided by University of Texas Institute for Geophysics (Figure **F31C**). The air gun was configured at 30/30 inch^3 (generator/injector) in "harmonic" mode. Source depth was nominally 2.0 m below sea level (mbsl), pressure was 2000 psi, and injector delay was 37 ms. The GI air gun was deployed and suspended directly from the *L/B Myrtle* forward starboard crane during operations, without using a flotation buoy. A 30 m "umbilical" tube carries a high-pressure air, electrical-trigger signal, and source-signature signal to the GI air gun. Compressed air was produced using a Max-Air 90 STD (10.8 standard cubic feet per minute [scfm]) electric (220 VAC, single phase) compressor and stored in a Max-Air four-cylinder air receiver system. A second Max-Air 90 (diesel) compressor was pro-

Figure F31. VSP operations during Expedition 364. A. The five SlimWave sondes with locking arms extended during predeployment test. The red bar on the right side of the image is a weight (not used for Expedition 364). B. Geovista winch and controller box. C. Sercel Mini GI air gun deployed from crane. D. Main (right) and backup (left) compressors and air tank reservoir on deck of the *L/B Myrtle*. E. Sercel surface panels during a VSP deployment. F. Two recording laptops operated with Sercel surface panels to right.

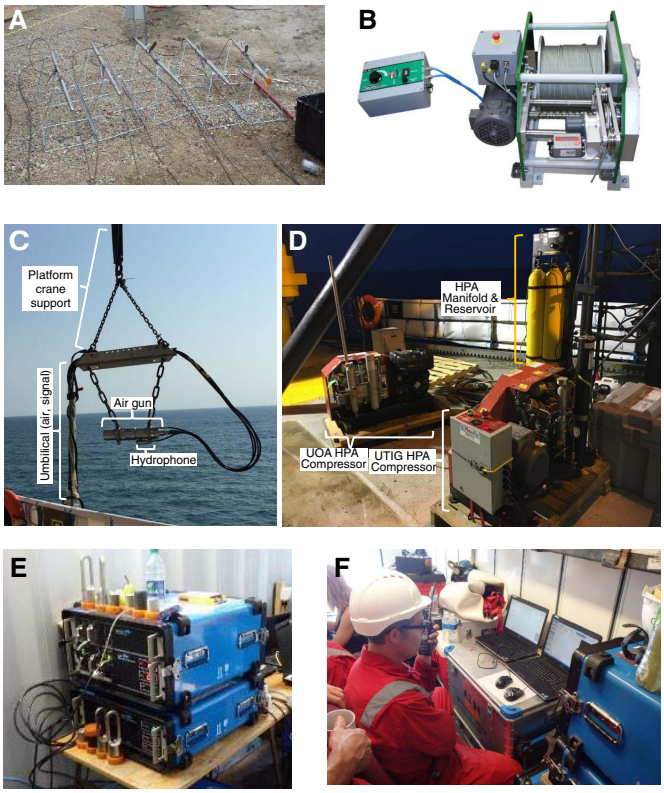

vided by University of Alberta (UoA; Canada) as a backup but was not used.

A Real Time Systems Hotshot portable controller was used to control source timing. Normally, five shots were produced and recorded at each receiver location at 10 s intervals. Trigger signals were provided to the Sercel recording system using a transistor-transistor logic rising edge signal from the controller, synchronized to the source aim point.

During the first two VSP deployments (upper and middle logging sessions, 14 April and 1 May 2016, respectively) firing of the Hotshot system was controlled by software on an attached laptop computer. This system was able to optimize the waveforms produced by the air gun. This laptop was not available during the lower session deployment (28 May), so the system was manually triggered. This sped up data acquisition at the cost of loss of the optimization of the air gun waveform.

Total cycle time required to record five shots, withdraw the receiver arms, reposition the receiver array, lock the arms, and re-arm for the next shots was 3–5 min. At this rate, the single 10.8 scfm compressor at continuous duty was just able to keep up with firing. Between acquisition cycles, the GI air gun was fired as required to be compliant with the protected species permit.

Sercel downhole SlimWave seismic recording system

The recording system for the Expedition 364 VSP was a Sercel SlimWave provided by UoA. This included downhole tools, a downhole telemetry package, a topside recording system, a "smart" winch, and deployment sheaves.

The downhole tool string was composed of five three-component wall-locking geophone sondes (Figure **F31A**) located at a spacing of 15 m on center between each set of sensors. The sondes are powered and transmit data through the wireline. Each sonde is approximately 2 m in length, and they are connected to each other with heavy $^{7}/_{16}$ inch interconnect cables approximately 13 m long. An end cap is placed below the bottommost sonde. The topmost sonde is then connected with one of the interconnect cables to the telemetry/natural gamma sonde. The telemetry unit is then connected to a shorter 3.97 m long interconnect cable that attaches to the wireline. The sondes each contain a locking arm. Normally, this tool string is configured for use in 7 inch (178 mm) diameter boreholes. However, the topmost 500 m of the borehole was drilled with a 7⅞ inch (200 mm) diameter, and new arms that could lock in a 9⅝ inch (251 mm) diameter borehole were purchased specially for this project and installed in the sondes.

The downhole telemetry system includes an instrument to record NGR. The telemetry package includes a demarcation line that indicates the "tool zero" that becomes the depth reference point. It must be noted that the bottommost sonde is consequently located 75 m beneath this point. This telemetry/natural gamma sonde is subsequently connected to the wireline via the interconnect cable the length (3.97 m) of which must be known to properly determine the depth of the sondes.

In deployment for Expedition 364, the height of the drill table above the seafloor was ~34 m (Figure **F30**). As such, the depth was "zeroed" at –30 m when the top of the wireline cable head was level with the drill table, accounting for the 3.97 m interconnect cable between the cable head and the zero depth reference mark on the telemetry tool. All depths reported directly in the headers of the SEG-Y data files are in wireline log depth below seafloor.

The topside system controls and records the VSP data and includes two surface panels and two laptops (Figure **F31F**). A USB-driven hard-drive system is added to this for redundancy; it records a second backup of the data simultaneously. The system is connected to a GPS antenna for timing purposes, with the trigger time recorded to the data files to the nearest microsecond. These units are capable of operating on either North American 110 V or European 220 V standard mains; they were run by the 110 V power within the logging container.

A Model 570 winch S/N 5877 was used with 3000 m of $^{7}/_{16}$ inch four-conductor cable. This winch came equipped with a six-way slip ring, integral depth encoder, automatic level-wind, cable tension gauge, electronic torque limiter, wireless auxiliary remote controller, and 1.5 kW electric DC motor (220 V AC) (Figure**F31B**). The winch was mounted to the mesh rig floor using large ratchet straps. One issue with the deployment configuration was the distance between the winch and its source of power and the position of the Sercel recording unit. A 50 m long heavy power cord allowed connection to the 220 V power plug on the ESO container. The data lines carrying signal from the winch to the Sercel recording system in the logging container were sufficiently long, but the smaller cable for the depth encoding was lengthened prior to operations.

The depth downhole encoding was provided to the Sercel system to the nearest centimeter by an electronic counting wheel on the winch head. During operation, the VSP chain would be moved upward with a count given by the Sercel system operator to the winch operator. The alignment between actual and desired depths is usually better than ±5 cm. A noncalibrated natural gamma ray log is

housed within the telemetry unit. This gamma ray log can be compared to those acquired from the wireline tools to quantify any depth uncertainties.

UoA certified sheave wheels (14 inches, Frank Henry Starlite, and proof load tested to 26,400 lb) were used for both the wireline logging and VSP operations.

The overall system configuration is shown in Figure **F31**. The original plans called for the inclusion of a hydrophone and a three-component gimballed geophone seafloor package. These components would have added information useful to confirm timing of the signals, but they could not be integrated to the Sercel system and were not used in this deployment. The placement of the drill system required that the winch be positioned at the edge of the platform, so the air gun–firing system and the Sercel recording system were separated from one another with no line of sight possible. Due to this arrangement, the recording and winch movement were coordinated using hand-held radios.

Field protocol

Field operations during each VSP run began with testing the trigger and electronics during the marine mammal watch for at least 1 h of daylight, which was a requirement of the Marine Mammal and Protected Species monitoring. Upon receiving the marine mammal observer go-ahead, a "soft-start" was employed with the air gun; initial air gun shots during each run were manually triggered at 500 psi in order to warn any species that might be nearby and not observed and gradually ramped up to the full operating pressure of 2000 psi. During any delays, a maximum air gun firing interval of 5 min was maintained to keep the area clear of marine mammals.

The VSP sondes were deployed downhole one at a time using the starboard crane until the entire tool string including the uppermost telemetry unit was assembled downhole with the cable header sitting on the makeup plate. At this point, the wireline cable was run through two sheave wheels (one attached to the deck to redirect the wireline upward and one suspended from the driller's crane to redirect the wireline downward) and attached to the cable header (Figure **F32**).

Tool measurement principle

Although technically challenging, the geometry of a zero-offset VSP is simple in principle and consists of a source on the surface generating seismic waves that are recorded on receivers within the borehole. The most immediate information retrieved from a VSP is the one-way traveltime of seismic *P*-waves. This time-to-depth relationship is important because it provides a reference against which reflection seismic profiles may be calibrated. Advanced processing of the VSP allows for accurate determination of the depth of reflections seen in the surface seismic images. In addition, velocity data extracted from a VSP complement other velocity data obtained from surface seismic measurements, downhole sonic logs, and MSCL and discrete laboratory measurements, for which velocity measurements utilize a range of seismic frequencies.

During Expedition 364, the seismic source in the survey was a dual-solenoid 30/30 cm^3 GI gun. The second solenoid provides a brief burst of air at a computer-optimized delay time (37 ms) that prevents collapse of the air bubble from its maximum volume and reduces oscillatory noise. The sharp packet of energy released by this seismic pulse travels downward through the lithology and is recorded as particle acceleration on the sonde's three geophones. The wavefield was sampled at 250 µs intervals and digitally encoded downhole before transmission to surface for storage.

The Sercel SlimWave system uses triggers that automatically record when the air gun is fired. For each shot, 3 s of data was re-

Figure F32. VSP system configuration during field deployment, Expedition 364.

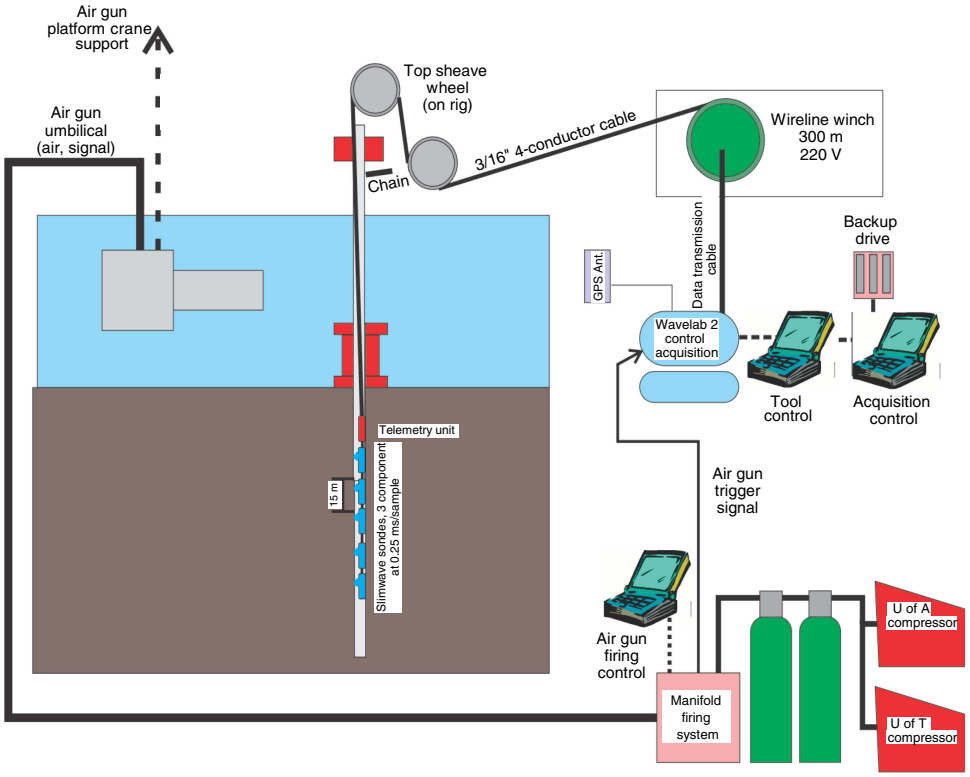

corded on a laptop and automatically backed up to an external hard-drive system. For each VSP deployment, the tool string was lowered to the bottommost planned receiver depth for the first shot. As the sonde is moved upward in the hole, receivers are located with a ±5 cm vertical accuracy. At each receiver depth, the receiver is coupled to the borehole using locking arms. For stacking purposes, five shots were fired at each recording depth. The system additionally uses a GPS timing receiver that provides a timestamp to each individual record according to the GPS time system (which differs from UTC by 17 s at the time of acquisition).

Data processing

Wireline logging

Slimline wireline logging data were processed onshore using the WellCAD software package. The processing procedure is described below. Except in specific cases, only uplogs were used to process the data.

Depth adjustments

One key processing task involves evaluating the depth of each log run and referencing the data to the rig floor and seafloor. Because the logging for Expedition 364 was performed from a platform resting directly on the seafloor, no corrections for ship heave and tides were necessary. Using WellCAD, the original logs were depth-adjusted to the rig floor (wireline log depth below rig floor; WRF). This adjustment included several corrections:

- If any, difference between loggers zero point and rig table (Figure **F30**; Zero logger offset correction column in Table **T4**),
- If any, difference in zero tool depths (discrepancies in depths between initial zeroing and zeroing on removal of the tool, which were generally <1.5 m; see Final tool correction column in Table **T4**),
- Corrections specific to certain tools when combined into specific tool strings (Table **T7**), and
- When necessary, manual shift by the Petrophysics Staff Scientist to a reference log. In most cases, gamma ray logs or borehole images of the pipe entrance were used as reference logs (see Depth shift adjustments column in Table **T4**).

Logs were subsequently shifted to the seafloor reference (WSF scale), which was recognized at 33.94 m below the rig table by the step in gamma radiation (QL40-SGR tool) at the water/sediment interface. Slight discrepancies (<0.2 m) may exist between the seafloor depths determined from the downhole gamma ray logs and those determined by the drillers.

Invalid data

Invalid log values were replaced by a null value of –999.25 when:

- Logging in pipe using the DLL3, EM51, and for some channels of the QL40-ABI40, QL40-OBI40, QL40-Ocean, and QL40-FWS;
- Approaching the metallic pipe (DLL3, EM51, and some channels of the QL40-ABI40 and QL40-OBI40) in open-hole conditions;
- The lowermost data points are affected by the cessation of measurement; and
- Data are affected by halts in the measurement.

Log merges

Where applicable for the processed logs, overlapping log runs were merged to give one continuous log. In the overlapping regions, data were checked by the Petrophysics Staff Scientist to make sure distinctive peaks and troughs correlated and where necessary, a vertical shift was applied (see Depth shift adjustments column in Table **T4**).

Table T7. Tool specific vertical shift, when combined into specific tool strings. Negative value = upward shift. **Download table in CSV format.**

Tool strings	Tool-specific corrections (m)		
	QL40-FWS	QL40-FTC (T°)	QL40-Ocean
QL40SGR+QFWS+QL40Ocean	–1.54		–0.31
QL40SGR+QFWS+FTC	–0.93	–0.08	

Tool-specific processing and quality control

Data quality is assessed in terms of reasonable values for the logged formation, repeatability between different passes of the same tool, and correlation between logs affected by the same formation property (e.g., the electrical resistivity and sonic logs normally correlate). Repeatability between data acquired on downward and upward acquisition of logs was checked by the Petrophysics Staff Scientist. The overall quality of the downhole logging data for Expedition 364 is considered to be very good.

Log quality is mainly influenced by borehole conditions. In Hole M0077A, the borehole quality is generally excellent, with the exception of the upper 400 m, where the hole is locally elliptical and there are karst cavities in the carbonates. Both the sonic (QL40-FWS) and acoustic (QL40-ABI) televiewer logs were affected by the borehole quality over this interval. Deeper measurements were generally less sensitive to these borehole conditions. Below 400 m WSF, the hole is almost in gauge with the drill bit diameter and the log data quality is generally excellent, with the exception of the EM51 and QL40-CAL logs, for which there were communication issues during acquisition (see below).

QL40-SGR. The QL40-SGR was run both in open hole and through pipe over certain intervals. Gamma ray logs recorded through drill pipe should be used qualitatively only, due to attenuation of the incoming signal. Faster logging speeds reduce resolution, and the gamma ray data become noisier. It is therefore recommended that the gamma ray acquired with the QL40-ABI and QL40-OBI tool strings be used in postexpedition studies because these data were acquired at slower logging speeds. All the processed gamma ray data available online come from these tool strings; in most cases, several passes have been merged.

The spectral components of the gamma ray (U, Th, and K) should be used with care because the total counts in the formation were low, with frequent negative values indicative of statistical unreliability. K and Th values are less than 3 counts/s, and Th is null over the three logged sessions. Nonetheless, the total gamma ray values appear to be reliable and correlate well with the NGR data measured on whole-round cores. Below 700 m WSF, a vertical depth offset of up to 1 m is consistently observed between the core (deeper) and the log data (shallower) (Figure **F33**).

QL40-FWS sonic data. Sonic waveforms were recorded while running downhole in the steel pipe to verify that the tool was working. The QL40-FWS data were subsequently processed in WellCad to calculate the *P*-wave velocity. Due to the good data quality below 460 m WSF, waveform picking was undertaken automatically using the standard threshold pickup algorithm module. Subsequently, any mispicked waveforms were identified and manually adjusted. Time picks were saved, and the acoustic velocities were calculated using the R1 and R2 receivers (spacing = 20 cm). For the QL40-FWS tool,

Figure F33. Core data (mbsf) and wireline downhole logging data (WSF) that show vertical offsets between the two data sets, Site M0077.

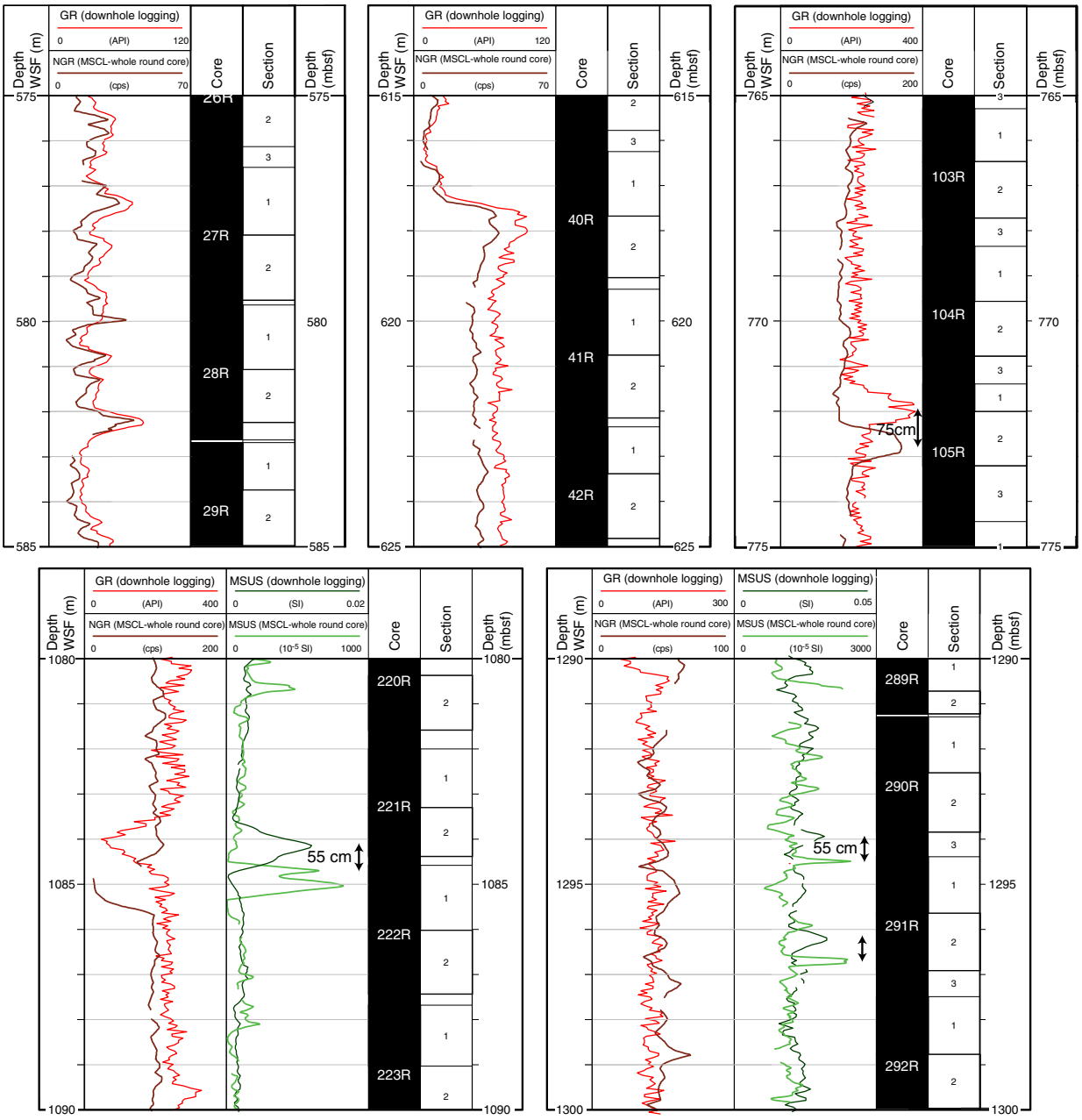

the depth measurement point corresponds to the emitter depth, located 60 cm below the first receiver (R1). An uphole depth correction of 70 cm (60 + 10) was thus applied to properly reposition the measurement point in depth (considered here as in the middle of receivers R1 and R2). All the velocities appear to be accurate because they correlate well with the resistivity log and/or acoustic borehole images and the discrete *P*-wave measurements. In the upper ~460 m of the hole, the data quality was not good enough for automatic picking of the first arrival; therefore, no *P*-wave data are provided for this region. Further postexpedition processing is necessary to undertake manual picking of the waveforms.

QL40-Ocean. The QL40-Ocean data in the upper session should be used qualitatively because the tool was run shortly after the hole was circulated with seawater and data were recorded uphole during Run 5. The quality of these logs is best when they are acquired downhole once the borehole fluid has reached an equilibrium temperature with the formation and before other runs that may alter the temperatures. The fluid temperature values provided by the tool are thus likely different than the temperature of the ambient formation, but relative variations may be retained.

QL40-CAL. Due to tool communication issues, the caliper arms did not open properly over some logged intervals. For this reason, data indicating diameters smaller than 15 cm are assumed to be incorrect and were deleted.

QL40-FTC. As for the QL40-Ocean, the quality of the QL40-FTC logs is best when they are acquired downhole once the borehole fluid has reached an equilibrium temperature with the formation and before other runs that may alter the temperatures. The QL40-FTC data should be used qualitatively because the tool was run in shortly after the hole was drilled (middle session) or circu-

lated with seawater (lower session). The fluid temperature values provided by the tool are thus likely different than the ambient temperature of the formation.

QL40-OBI. Brightness and contrast of the QL40-OBI images were automatically adjusted during processing. In some intervals, several passes have been oriented and merged on the same presentation. Image quality is good in the upper session (0–500 m WSF) and Lower A session (938–1334 m WSF). In the Lower A session, the QL40-OBI images present an apparent ~3 m long cyclic-like change in color, which is interpreted as resulting from a change in the LED intensity of the tool, which was run at this depth beyond the temperature limitation of the tool. The QL40-OBI image correlates well with the QL40-ABI image in the Lower A session. In the Lower B session (935–698 m WSF), no features are observed on the QL40-OBI images although the images were acquired at high resolution and the tool was functioning properly. The lack of features is likely due to the presence of a mudcake on the borehole wall that was not removed when the hole was flushed with seawater in preparation for logging.

Processed QL40-OBI images available in the JRSO online log database are provided in PDF (1:5 and 1:50 scales), depth-corrected to the seafloor (WSF scale), and displayed as an unwrapped borehole cylinder. QL40-OBI images are oriented with respect to magnetic north.

QL40-OBI images can be used to reorient cores when distinctive features are observed both on the borehole image and in the core. A dipping plane in the borehole (e.g., a fault) thus appears as a sinusoid on the image, and the height of this sinusoid is proportional to the dip of the plane. The lowest part of the sinusoid indicates the azimuth of the plane. At Chicxulub, however, the presence of a strong local magnetic anomaly (Pilkington and Hildebrand, 2000; Rebolledo-Vieyra et al., 2010) causes some deviation in the compass needle at the surface, which raises some uncertainty regarding whether the north direction picked up by the tool is correct. Postexpedition paleomagnetism studies will be performed to verify whether the QL40-OBI tool was properly oriented.

QL40-ABI. The QL40-ABI40 data were processed using the WellCAD software. "No Data" or "NULL" traces in the images were removed using an algorithm that replaces bad traces with the closest trace containing valid data points. Traveltime images were corrected for decentralization effects of the probe within the borehole. Assuming the decentralization effect on the data is approximately sinusoidal, "Centralize Process" was used to remove this trend and correct the input data according to a best-fit sinusoid.

Acoustic caliper values were obtained with the Traveltime-to-Caliper Module using the WndTime log (Table **T4**) and by assuming an acoustic wave velocity through the borehole fluid of 1500 m/s.

Processed QL40-ABI images are provided in PDF (1:5 and 1:50 scales) in the JRSO online log database. They are depth-corrected to the seafloor (WSF scale) and are displayed as an unwrapped borehole cylinder. Images were not normalized. In some borehole intervals, several passes were oriented and merged on the same presentation.

QL40-ABI images correlate well with QL40-OBI images and, where available, with other downhole logs (sonic, resistivity, and NGR) and with core line scan images. QL40-ABI log quality is generally excellent with the exception of the upper 400 m, where the hole was elliptical or larger than the optimal size for the tool or where karst was present. As with the QL40-OBI, there is uncertainty regarding the magnetic north picked by the tool during data acquisition. This uncertainty will be quantified during postexpedition analysis.

DLL3 and EM51. The DLL3 performs well in high-resistivity formations. Performance is also better in higher conductivity mud. Due to the borehole width and the low resistivity of the formation in the upper interval, the DLL3 provided measurements that are not quantitatively reliable, especially the shallow readings. The induction conductivity measured by the EM51 tool (magnetic susceptibility and conductivity), which is more effective in high-conductivity formations, should be preferred in the upper interval.

In the middle session, the DLL3 was not run. Due to tool communication issues, the EM51 data are poor quality. Only a few data points were acquired, every 1 to 5 m. The processed logs contain interpolated data (maximum gap = 2 m). The resulting data set, however, shows that the general log trend is in good agreement with the electrical and the magnetic susceptibility measurements performed on whole-round cores (see Figures **F43** and **F44** in the Site M0077: Post-Impact Sedimentary Rocks chapter [Gulick et al., 2017b]), although the induction and magnetic susceptibility logs have poor vertical resolution and show values that are respectively higher and lower than those from the cores.

Both the DLL3 and the EM51 worked well in the lower part of the hole. A spike at ~850.7 m WSF was removed and was probably caused by the presence of metal from a broken bit.

VSP

A software problem during the middle VSP caused the recorded depth to "freeze" during Shots 49–99 (570–690 m WSF); this error was corrected manually in the data headers by referencing the depths recorded on paper and the Adhered to shot plan Excel file. Particularly poor data traces were manually selected and removed. The remaining data traces were stacked together by receiver depth to improve signal-to-noise ratio. First breaks were manually selected at the minimum value of the first trough for each trace, and *P*-wave velocities were differentially calculated with the two-stage least-squares regression method. First, a moving window of 21 points found the slope for the VSP with a required truncation of 10 points at both ends. Next, velocity zones were selected visually by identifying changes in slope in the first-arrival traveltimes.

Data delivery

Processed and raw data from all downhole logs are available in the JRSO online log database. Processed standard wireline data are available in ASCII format. VSP processed first breaks are provided as tab-delimited ASCII. All processed depths are depth-corrected to the seafloor (WSF scale). QL40-ABI and QL40-OBI image files are available in PDF and JPEG formats.

Wireline raw data are provided in DLIS format with depths in meters below loggers zero level (BZL). VSP raw data are in SEG-Y format with wireline log depth below seafloor depths.

Downhole logging operations

During Expedition 364, the wireline logging and VSP data were acquired in three logging sessions (upper, middle, and lower) at ~0–503 m DSF (upper session), ~506–699 m DSF (middle session), and 700–1334 m DSF (lower session) (Figure **F26**). In the lower session, wireline logs were acquired in two steps to avoid an interval of potential hole instability (mud circulation loss zone), identified as Lower A (939 m DSF to total depth) and Lower B (935–701 m DSF) sessions.

In preparation for logging, the boreholes were either flushed of debris by circulating seawater (upper and lower session) or left filled with drill mud (middle session). The BHA was pulled up to 20.1 m WSF (upper session), 507.3 m WSF (middle session), and 938.7 m WSF (Lower A session). The BHA was pulled out entirely before logging the Lower B session.

Upper logging session

The first downhole logging measurements in Hole M0077A were conducted after completion of open-hole drilling to 503 m DSF (See **Operations**). Between 78 and 82 m DSF, mud circulation was lost, and the hole was cemented from 100 to 50 m DSF before being drilled again. With the exception of this interval, the hole was reported to be in good condition. Seawater was circulated to clean the hole, the pipe was pulled up, the drill bit was changed, and the pipe was lowered down again and positioned at 20 m DSF.

Two stand-alone tools and seven tool strings were deployed in the open-hole interval in the following order (Figures **F26**, **F27**, **F28**): DLL3, QL40-SGR + QL40-ABI40 tool string, VSP, EM51, QL40-SGR + QL40-ABI40 tool string, QL40-SGR + QL40-FWS + QL40-Ocean tool string, and QL40-SGR + QL40-OBI40 tool string. The QL40-SGR was included at the top of each wireline tool string to allow precise depth match processing between logging tool strings and passes. The description of the acquisition parameters and logged intervals can be found in the Table **T4**.

On 14 April 2016 at 1230 h, the DLL3 descended into the pipe (Run 1). A downlog was taken at ~30 m/min to ~465 m WSF. The hole was logged up to the surface in two passes at ~30 m/min. Resistivity values were low (<0.7 Ωm) for the RLLD (deep depth of penetration) and showed negative values for the RLLS (shallow depth of penetration), indicating low-resistivity formations. It was decided to run the EM51 induction tool at a later stage because it works well in conductive formations.

The QL40-SGR + QL40-ABI tool string was rigged up and sent down the hole at ~1355 h (Run 2) on 14 April. The tool string was equipped with one 8 inch centralizer, located on the QL40-ABI. A downlog was acquired at 20 m/min and low resolution to ~165 m WSF only to allow the start of the VSP operations during daylight. An uplog was recorded in several passes at a medium resolution and a velocity of 1.5 m/min. During acquisition, the acoustic signal was frequently lost due to either the presence of cavities in the carbonate formation or borehole enlargement beside the echo time window. The pipe was observed on the acoustic images at 20.12 m WSF. The echo time window was manually chosen to increase data quality in the open hole because it was too large compared to the pipe internal diameter (6 inch). As a result, the acoustic signal within the pipe could not be used for acoustic caliper calibration. A last pass was thus acquired with an automatic selection of the echo time window in the pipe over a ~20 m long interval from ~18 m WSF to enable calculation of the acoustic velocity of the borehole fluid. The acquisition of the uplog was stopped after the tool passed the seafloor, the depth of which was given by the step in the total gamma ray log at 33.94 meters below rig floor (mbrf). At 1615 h, the tool string was back on deck.

On 14 April at 1645 h, firing of the air guns was initiated, and marine mammal observation procedures started. The tool string reached the bottom of Hole M0077A at ~500 m WSF. VSP data were acquired uphole from 500 to 200 m WSF at a sonde spacing of 1.25 m and from 200 to 47.5 m WSF at a spacing of 2.5 m. Data acquisition commenced at 1720 h and ceased at 2326 h. All five Sercel sondes were employed. However, the arm-locking motor on one of the units required excessive power to operate, causing some concern, and to reduce the risk that the arm might not retract in the latter two VSP deployments (middle and lower sessions), this unit was not deployed again. Recovery of the tool string was complicated because the top edges of each sonde caught at the bottom of the pipe hanging from the drill floor. The tools were safely removed once the pipe was rotated. This problem was avoided in future deployments by smoothing the top edges of each sonde with wound electrical tape. The VSP tool was back to the surface at 0330 h on 15 April.

On 15 April at 0330 h, the standalone EM51 was sent downhole (Run 3) to (1) check that the borehole was still open following the VSP measurements, (2) acquire accurate conductivity values in the low-resistivity formation, and (3) acquire magnetic susceptibility data. A downlog was acquired, followed by an uplog at 30 m/min from ~498 m WSF to the pipe entrance.

The QL40-SGR + QL40-ABI tool string was then rerun at 0430 h (Run 4), and an uplog was acquired at a velocity of 1.5 m/min from ~498 to ~160 m WSF; logging was completed at 0900 h.

The QL40-SGR + QL40-FWS + QL40-Ocean tool string was successively sent (Run 5). The tool string was equipped with two 8 inch centralizers, located on the QL40-FWS and QL40-Ocean. No downlog was acquired. An uplog was taken from ~493 m WSF with evidence of communication issues with the QL40-SGR and QL40-Ocean. At ~460 m WSF, the acquisition was stopped and the problem resolved. Only QL40-FWS data are available in the ~493–460 m WSF interval. Due to time constraints, it was decided not to relog the lowest part of the hole and to proceed with the logging uphole. An uplog was thus taken from ~462 m WSF to the pipe entrance at a velocity of 4.5 m/min. Acquisition was stopped after entering the pipe.

During drilling operations, mud circulation was lost between ~120 and ~85 m DSF. The last tool string, consisting of the QL40-SGR + QL40-OBI, was run (Run 6) over this interval to check for the presence of cavities in the carbonates that could explain the circulation loss. An uplog was acquired in two passes at very high and high resolution from ~91 to ~54 m WSF. Rig down was completed at 1515 h.

On 16 April at 0300 h, wireline logging was rigged up for operational purposes following the loss of a 160 m long pipe section in the hole. The stand-alone EM51 was sent downhole first to locate the fallen pipe entrance, which was found at ~302.66 m WSF. The downhole log was stopped at ~ 303.06 m WSF, and the tool was brought back to the surface. The QL40-SGR + QL40-ABI tool string was successively sent downhole to check the pipe quality (joint quality and pipe deformation) and its tilt. Several attempts to enter the pipe failed. The tension drop suggested that the top of the pipe was blocked. The tool was brought back to the surface at 0516 h, and reentry cones were built up to facilitate the entry of the tool into the fallen pipe. At 0540 h, the tool entered the pipe as indicated by a change in the signal echo at 340 mbrf. The pipe joints were counted while going down. The last joint was found at 493.81 m WSF, and the pipe exit was located at 497 m WSF, ~6.80 m above the base of the hole. The acoustic echo indicated that the pipe was not damaged (the joint was in good shape and caliper circular), and the tilt increased downpipe from 0.4° to 1.3°. Rig down was completed at 0730 h.

Middle logging session

The second session of downhole logging measurements in Hole M0077A was conducted after completion of coring to 699.09 m DSF. The borehole conditions were expected to be excellent and the hole very stable, except possibly in the lowest 20 m. The pipe was pulled up and positioned at 506 m DSF because there were concerns that the hole quality between 500 and 505 m DSF could cause problems for logging. The hole was not flushed before logging and remained filled with drilling fluid. Consequently, it was not possible to run the wireline QL40-OBI tool in this interval, as the device camera requires air or clear water to properly image the borehole wall.

Wireline and VSP tools were deployed for acquisition in the open hole in the following order (Figures **F26**, **F28**; Table **T4**): EM51, QL40-SGR + QL40-FWS + QL40-FTC tool string, QL40-SGR + QL40CAL + QL40-ABI40 tool string, and VSP. Another tool string composed of the QL40-SGR + QL40-ABI40 was run at a later stage over a 3 m long interval; afterward, the hole was cased and cemented. The QL40-SGR was included in each wireline tool string to allow precise depth match processing between logging strings and passes.

Rig up started on 1 May 2016 at 1745 h. At 1822 h, the EM51 descended into the pipe (Run 1). A downlog was taken at ~30 m/min to the bottom of the hole. Communication with the tool was good at the surface but got lost during the downlog. An uplog was acquired at 30 m/min from ~698 m WSF to the pipe entrance, with frequent communication errors. The zero tool at the surface indicated an important depth offset of –42.5 m.

The QL40-SGR + QL40-FWS + QL40-FTC tool string was successively sent down the hole at ~2115 h (Run 2). The tool string was equipped with two 6 inch centralizers located on the QL40-SGR and QL40-FTC. The log was acquired while going from 483 to ~699 m WSF. The probe was stopped short of the bottom of the hole to avoid heavy mud or debris being deposited on the QL40-FTC sensors. The uplog was performed from ~699 to ~478 m WSF and across the seafloor boundary.

The QL40-SGR + QL40CAL + QL40-ABI40 tool string was run downhole at 0040 h on 2 May (Run 3). The tool string was equipped with two 6 inch centralizers located on the QL40-SGR and QL40-ABI. The QL40-caliper was included in the string to add weight to the tool string and ensure the possibility of lowering it through the pipe and BHA. The tool string was lowered to ~698 m WSF, and the bottom of the hole was not tagged to avoid deposition of heavy mud or debris on the acoustic window of the QL40-ABI. Because of the good hole quality, the QL40-ABI40 logs up were set to maximum resolution and acquired at low velocity (0.6 m/min) to obtain high-resolution borehole wall acoustic images. Uplogs were acquired in seven passes from ~698 to ~504 m WSF using various acoustic windows. Two additional passes were acquired in the pipe for high-resolution borehole wall acoustic imaging over a ~3.5 m long interval with an automatic selection of the echo time window to allow for caliper calibration. At 0855 h, the tool string was back to the surface.

The VSP system was prepared for deployment by 0000 h on 2 May. VSP operations started at 0800 h, with marine mammal observation activities taking place during rig up. At 0930 h, the tool was lowered to 695 m WSF, 5 m above the base of the hole, and the first shots were recorded at 1320 h. A VSP was acquired from 695 to 462.5 m WSF at a 1.25 m spacing. Only four of the five sondes were used. Data were not acquired near the bottom of the pipe to avoid locking the tool in this region. There were no problems reentering the pipe at the end of VSP data acquisition, with the last shots performed at 1728 h. VSP operations were completed at 1800 h. A decision was made to fill the data gaps at the bottom of the hole and below the pipe entrance at a later stage during the third phase of VSP operations.

On 4 May, following casing of the hole and cementation, a tool string including the QL40-SGR and QL40-ABI40 was sent downhole at 1124 h. This acquisition was performed to investigate the possibility of acoustically imaging the borehole formation through the steel casing for further through-pipe logging at depth in the event of the hole being too unstable to allow for open-hole logging (Run 4). The tool string was equipped with two 6 inch centralizers located on the QL40-SGR and QL40-ABI and was sent downhole below the pipe entrance. An uplog was acquired from 520.36 to 515.64 m WSF at high resolution and a velocity of 0.6 m/min. The pipe signal was blanked using an acoustic window starting behind the pipe arrival. The tool string was back up to the surface at 1320 h, and rig down was completed at 1345 h.

Lower logging session

The third session of downhole logging measurements in Hole M0077A was conducted after completion of coring to a total depth of 1334.69 m DSF. Borehole conditions were expected to be excellent and the hole very stable, with the exception of a 2 m thick interval located around 938 mbsf where mud circulation was lost. Because of high hole instability risks at this depth and because of the presence of centralizers on the wireline tool strings, it was decided to open-hole log the bottommost 634 m of the hole in two steps (from total depth to 940 m DSF and from 935 to 700 m DSF). Because the geophones were not equipped with centralizers, the VSP operations were successively performed in the open hole along the entire lower interval, but no data were acquired at the possibly unstable depth.

Logging operations started on 26 May 2016. The pipe was pulled up and positioned at 940 m DSF, just below the possible unstable zone, and the hole was flushed with seawater in preparation for wireline logging.

Lower A session

Rig up started on 26 May at 0615 h. At 0715 h, the DLL3 was run first (Run 1) to check for the absence of bridges in the hole. Two logs were recorded at 30 m/min, down and up, between 1336.6 and 938 m WSF. The discrepancy in depth between the total drillers depth (1334.69 m DSF) and the wireline depth may be partly linked to the light weight of the DLL3 tool combined with the length of cable making the bottom of the hole difficult to tag. Formation resistivity values were low (<1 Ωm) and at the limit of the measurement range of the tool.

The QL40-SGR + QL40-FWS + QL40-FTC tool string was successively sent down the hole at ~0950 h (Run 2). The tool string was equipped with two 5 inch centralizers placed on the QL40-SGR and QL40-FTC. The downlog was acquired to ~1334 m WSF, and the probe was not lowered to the bottom of hole to avoid heavy mud or debris being deposited on the QL40-FTC sensors. The uplog was performed at 4.7 m/min from ~1334 to ~939 m WSF and through the seafloor.

The EM51 stand-alone tool was sent downhole at 1351 h (Run 3). A downlog was recorded to ~1334 m WSF, and an uplog was performed in several passes due to a fault with the winch that could have damaged the cable. The uplog was stopped at the pipe entrance.

The QL40-SGR + QL40CAL + QL40-ABI40 tool string followed at 1620 h (Run 4). The tool string was equipped with two 5 inch centralizers located on the QL40-SGR and QL40-ABI. A downlog was performed at low resolution to ~1334 m WSF, and the bottom of the hole was not tagged to avoid damaging or muddying the acoustic window of the QL40-ABI. The uplog was acquired in three passes from ~1334 to ~942 m WSF using various acoustic windows. The caliper arms were opened over short intervals for further comparison with the acoustic traveltime caliper. To check the tool orientation, successive passes were made across intervals where fractures were clearly visible. A high-resolution image of the drill bit and a through-seafloor log were acquired before the tool was recovered.

The last tool string, consisting of the QL40-SGR + QL40CAL + QL40-OBI40 tools (Run 5), was lowered in the hole at 2323 h. The tool was sent to the bottom of the hole in order to record the optical imagery of the borehole wall. However, due to the high temperature in the borehole and that of the tool head (67°C), the head LEDs couldn't be switched on, and the decision was made to retrieve the tool to a shallower depth. The LEDs were successfully switched on at ~1044 m WSF, where the temperature of the tool head was 5°C cooler. The logs were taken from here to the entrance of the pipe. The tool string was back to the surface at 0224 h on 27 May, and rig down was completed by 0300 h.

Lower B session

Following wireline operations in the Lower A interval, the drill string was entirely removed from the hole, and wireline logs were recorded in the upper part of the lower section from 935 to 700 m DSF. Centralized tools were not run deeper than 937 m WSF to avoid the unstable zone. The noncentralized tools were run to 956 m WSF in order to ensure overlap with the data previously acquired in the lowest part of this interval.

Rig up started on 27 May at 0715 h. The DLL3 was run first (Run 6). Downlogs and uplogs were recorded between ~957 and 698 m WSF at a velocity of 30 m/min. The tool was lowered without any problem below the unstable zone.

The QL40-SGR + QL40-FWS + QL40-FTC tool string was successively deployed at ~0926 h (Run 7), and a downlog was acquired to ~935 m WSF. The tool string was equipped with two 5 inch centralizers located on the QL40-SGR and QL40-FTC. This tool string was not lowered below the unstable zone. The uplog was acquired at 4.5 m/min to ~696 m WSF.

The QL40-SGR + QL40-CAL + QL40-ABI tool string was run into the hole at 1143 h (Run 8) and sent to ~936 m WSF. The tool string was equipped with two 5 inch centralizers located on the QL40-SGR and the QL40-ABI. An uplog was acquired at medium resolution in three passes at a velocity of 0.8 m/min. The uplog was interrupted at ~829 m WSF because the tool was not centralized any longer, which led to a poor quality acoustic image. Caliper arms were opened to try to centralize the tool without success. The decision was made to bring the tool back to surface and replace the 5 inch centralizers with 6 inch centralizers.

The EM51 was successively deployed in the hole at 1612 h (Run 9). Downlogs and uplogs were recorded between ~956 and 697 m WSF at 30 m/min. This tool was lowered without any problem below the unstable zone.

The QL40-SGR + QL40-CAL + QL40-ABI tool string was sent back in hole again at 1840 h (Run 10) equipped with two 6 inch centralizers located on the QL40-SGR and the QL40-ABI. An uplog was taken in several passes from ~853 to 678 m WSF.

Because the lost-circulation zone at around 938 mbsf appeared stable, it was decided to run the QL40-SGR + QL40-FTC tool string down to the total depth of the hole, given that the lower interval deeper than 950 m WSF remained undisturbed from wireline logging operations over a 14 h period. The tool string was sent downhole at 2351 h. A downhole log was acquired at low velocity from 698 to 1334 m WSF (Run 11). Several passes were required because the probe intercepted the borehole wall at ~754 and 850 m WSF, a depth at which a reduction in borehole diameter was observed on the QL40-ABI signal. The bottom of the hole was not tagged to avoid muddying the QL40-FTC sensors. On its way up, the decision was made to record fluid temperature and conductivity over a given time at 937.5 m WSF, which corresponded to the depth of the fractured zone where mud circulation was lost and a sharp increase in fluid temperature and conductivity was observed. This record was made at a time interval of 500 ms for a duration of 7 min. The tool was back to the surface at 0400 h on 28 May, and mud was observed to be present on the tool sensor, which may have affected the static measurements.

The QL40-SGR + QL40-OBI tool string was the last to be run in the hole at 0420 h (Run 12). The tool string was set up with 6 inch centralizers located on the QL40-SGR and QL40-OBI. Due to time constraints, an uplog was recorded in several passes between 767 and 693 m WSF over an interval where interesting features were expected from through-liner core observations. The recorded optical images did not seem consistent with the expected lithologic variations, and the decision was made to decrease the resolution and bring the tool back to the surface. Rig down was completed at 0700 h on 28 May.

VSP

The VSP team was deployed to the rig on 25 May 2016. Preparations for logging were made, and a full test of the air gun in the water was carried out on 26 May. As before, marine mammal observation activities proceeded before testing of the air gun.

VSP started with the rig up at 0630 h on 28 May. The start of data acquisition was delayed, first because the crane was being used for operational purposes and then because of issues related to the depth encoder wire. These issues were solved, and the first shot was recorded at a 1007 h with the bottom sonde at 1325 m WSF. Data were acquired uphole with a spacing of 5 m to 650 m WSF to overlap with the middle interval VSP acquisition and allow for correction of gaps. The last shots were fired at 1317 h.

An attempt to reshoot through pipe around 440 m WSF was performed to improve data quality across zones in the upper VSP interval that were less successful due to poor coupling. The inner casing, however, was not cemented, and only poor quality data were obtained. The VSP tool was back to surface at 1340 h, and rig down ended at 1530h.

Microbiology

Offshore sampling and sample preparation

Core handling and sampling

Samples of whole core were obtained for microbiology analyses immediately after core recovery on deck. Samples of core were typically ~5–10 cm in length and were obtained at the core catcher end of the recovered core. Core samples were obtained using sterile chisels or hammers. The exterior of the core was carefully removed, and the interior material was used for subsequent sampling. As a

consequence of the adopted procedure, the resultant material was either a ~3 cm diameter whole round or a fragment of interior material. In cases where the rock (typically granitoids) was not easily divided using a chisel, a water-cooled diamond circular saw was used. To minimize contamination, the outer ~1 cm of the core was returned for curation and was not used in subsequent microbiological analysis.

Sawing of core slices can potentially lead to contamination of the entire cut surface with microbial cells stemming from drilling mud (Inagaki et al., 2015) and/or from the water used to cool the saw. To reduce the likelihood of contamination, visible sticky gray-colored drilling fluid was first removed under running tap water. Next, the rocks were sprayed with RNase-Away (Thermofisher), a reagent that destroys nucleases and foreign DNA on surfaces. The surfaces of the core slices were then heat sterilized using 70 vol% ethanol and burning off the excessive ethanol. Care was taken not to overheat and possibly sterilize the pristine interior of the core samples.

Irrespective of the sampling method (chisel or saw), the core slices were then wrapped in several layers of autoclaved aluminum foil, and the center of each slice was crushed with a hammer without breaking or damaging the aluminum foil. The aluminum foil was further wrapped tightly to prevent shifting of crushed pieces. Using a flame-sterilized spatula and tweezers, pieces from the center of each sample were transferred into appropriate bags or vials.

At all times, individuals involved in collecting and processing the core wore vinyl gloves to prevent cross-contamination with skin-associated bacterial and/or human cells, which can constitute a major source of contaminant DNA. Samples were collected every 3 to 9 m from the marine Post-Impact Sedimentary Rocks interval and every 9 m from the underlying Upper Peak Ring and Lower Peak Ring intervals.

Contamination control

Drilling fluid samples were collected alongside samples used for microbial analysis to allow for the enumeration and anaerobic cultivation of contaminant microbes in the drilling fluid, and for the extraction of nucleic acids from drilling fluid to compare with interior nucleic acid samples. Samples of drilling fluid were taken from (1) the sides of the core, (2) fluid flowing up from the borehole, and (3) drilling fluid prior to its use in the hole. Samples of fresh components of the dry mud were also collected prior to its mixing with seawater. No perfluorocarbon tracers (e.g., Smith et al., 2000a, 2000b) were used during this expedition.

Subsampling for microbial enumerations

For cell enumeration, small pieces of rock (~1 g in total and maximum 3 mm in diameter) were transferred into 10 mL sterile serum bottles prefilled with 4 mL 4 vol% formaldehyde and 3.5% wt/vol NaCl. The labeled serum flasks were sealed with sterile rubber stoppers, crimped with aluminum seals, and immediately put into storage and kept at 4°C in the dark.

Subsampling for microbial cultivation

For microbial cultivation, material from the interior of the core was transferred into a 20 mL sterile serum bottle. The size of the sample varied from ~1 to ~5 g depending on the material and the ease with which the core could be broken up. The serum bottle was sealed with a sterile rubber stopper and aluminum seals using a crimping device. The bottles with samples were subsequently flushed with sterile-filtered nitrogen gas for 5 min to create an anoxic headspace. Gas was injected through a 0.2 µM pore size filter disc (Millipore) using a needle inserted into the rubber stopper. A second needle was pushed through the rubber stopper to release pressure and to enable nitrogen flow. New sterile needles were used for each sample. The labeled bottles were immediately stored at 4°C in the dark.

Subsampling for RNA extraction and analysis

A piece of ~2 g of sample was ground in an RNase-Away treated and autoclaved steel or stone mortar in the presence of 5 mL LifeGuard Solution (MOBIO; Carlsbad, CA [USA]) to minimize degradation of RNA during sampling. These samples were transferred with a sterile plastic spoon into 15 mL sterile centrifuge tubes. The tubes were labeled and transferred in separate Whirl-Pak bags and immediately frozen at –80°C. Double bagging was used to prevent labels getting lost as a result of the samples being deeply frozen and then transported. If sufficient RNA can be extracted, these samples will be used to study the diversity and function of metabolically active microbes (e.g. Coolen and Orsi, 2015).

Subsampling for DNA extraction and analysis

For subsequent environmental DNA analysis, duplicate larger sized pieces of rock (~10–30 g) were taken from core samples and transferred into labeled sterile Whirl-Pak bags and double bagged to prevent potential loss of labels. The samples were immediately frozen at –80°C. These samples will be analyzed for taxonomic and functional diversity of life before and after the impact.

Subsampling for organic and isotopic geochemistry

The largest remaining pieces of rock (>30 g) from the same sampled intervals that will be analyzed for (molecular) microbiology were sampled for organic and isotopic geochemistry. To prevent contamination with organics, direct contact with plastic was avoided by wrapping these samples first in autoclaved aluminum foil followed by putting them in a canvas bag. They were then double-bagged in Whirl-Pak bags and stored at –80°C.

Samples for microbiology and for organic and isotopic geochemistry were not analyzed offshore or at the OSP at MARUM. Instead, immediately after the expedition, all mud and rock samples were shipped on dry ice to the University of Edinburgh (Scotland, UK) and Curtin University (Australia), while the vials for cell enumeration and cultivation were shipped refrigerated to the University of Edinburgh for downstream analyses.

Onshore sampling and sample processing

Core handling and sampling

During core spitting at MARUM, additional quarter rounds (1–1.5 cm in diameter) were occasionally sampled using a water-cooled circular saw only. Without crushing the samples, the outer surface was cleaned under running tap water, and the surface was sterilized using RNase-Away and flamed with 70% ethanol as described above. The pieces were then wrapped in autoclaved aluminum foil and double bagged in labeled Whirl-Pak bags and stored at –80°C in a freezer at MARUM.

Core samples were collected in the proximity of locations in the core where samples were previously obtained offshore. DNA will be extracted from these intervals to allow direct comparison of the microbial diversity in samples that were immediately frozen upon core recovery (as is currently the standard procedure) with samples taken from intact core that have been kept refrigerated for 4 months. If no significant changes in the community structure have

occurred, it means that samples taken from the split cores during the OSP are suitable for DNA-based community structure analysis. In that case, DNA as well as geolipids will be extracted from additional samples taken from targeted features that were not necessarily near the core ends. These additional samples include (1) sections of granitoids in the Lower Peak Ring interval with mineral overgrowth veins; (2) samples that record the recovery of life shortly after the impact; (3) a sample from the early, middle, and end of the Paleocene/Eocene Thermal Maximum (PETM); (4) samples covering five consecutive precession cycles; and (5) samples from ash layers within the Post-Impact Sedimentary Rocks interval.

Cell enumerations

Cell sediment preparations will be either filtered or observed directly after staining with Sybr green, acridine orange, or 4′,6-diamindino-2-phenylindole (DAPI) under fluorescence microscopy. The different dyes have different effectiveness in different substrates. In some cases, multiple dyes will be used on single samples to count cells.

Cultivation procedures

Cultivation will be carried out for a range of metabolic groups using a diversity of media. Samples collected for cultivation are divided up into 10 mL serum bottles under anaerobic conditions. To each serum bottle, ~1–5 mL of media is added. The objective is to maximize the rock/media ratio to ensure that the resulting fluid is geochemically driven by the rock and not by the media, thus producing a fluid that has a higher chance of being similar to in situ fluids. Once the media is added, the bottles are closed with sterile rubber stoppers and crimped with aluminum seals. Downhole temperature data will be used to determine incubation temperatures. Three incubation temperatures will be used: 50°C (506–802 mbsf), 60°C (802–1125 mbsf), and 70°C (1125–1333 mbsf). These temperatures reflect the upper range of temperatures in the core required to support the selective growth of indigenous thermophiles and to minimize growth of potential mesophilic contaminants.

The media used for enrichments are as follows.

Target group: heterotrophs

Subsurface heterotroph minimal medium I is a simple medium with supplemental N, P, and S and a few organic sources including yeast extract. A volume of 500 mL of the medium contains 0.1 g NH_4Cl, 0.1 g K_2HPO_4, 0.1 g Na_2SO_4, 0.05 g iron citrate, 0.2 g yeast extract, 0.2 g peptone, 0.2 g casamino acids, and 0.2 g sodium acetate. As a reducing agent, 0.6 g/L of cysteine is added. Samples are gassed under 100% N_2 or 20% CO_2 and 80% N_2 headspace.

Subsurface minimal medium II is a medium that provides N, P, and S and carbon in a variety of forms from simple organic compounds (e.g., acetate) to long-chain sugars such as xylan and yeast extract. This is a more complex organics mix compared to subsurface minimal medium I. A volume of 500 mL of medium contains 0.1 g NH_4Cl, 0.1 g K_2HPO_4, 1 g KNO_3, 1 g Na_2SO_4, 0.5 g iron citrate, 0.1 g yeast extract, 0.1 g peptone, 0.1 g sodium acetate, 0.1 g casamino acids, 0.1 g sodium formate, 0.1 g xylan, 0.1 g fructose, and 0.1 g sodium pyruvate. Additionally, 1.25 g $NaHCO_3$ was dissolved in 25 mL water, autoclaved separately, and then added to the medium. Samples are gassed under a 20% CO_2 and 80% N_2 headspace.

Subsurface minimal medium III was used to enrich microorganisms that utilize simple organic compounds. A volume of 500 mL of medium contains 5 g K_2HPO_4, 0.5 g NH_4Cl, 0.25 g KCl, 0.25 g $MgSO_4 \cdot 7H_2O$, 0.5 g sodium gluconate, 0.5 g sodium acetate, 0.5 g sodium formate, and 0.5 g sodium fumarate. Samples are gassed under an 80% CO_2 and 20% N_2 headspace.

Target group: chemolithotrophs

Chemolithotrophs were cultivated using a simple medium that contains a range of electron acceptors such as sulfate, iron, and nitrate but without the addition of organics. Electron donors are supplied as H_2 or other sources available in the rock. A volume of 500 mL of medium contains 0.1 g NH_4Cl, 1.0 g K_2HPO_4, 1 g KNO_3, 1 g Na_2SO_4, 0.5 g iron citrate, 1.5 mg $NiCl_2 \cdot 6H_2O$, and 5.0 g $NaHCO_3$. Samples are gassed under an 80% H_2 and 20% CO_2 headspace. As a reducing agent, 0.6 g/L of cysteine is added.

Target group: chemolithotrophs/heterotroph communities

A medium that has both organics and H_2 available as an electron donor was used to select for organisms that could be heterotrophs and/or chemolithotrophs or members of both groups interacting in communities. In this case, Wolfe's vitamin and trace element solution was added along with a tungstate selenate solution to provide additional nutrient sources in case these made a difference to growth compared to previous media. A volume of 500 mL of medium contains 0.5 g NH_4Cl, 0.4 g K_2HPO_4, 0.1 g $MgCl_2 \cdot 6H_2O$, 0.5 g yeast extract, 0.1 g $MgSO_4 \cdot 7H_2O$, 0.05 g $CaCl_2$, 2.5 g $NaHCO_3$, 0.25 g L-cysteine, 10 mL Wolfe's trace element solution, 10 mL Wolfe's vitamin solution, 0.5 mL tungstate selenate solution, and 0.25 mL $FeCl_3$. Samples are gassed under an 80% H_2 and 20% CO_2 headspace.

DNA extraction

DNA will be extracted using a variety of methods depending on the sample type. Most common among these are the use of the Mo Bio DNA extraction kits (MO BIO Laboratories). Modifications to the protocol will be used where appropriate. Successfully extracted DNA will be amplified for bacterial, archaeal, and eukaryotic genes with sequencing performed by MiSeq and for 454 sequencing. Other methods may be used. Quantitative polymerase chain reaction (PCR) will be used to quantify microbial taxa.

RNA extraction

RNA will be extracted after Lever et al. (2015) to study the microbial communities that were alive and active at the time of sampling. DNA can be preserved in the geosphere for at least several hundreds of thousands of years (e.g., Coolen et al., 2006; Randlett et al., 2014) and could therefore also reveal taxa that were alive in the past. This approach uses buffers that protect the RNA and prevent adsorption of nucleic acids to the mineral matrices that would otherwise lead to loss of RNA. To increase the likelihood that sufficient RNA can be recovered for downstream analyses, only samples that were shown to contain significant amounts of DNA will be extracted.

Organic and isotopic geochemistry

At the WA Organic and Isotopic Geochemistry Centre (WA-OIGC; Curtin University), samples will be ground and subjected to Rock Eval pyrolysis via collaboration with international partners. The powders will be extracted with organic solvents in a microwave extractor to obtain organic matter. Aliquots will be taken and analyzed by gas chromatography–mass spectroscopy (GC-MS), liquid chromatograpy (LC)-MS, and GC×GC time of flight (TOF)-MS. The extracted residues will be demineralized and subjected to hydropyrolysis. Organic extracts will be further separated for compound-specific carbon, hydrogen isotopes of biomarkers, and sulfur isotopes of organosulfur compounds. Selected polyaromatic hydro-

carbons (PAHs), diamondoids, and fullurenes will be targeted by GC-MS and LC-MS as required (Brocks and Grice, 2011; Brocks and Summons, 2014; Grice and Brocks, 2011; Grice and Eiserbeck, 2014; Peters et al., 2005; Whiteside and Grice, 2016).

References

Agnini, C., Fornaciari, E., Raffi, I., Rio, D., Röhl, U., and Westerhold, T., 2007. High-resolution nannofossil biochronology of middle Paleocene to early Eocene at ODP Site 1262: implications for calcareous nannoplankton evolution. *Marine Micropaleontology,* 64(3–4):215–248. **https://doi.org/10.1016/j.marmicro.2007.05.003**

Alegret, L., and Thomas, E., 2001. Upper Cretaceous and lower Paleogene benthic foraminifera from northeastern Mexico. *Micropaleontology,* 47(4):269–316. **https://doi.org/10.2113/47.4.269**

Amante, C., and Eakins, B.W., 2009. *ETOPO1 1 Arc-Minute Global Relief Model: Procedures, Data Sources and Analysis.* NOAA Technical Memorandum NESDIS NGDC-24. National Geophysical Data Center, NOAA. **https://doi.org/10.7289/V5C8276M**

Berggren, W.A., and Aubert, J., 1975. Paleocene benthonic foraminiferal biostratigraphy, paleobiogeography and paleoecology of Atlantic-Tethyan regions: Midway-type fauna. *Palaeogeography, Palaeoclimatology, Palaeoecology,* 18(2):73–192. **https://doi.org/10.1016/0031-0182(75)90025-5**

Berggren, W.A., and Pearson, P.N., 2005. A revised tropical to subtropical Paleogene planktonic foraminiferal zonation. *Journal of Foraminiferal Research,* 35(4):279–298. **https://doi.org/10.2113/35.4.279**

Bolli, H.M., Beckmann, J.-P., and Saunders, J.B., 1994. *Benthic Foraminiferal Biostratigraphy of the South Caribbean Region:* Cambridge, United Kingdom (Cambridge University Press).

Bown, P.R., Rutledge, D.C., Crux, J.A., and Gallagher, L.T., 1998. Lower Cretaceous. *In* Bown, P.R. (Ed.), *Calcareous Nannofossil Biostratigraphy:* Dordrecht, The Netherlands (Kluwer Academic Publishing), 86–131.

Brocks, J.J., and Grice, K., 2011. Biomarkers (molecular fossils). *In* Reitner, J., and Thiel, V. (Eds.), *Encyclopedia of Geobiology:* Dordrecht, The Netherlands (Springer), 147–167. **https://doi.org/10.1007/978-1-4020-9212-1_30**

Brocks, J.J., and Summons, R.E., 2014. Sedimentary hydrocarbons, biomarkers for early life. *In* Karl, D.M., and Schlesinger, W.H. (Eds.), *Treatise on Geochemistry* (2nd edition) (Volume 10): *Biogeochemistry.* Holland, H., and Turekian, K.K. (Series Eds.): Oxford, United Kingdom (Elsevier), 61–103. **https://doi.org/10.1016/B978-0-08-095975-7.00803-2**

Carslaw, H.S., and Jaeger, J.C., 1959. *Conduction of Heat in Solids* (2nd edition): Oxford, United Kingdom (Clarendon Press).

Chung, F.H., 1974. Quantitative interpretation of X-ray diffraction patterns of mixtures. I. Matrix-flushing method for quantitative multicomponent analysis. *Journal of Applied Crystallography,* 7(6):519–525. **https://doi.org/10.1107/S0021889874010375**

Cockell, C.S., Voytek, M.A., Gronstal, A.L., Finster, K., Kirshtein, J.D., Howard, K., Reitner, J., Gohn, G.S., Sanford, W.E., Horton, J.W., Jr., Kallmeyer, J., Kelly, L., and Powars, D.S., 2012. Impact disruption and recovery of the deep subsurface biosphere. *Astrobiology,* 12(3):231–246. **https://doi.org/10.1089/ast.2011.0722**

Collette, A., 2013. *Python and HDF5: Unlocking Scientific Data:* Boston (O'Reilly Media).

Collier, J., Schumacher, S., Behrens, C., Driemel, A., Diepenbroek, M., Grobe, H., Kim, T., Schindler, U., Sieger, R., and Wallrabe-Adams, H.-J., 2015. Rescued from the deep: publishing scientific ocean drilling long tail data. *GeoResJ,* 6:17–20. **https://doi.org/10.1016/j.grj.2015.01.003**

Coolen, M.J.L., Boere, A., Abbas, B., Baas, M., Wakeham, S.G., and Sinninghe Damsté, J.S., 2006. Ancient DNA derived from alkenone-biosynthesizing haptophytes and other algae in Holocene sediments from the Black Sea. *Paleoceanography,* 21(1):PA1005. **https://doi.org/10.1029/2005PA001188**

Coolen, M.J.L., and Orsi, W.D., 2015. The transcriptional response of microbial communities in thawing Alaskan permafrost soils. *Frontiers in Microbiology,* 6:197. **https://doi.org/10.3389/fmicb.2015.00197**

Coolen, M.J.L., and Overmann, J., 2007. 217 000-year-old DNA sequences of green sulfur bacteria in Mediterranean sapropels and their implications for the reconstruction of the paleoenvironment. *Environmental Microbiology,* 9(1):238–249. **https://doi.org/10.1111/j.1462-2920.2006.01134.x**

Corinaldesi, C., Beolchini, F., and Dell'Anno, A., 2008. Damage and degradation rates of extracellular DNA in marine sediments: implications for the preservation of gene sequences. *Molecular Ecology,* 17(17):3939–3951. **https://doi.org/10.1111/j.1365-294X.2008.03880.x**

de Winter, N.J., and Claeys, P., 2016. Micro X-ray fluorescence (μXRF) line scanning on Cretaceous rudist bivalves: a new method for reproducible trace element profiles in bivalve calcite. *Sedimentology,* 64(1):231–251. **https://doi.org/10.1111/sed.12299**

Diepenbroek, M., Grobe, H., Reinke, M., Schindler, U., Schlitzer, R., Sieger, R., and Wefer, G., 2002. PANGAEA—an information system for environmental sciences. *Computers & Geosciences,* 28(10):1201–1210. **https://doi.org/10.1016/S0098-3004(02)00039-0**

Diepenbroek, M., Grobe, H., Reinke, M., Schlitzer, R., and Sieger, R., 1999. Data management of proxy parameters with PANGAEA. *In* Fischer, G., and Wefer, G. (Eds.), *Use of Proxies in Paleoceanography: Examples from the South Atlantic:* Heidelberg, Germany (Springer-Verlag), 715–727. **https://doi.org/10013/epic.11224**

Droser, M.L., and Bottjer, D.J., 1991. Trace fossils and ichnofabric in Leg 119 cores. *In* Barron, J., Larsen, B., et al., *Proceedings of the Ocean Drilling Program, Scientific Results,* 119: College Station, TX (Ocean Drilling Program), 635–641. **https://doi.org/10.2973/odp.proc.sr.119.206.1991**

Duliu, O.G., 1999. Computer axial tomography in geosciences: an overview. *Earth-Science Reviews,* 48(4):265–281. **https://doi.org/10.1016/S0012-8252(99)00056-2**

Dunham, R.J., 1962. Classification of carbonate rocks according to depositional texture. *In* Ham, W.E. (Ed.), *Classification of Carbonate Rocks.* AAPG Memoir, 1:108–121. **http://archives.datapages.com/data/specpubs/carbona2/data/a038/a038/0001/0100/0108.htm**

Ellis, D.V., and Singer, J.M., 2007. *Well Logging for Earth Scientists* (2nd edition): New York (Elsevier).

Embry, A.F., III, and Klovan, J.E., 1972. Absolute water depth limits of late Devonian ecological zones. *Geologische Rundschau,* 61(2):672–686. **https://doi.org/10.1007/BF01896340**

Goff, J.A., Gulick, S.P.S., Perez Cruz, L., Stewart, H.A., Davis, M., Duncan, D., Saustrup, S., Sanford, J., and Urrutia Fucugauchi, J., 2016. Solution pans and linear sand bedforms on the bare-rock limestone shelf of the Campeche Bank, Yucatán Peninsula, Mexico. *Continental Shelf Research,* 117:57–66. **https://doi.org/10.1016/j.csr.2016.02.005**

Goldberg, D., 1997. The role of downhole measurements in marine geology and geophysics. *Reviews of Geophysics,* 35(3):315–342. **https://doi.org/10.1029/97RG00221**

Gradstein, F.M., Ogg, J.G., Schmitz, M.D., and Ogg, G.M. (Eds.), 2012. *The Geological Time Scale 2012:* Amsterdam (Elsevier).

Grice, K., and Brocks, J.J., 2011. Biomarkers (organic, compound-specific isotopes). *In* Reitner, J., and Thiel, V. (Eds.), *Encyclopedia of Geobiology:* Dordrecht, The Netherlands (Springer), 167–182. **https://doi.org/10.1007/978-1-4020-9212-1_29**

Grice, K., and Eiserbeck, C., 2014. The analysis and application of biomarkers. *In* Falkowski, P.G., and Freeman, K.H. (Eds.), *Treatise on Geochemistry* (2nd edition) (Volume 12): *Organic Geochemistry.* Holland, H., and Turekian, K.K. (Series Eds.): Oxford, United Kingdom (Elsevier), 47–78. **https://doi.org/10.1016/B978-0-08-095975-7.01006-8**

Gulick, S., Morgan, J., Mellett, C.L., Green, S.L., Bralower, T., Chenot, E., Christeson, G., Claeys, P., Cockell, C., Coolen, M., Ferrière, L., Gebhardt, C., Goto, K., Jones, H., Kring, D., Lofi, J., Lowery, C., Ocampo-Torres, R., Perez-Cruz, L., Pickersgill, A.E., Poelchau, M., Rae, A., Rasmussen, C., Rebdolledo-Vieyra, M., Riller, U., Sato, H., Smit, J., Tikoo, S., Tomioka, N., Urrutia Fucugauchi, J., Whalen, M., Wittmann, A., Yamagachi, K., Xiao, L., and Zylberman, W., 2017a. Expedition 364 summary. *In* Morgan, J., Gulick, S., Mellett, C.L., Green, S.L., and the Expedition 364 Scientists, *Chicxulub: Drilling the K-Pg Impact Crater.* Proceedings of the Interna-

tional Ocean Discovery Program, 364: College Station, TX (International Ocean Discovery Program). **https://doi.org/10.14379/iodp.proc.364.101.2017**

Gulick, S., Morgan, J., Mellett, C.L., Green, S.L., Bralower, T., Chenot, E., Christeson, G., Claeys, P., Cockell, C., Coolen, M., Ferrière, L., Gebhardt, C., Goto, K., Jones, H., Kring, D., Lofi, J., Lowery, C., Ocampo-Torres, R., Perez-Cruz, L., Pickersgill, A.E., Poelchau, M., Rae, A., Rasmussen, C., Rebdolledo-Vieyra, M., Riller, U., Sato, H., Smit, J., Tikoo, S., Tomioka, N., Urrutia Fucugauchi, J., Whalen, M., Wittmann, A., Yamagachi, K., Xiao, L., and Zylberman, W., 2017b. Site M0077: Post-Impact Sedimentary Rocks. *In* Morgan, J., Gulick, S., Mellett, C.L., Green, S.L., and the Expedition 364 Scientists, *Chicxulub: Drilling the K-Pg Impact Crater.* Proceedings of the International Ocean Discovery Program, 364: College Station, TX (International Ocean Discovery Program). **https://doi.org/10.14379/iodp.proc.364.105.2017**

Hall, B., and Govert, A., 2016. Techniques for using core CT data for facies identification and analysis [paper presented at the Unconventional Resources Technology Conference, San Antonio, Texas, 1–3 August 2016]. (Abstract 2434059)

Holbourn, A., Henderson, A.S., and MacLeod, N., 2013. *Atlas of Benthic Foraminifera:* Chichester, United Kingdom (John Wiley & Sons, Ltd.). **https://doi.org/10.1002/9781118452493**

Hoehler, T.M., and Jørgensen, B.B., 2013. Microbial life under extreme energy limitation. *National Review of Microbiology,* 11(2):83–94. **https://doi.org/10.1038/nrmicro2939**

Imai, N., Terashima, S., Itoh, S., and Ando, A., 1995. 1994 compilation of analytical data for minor and trace elements in seventeen GSJ geochemical reference samples, "igneous rock series." *Geostandards and Geoanalytical Research,* 19(2):135–213. **https://doi.org/10.1111/j.1751-908X.1995.tb00158.x**

Inagaki, F., Hinrichs, K.-U., Kubo, Y., Bowles, M.W., Heuer, V.B., Long, W.-L., Hoshino, T., Ijiri, A., Imachi, H., Ito, M., Kaneko, M., Lever, M.A., Lin, Y.-S., Methé, B.A., Morita, S., Morono, Y., Tanikawa, W., Bihan, M., Bowden, S.A., Elvert, M., Glombitza, C., Gross, D., Harrington, G.J., Hori, T., Li, K., Limmer, D., Liu, C.-H., Murayama, M., Ohkouchi, N., Ono, S., Park, Y.-S., Phillips, S.C., Prieto-Mollar, X., Purkey, M., Riedinger, N., Sanada, Y., Sauvage, J., Snyder, G., Susilawati, R., Takano, Y., Tasumi, E., Terada, T., Tomaru, H., Trembath-Reichert, E., Wang, D.T., and Yamada, Y., 2015. Exploring deep microbial life in coal-bearing sediment down to ~2.5 km below the ocean floor. *Science,* 349(6246):420–424. **https://doi.org/10.1126/science.aaa6882**

Inwood, J., Brewer, T., Braaksma, H., and Pezard, P., 2008. Integration of core, logging and drilling data in modern reefal carbonates to improve core location and recovery estimates (IODP Expedition 310). *Journal of the Geological Society,* 165(2):585–596. **https://doi.org/10.1144/0016-76492007-041**

Leckie, R.M., and Olson, H.C., 2003. Foraminifera as proxies of sea-level change on siliciclastic margins. *In* Olson, H.C., and Leckie, R.M. (Eds.), *Micropaleontologic Proxies of Sea-Level Change and Stratigraphic Discontinuities.* Special Publication - SEPM (Society for Sedimentary Geology), 75:5–19. **https://doi.org/10.2110/pec.03.75.0005**

Le Maitre, R.W., Steckeisen, A., Zanettin, B., Le Bas, M.J., Bonin, B., and Bateman, P. (Eds.), 2002. *Igneous rocks: A Classification and Glossary of Terms* (2nd edition.): Cambridge, United Kingdom (Cambridge University Press).

Leroy, C.C., 1969. Development of simple equations for accurate and more realistic calculation of the speed of sound in seawater. *Journal of the Acoustical Society of America,* 46(1B):216–226. **https://doi.org/10.1121/1.1911673**

Lirer, F., 2000. A new technique for retrieving calcareous microfossils from lithified lime deposits. *Micropaleontology,* 46(4):365–369. **http://www.micropress.org/micropen2/articles/1/3/7343_articles_article_file_1363.pdf**

Moore, D.M., and Reynolds, R.C., Jr., 1997. *X-ray Diffraction and the Identification and Analysis of Clay Minerals* (2nd edition): Oxford, United Kingdom (Oxford University Press).

Norrish, K., and Chappell, B.W., 1967. X-ray spectrography. *In* Zussman, J. (Ed.), *Physical Methods in Determinative Mineralogy:* New York (Academic Press), 161–124.

Okada, H., and Bukry, D., 1980. Supplementary modification and introduction of code numbers to the low-latitude coccolith biostratigraphic zonation (Bukry, 1973; 1975). *Marine Micropaleontology,* 5:321–325. **https://doi.org/10.1016/0377-8398(80)90016-X**

Olsson, R.K., Hemleben, C., Berggren, W.A., and Huber, B.T. (Eds.), 1999. Atlas of Paleocene planktonic foraminifera. *Smithsonian Contributions to Paleobiology,* 85. **https://doi.org/10.5479/si.00810266.85.1**

Pearson, P.N., Olsson, R.K., Hemleben, C., Huber, B.T., and Berggren, W.A., 2006. Atlas of Eocene planktonic foraminifera. *Special Publication - Cushman Foundation for Foraminiferal Research,* 41.

Perch-Nielsen, K., 1985. Cenozoic calcareous nannofossils. *In* Bolli, H.M., Saunders, J.B., and Perch-Nielsen, K. (Eds.), *Plankton Stratigraphy:* Cambridge, United Kingdom (Cambridge University Press), 427–554.

Peters, K.E., Walters, C.C., and Moldowan, J.M., 2005. *The Biomarker Guide* (2nd edition): Cambridge, United Kingdom (Cambridge University Press).

Pilkington, M., and Hildebrand, A.R., 2000. Three-dimensional magnetic imaging of the Chicxulub crater. *Journal of Geophysical Research: Solid Earth,* 105(B10):23479–23491. **https://doi.org/10.1029/2000JB900222**

Postuma, J.A., 1971. *Manual of Planktonic Foraminifera:* Amsterdam (Elsevier).

Randlett, M.-È., Coolen, M.J.L., Stockhecke, M., Pickarski, N., Litt, T., Balkema, C., Kwiecien, O., Tomonaga, Y., Wehrli, B., and Schubert, C.J., 2014. Alkenone distribution in Lake Van sediment over the last 270 ka: influence of temperature and haptophyte species composition. *Quaternary Science Reviews,* 104:53–62. **https://doi.org/10.1016/j.quascirev.2014.07.009**

Rider, M.H., 1996. *The Geological Interpretation of Well Logs* (2nd edition): Caithness, Scotland (Whittles Publishing).

Rebolledo-Vieyra, M., Urrutia-Fucugauchi, J., and López-Loera, H., 2010. Aeromagnetic anomalies and structural model of the Chicxulub multiring impact crater, Yucatán, Mexico. *Revistas Mexicana de Ciencias Geológicas,* 27:185–195. (in Spanish with English abstract) **http://www.redalyc.org/pdf/572/57214937016.pdf**

Schlumberger, 1989. *Log Interpretation Principles/Applications:* Houston (Schlumberger Education Services), SMP–7017.

Schlumberger, 1994. *IPL Integrated Porosity Lithology:* Houston (Schlumberger Education Services), SMP-9270.

Schnitker, D., 1979. Cenozoic deep water benthic foraminifera, Bay of Biscay. *In* Montadert, L., Roberts, D.G., et al., *Initial Reports of the Deep Sea Drilling Project,* 48: Washington, DC (U.S. Government Printing Office), 377–413. **https://doi.org/10.2973/dsdp.proc.48.115.1979**

Serra, O., 1984. *Fundamentals of Well-Log Interpretation* (Volume 1): *The Acquisition of Logging Data:* Amsterdam (Elsevier).

Serra, O., 1986. *Fundamentals of Well-Log Interpretation* (Volume 2): *The Interpretation of Logging Data:* Amsterdam (Elsevier).

Siddiqui, S., and Khamees, A.A., 2004. Dual-energy CT-scanning applications in rock characterization [paper presented at the SPE Annual Technical Conference and Exhibition, Houston, Texas, 26–29 September 2004]. (Abstract SPE-90520-MS) **https://doi.org/10.2118/90520-MS**

Smith, D.C., Spivack, A.J., Fisk, M.R., Haveman, S.A., and Staudigel, H., 2000a. Tracer-based estimates of drilling-induced microbial contamination of deep sea crust. *Geomicrobiology Journal,* 17(3):207–219. **https://doi.org/10.1080/01490450050121170**

Smith, D.C., Spivack, A.J., Fisk, M.R., Haveman, S.A., Staudigel, H., and the Leg 185 Shipboard Scientific Party, 2000b. *Technical Note 28: Methods for Quantifying Potential Microbial Contamination during Deep Ocean Coring.* Ocean Drilling Program. **https://doi.org/10.2973/odp.tn.28.2000**

Stöffler, D., and Grieve, R., 2007. Impactites. *In* Fettes, D., and Desmons, J. (Eds.), *Metamorphic Rocks: A Classification and Glossary of Terms; Recommendations of the International Union of Geological Sciences Subcommission on the Systematics of Metamorphic Rocks:* Cambridge, United Kingdom (Cambridge University Press), 82–92.

Streckeisen, A., 1974. Classification and nomenclature of plutonic rocks recommendations of the IUGS subcommission on the systematics of igneous rocks. *Geologische Rundschau,* 63(2):773–786. **https://doi.org/10.1007/BF01820841**

TeKa, 2010. *TK04 Thermal Conductivity Meter: User's Manual Version 4.4.x:* Berlin (TeKa).

Terashima, S., Taniguchi, M., Mikoshiba, M., and Imai, N., 1998. Preparation of two new GSJ geochemical reference materials: basalt JB-1b and coal fly ash JCFA-1. *Geostandards and Geoanalytical Research,* 22(1):113–117. **https://doi.org/10.1111/j.1751-908X.1998.tb00550.x**

Vacquier, V., 1985. The measurement of thermal conductivity of solids with a transient linear heat source on the plane surface of a poorly conducting body. *Earth and Planetary Science Letters,* 74(2–3):275–279. **http://dx.doi.org/10.1016/0012-821X(85)90027-5**

van Hinsbergen, D.J.J., Kouwenhoven, T.J., and van der Zwaan, G.J., 2005. Paleobathymetry in the backstripping procedure: correction for oxygenation effects on depth estimates. *Palaeogeography, Palaeoclimatology, Palaeoecology,* 221(3–4):245–265. **http://dx.doi.org/10.1016/j.palaeo.2005.02.013**

van Konijenburg, J.-H., Wernli, R., and Bernoulli, D., 1998. Tentative biostratigraphy of Paleogene planktic foraminifera in thin-section, an example from the Gran Sasso d'Italia (central Appennines, Italy). *Eclogae Geologicae Helvetiae*, 91:203–216. **https://doi.org/10.5169/seals-168418**

Von Herzen, R., and Maxwell, A.E., 1959. The measurement of thermal conductivity of deep-sea sediments by a needle-probe method. *Journal of Geophysical Research,* 64(10):1557–1563. **https://doi.org/10.1029/JZ064i010p01557**

Wade, B.S., Pearson, P.N., Berggren, W.A., and Pälike, H., 2011. Review and revision of Cenozoic tropical planktonic foraminiferal biostratigraphy and calibration to the geomagnetic polarity and astronomical timescale. *Earth-Science Reviews,* 104(1–3):111–142. **https://doi.org/10.1016/j.earscirev.2010.09.003**

Wentworth, C.K., 1922. A scale of grade and class terms for clastic sediments. *Journal of Geology,* 30(5):377–392. **http://dx.doi.org/10.1086/622910**

Westerhold, T., Röhl, U., Raffi, I., Fornaciari, E., Monechi, S., Reale, V., Bowles, J., and Evans, H.F., 2008. Astronomical calibration of the Paleocene time. *Palaeogeography, Palaeoclimatology, Palaeoecology,* 257(4):377–403. **https://doi.org/10.1016/j.palaeo.2007.09.016**

Whiteside, J.H., and Grice, K., 2016. Biomarker records associated with mass extinction events. *Annual Review of Earth and Planetary Sciences,* 44(1):581–612. **https://doi.org/10.1146/annurev-earth-060115-012501**